Regulation of angiogenesis by CPEB-mediated translational control

Vittorio Calderone

UNIVERSITY OF BARCELONA (UB)

SCHOOL OF PHARMACY

DEPARTMENT OF BIOCHEMISTRY AND MOLECULAR BIOLOGY

DOCTORATE IN MEDICAL BIOTECHNOLOGY

Regulation of angiogenesis by CPEB-mediated translational control

Report submitted by **Vittorio Calderone**
to obtain the PhD degree at University of Barcelona

Thesis director: Raul Mendez de la Iglesia

PhD candidate: Vittorio Calderone

Vittorio Calderone, 2013

TABLE OF CONTENTS

ABSTRACT

Angiogenesis is a major pathological hallmark of chronic liver disease, playing a crucial role in the progression of liver fibrogenesis to cirrhosis, and in the onset and aggravation of portal hypertension, which determines the main complications of the disease. Even though it is clear that VEGF is the main effector of this pathological angiogenesis, the molecular mechanisms that govern the post-transcriptional activation of its synthesis during liver cirrhosis are largely unknown. In this work, we show that VEGF synthesis is regulated through sequential and non-redundant functions of two members of the cytoplasmic polyadenylation element-binding protein (CPEB) family of RNA-binding proteins: CPEB1 and CPEB4. Thus, CPEB1 promotes alternative processing of both VEGF and CPEB4 pre-mRNAs, shortening their 3' untranslated regions and excluding translation-inhibition elements from their mature transcripts. As the result of this alternative processing, CPEB4 is overexpressed and polyadenylates VEGF mRNA, further increasing its translation. Accordingly, both CPEB1 and CPEB4 are required for VEGF synthesis and the subsequent angiogenesis. Furthermore, the regulation of CPEB4 by CPEB1 and the auto amplification loop of CPEB4 ensues a coordinated switch-like induction of angiogenesis during portal hypertension. In accordance, all the proteins are sequentially overexpressed in patients and animal models of liver cirrhosis and portal hypertension, and both CPEB1 and CPEB4 knockout mice failed to activate angiogenesis upon portal hypertension induction. Through the analysis of *in vitro* angiogenesis assays, human samples and animal models, our findings highlight the crucial role of CPEBs on pathological neovascularization, in the setting of portal hypertension and cirrhosis, and identify CPEBs as potential new molecular targets for therapy of chronic liver disease and other neovascularization-dependent diseases, as cancer.

INTRODUCTION

CHAPTER I: Angiogenesis

1. Mechanism of angiogenesis

The vascular system is a highly branched network of endothelium-lined tubes that provides all tissues with crucial nutrients and respiratory gasses, and allows the circulation of signaling molecules and cellular components throughout the body. Vascular development is initiated by the organization of migrating mesoderm-derived endothelial progenitor cells that form the primary vascular plexus, in a process termed “vasculogenesis”. However, most of the vasculature is formed by the process known as “angiogenesis”, in which the primary network is expanded by formation of new vessels from the preexisting vascular tubes. Angiogenesis is a multistep process that includes sprouting morphogenesis, cell migration, extracellular matrix remodeling, stabilization and differentiation in arterioles, venules and capillaries.

Despite several factors are involved at different levels, either stimulating or inhibiting angiogenesis, last decade of research on vascular biology has identified the Vascular Endothelial Growth Factor (VEGF) as the most potent angiogenic factor. VEGF is able to initiate angiogenesis, activating endothelial “tip” cells that guide the blood vessel sprout, while neighboring “stalk” cells proliferate and form the body of the vascular branch. The VEGF-induced tip/stalk cell specification is achieved by the Notch-Dll4 signaling pathway **(Figure 1)**. Angiogenic sprouts eventually meet and connect in a process, called “anastomosis”, creating a closed and functional tubular system [1-4].

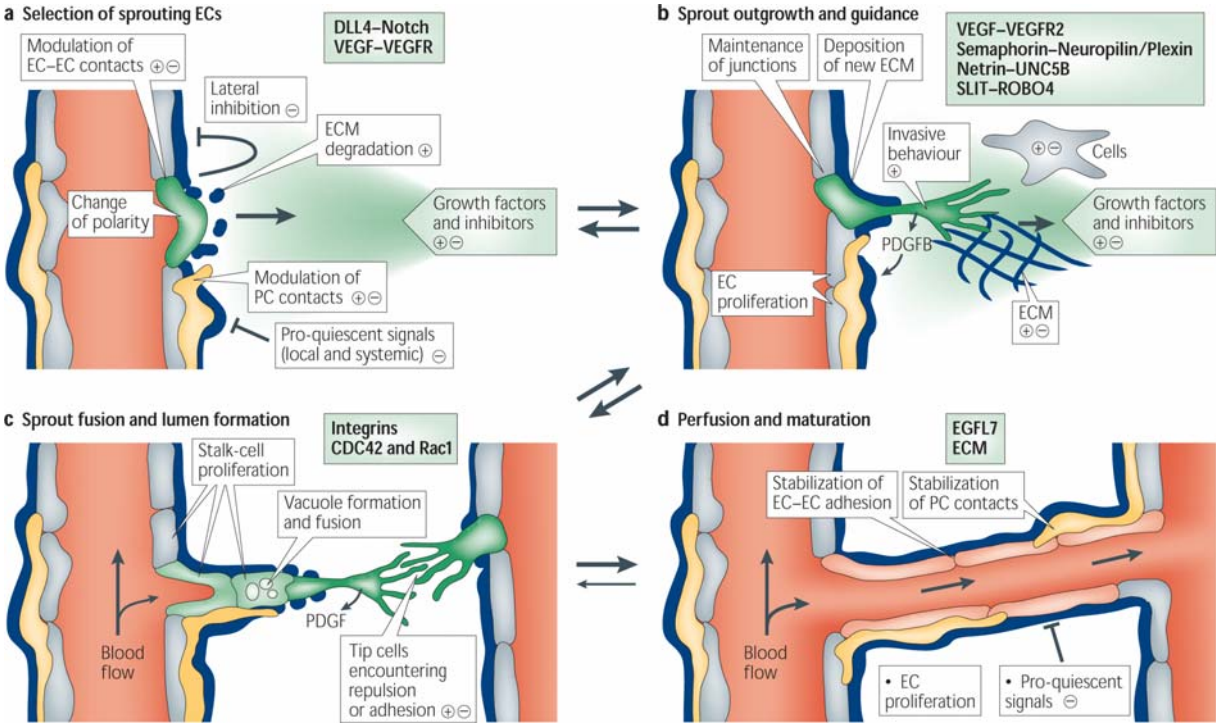

Figure 1. VEGF-induced angiogenesis model. **a**. VEGF induces activation and sprouting of certain endothelial cells (green), whereas others fail to respond (grey). **b**. The growing EC sprout is guided by VEGF gradients. Other signals may include attractive (+) or repulsive (–) matrix cues and guidepost cells in the tissue environment. **c**. Adhesive or repulsive interactions that occur when tip cells encounter each other regulate the fusion of adjacent sprouts and vessels. Lumen formation in stalk ECs involves the fusion of vacuoles but other mechanisms may also contribute. **d**. Fusion processes at the EC–EC interfaces establish a continuous and functional lumen. Modified from Ralf H. Adams and Kari Alitalo [3].

2. Vascular Endothelial Growth Factor as key regulator of angiogenesis

The development of a functional network of blood vessels depends on the balance of many stimulating or inhibiting factors. Quite a number of molecules can serve as regulator of angiogenesis including fibroblast growth factor (FGF), transforming growth factors (TGFα and TGFβ), angiogenin, interleukin-8, and angiopoietins. However, it's now assumed that the critical event in the regulation of angiogenesis is the signaling cascade induced by VEGF family of proteins. This family includes several factors such as VEGF (also known as VEGF-A), placenta growth factor (PIGF), VEGF-B, VEGF-C and VEGF-D.

The gene encoding human VEGF consists in eight exons separated by seven introns. The first 26 aminoacids of VEGF constitute the signaling peptide that achieves the secretion of the protein. By alternative splicing of *VEGF* gene, four isoforms, $VEGF_{121}$, $VEGF_{165}$, $VEGF_{189}$, and

$VEGF_{206}$, containing respectively, 121, 165, 189, and 206 aminoacids after removal of the signaling peptide, are generated. Less frequent spliced isoforms $VEGF_{145}$ and $VEGF_{183}$ have also been identified **(Figure 2)**. In mouse and rat, where *VEGF* gene is highly conserved, VEGF isoforms are shorter by one aminoacid. In VEGF secreting cells, the most frequent isoform is $VEGF_{165}$, a homodimer of molecular mass 45 kD. An important characteristic of VEGF isoforms is their ability to bind heparin, because this determines if the secreted protein will be accumulated in the extracellular matrix or will be released and thus become accessible for interaction with other cells. The isoforms $VEGF_{189}$ and $VEGF_{206}$ bind heparin with high affinity and are almost completely accumulated in the extracellular matrix; $VEGF_{121}$ is weakly acid and fails to bind to heparin, while $VEGF_{165}$, showing intermediate properties (it's soluble but certain amount of protein also remains bound to extracellular matrix), is characterized by optimal parameters of biological activity. Heparin-bound VEGF may be released in a soluble form after cleavage by plasmin or heparinase with formation of a biological active fragment.

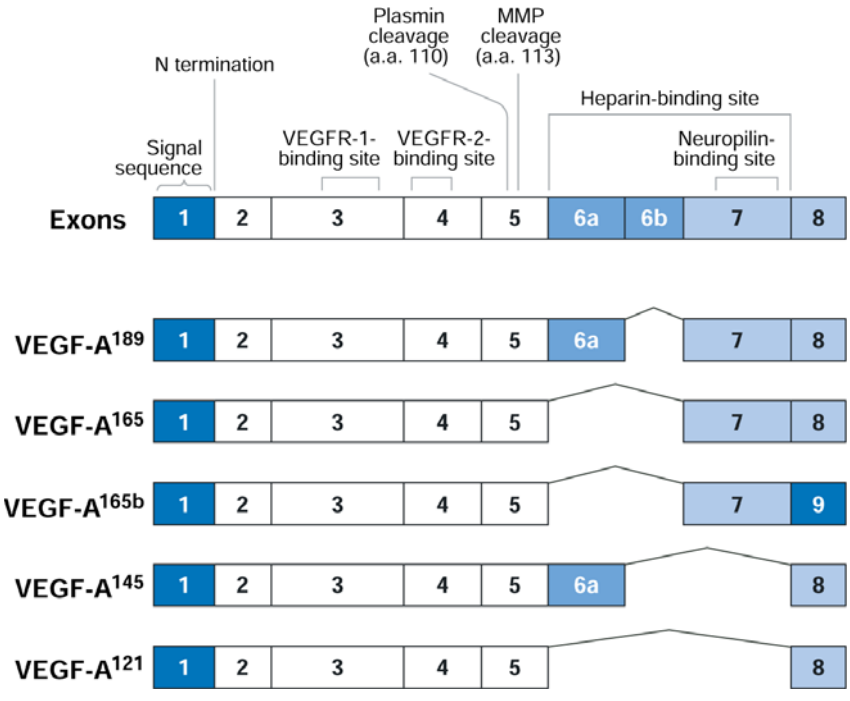

Figure 2. Structure of human VEGF-A and its most commonly expressed isoforms. The first exon encodes a hydrophobic leader sequence typical of secreted proteins. VEGF-A_{189} lacks a portion of exon 6, whereas VEGF-A_{165}, generally the most commonly expressed isoform, lacks all of exon 6. VEGF-A_{145} lacks both exons 6b and 7, and VEGF-A_{121} lacks all of exons 6

and 7. VEGF-A_{165b} is an inhibitory form of VEGF-A that lacks exons 6 and 8 and that terminates with a portion of the supposed 3' untranslated region, here designated as exon 9. VEGF receptor and heparin-binding sites, as well as protease cleavage sites, are shown. Murine isoforms are one amino acid (a.a.) shorter, e.g., mouse VEGF-A_{164} versus human VEGF-A_{165} . Exons are not drawn to scale. Modified from Janice A. Nagy et al [5].

VEGF exerts its biological effect by interaction with receptors expressed on the surface of endothelial cells. Three receptors have been identified, and bind different VEGF growth factors: VEGFR1 (FLT1), VEGFR2 (Flk1/KDR) and VEGFR3 (FLT4) (initial receptor names are indicated in parentheses). These receptors belong to the superfamily of receptor tyrosine kinase (RTK) **(Figure 3)**.

- VEGFR1, the first to be identified, shows a not well understood function. Several studies proposed VEGFR1 as a decoy receptor that acts as negative regulator of VEGF-A activity.
- VEGFR2 plays a key role in the regulation of angiogenesis mediating the effects of VEGF-A binding. Activation of VEGFR2 induces a number of signal transduction pathways that then make the endothelial cells competent for mitogenesis, sprouting and migration.
- VEGFR3 is bound preferentially by VEGF-C and it's involved in the regulation of lymphangiogenesis [6-8].

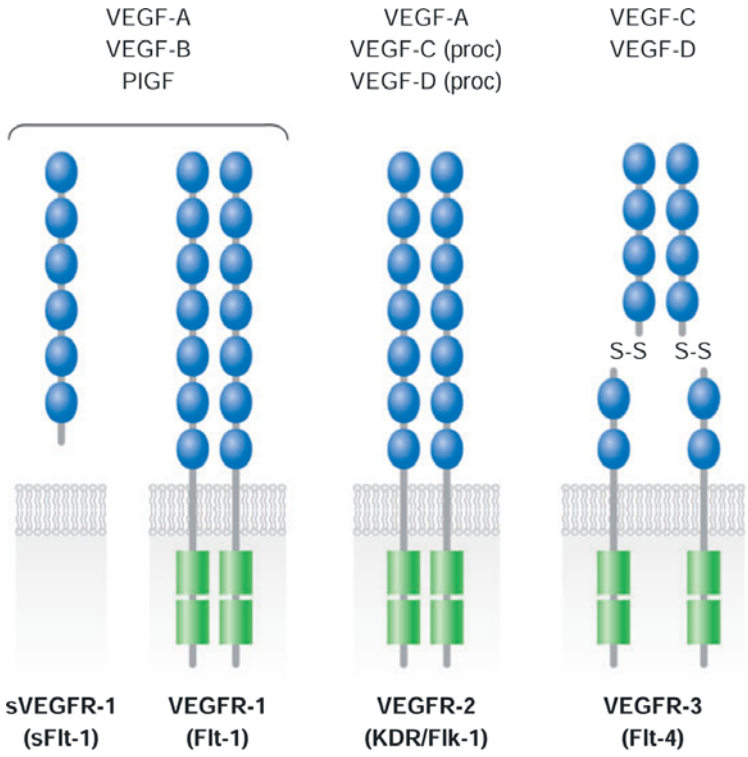

Figure 3. Schematic diagram of VEGF receptors and their ligands. Only proteolytically processed forms (proc) of VEGF-C and VEGF-D bind to VEGFR-2. Modified from Janice A. Nagy et al [5].

CHAPTER II: Physiological and pathological angiogenesis

1. Physiological angiogenesis

Angiogenesis, which is a crucial process during embryonic and fetal development, takes place also in the adult, in physiological conditions such as menstrual cycle and pregnancy, wound healing, and skeletal growth. A brief analysis of the role of angiogenesis in the regulation of these processes is proposed below.

Angiogenesis is a pivotal process in menstrual cycle. The cyclic establishment and differentiation of a receptive endometrium is driven by the action of estradiol and progesterone; both hormones have been shown to induce VEGF expression in uterine stroma cells. Moreover, recent studies also demonstrated that VEGF mRNA expression is temporally and spatially regulated in the corpus luteum following ovulation. Once fertilization occurs, angiogenesis is essential for embryo vascularization and maintenance of pregnancy [8].

Immediately after an injury, the formation of a temporary plug of platelet cells is achieved by the production of endothelial cell-secreted pro-coagulant factors in response to VEGF. In turn, platelet-secreted VEGF further increases its own local concentration to promote endothelial cell proliferation and facilitate extravasation of plasma fibronectin into the extracellular space. In addition, VEGF can signal to induce nitric oxide and prostacyclin production to increase microvascular permeability and endothelial cell migration [8].

Angiogenesis is essential during bone formation. The majority of bones in the skeleton develop through the process of endochondral ossification in which bone replaces avascular cartilage. VEGF-dependent angiogenesis is important for coupling cartilage resorption with bone formation [8,9].

2. Pathological angiogenesis

Pathological angiogenesis shares several characteristics with physiological angiogenesis. Under both conditions, a cascade of highly regulated cellular functions drives the formation of new blood vessels in response to increased demand for oxygen and nutrients.
In this session of the manuscript it's proposed an overview of the main pathological conditions, characterized by formation of new blood vessels. In particular, it's analyzed the importance of angiogenesis during cancer establishment and progression, and in intraocular disorders. Finally, it's proposed a focus on angiogenesis in liver diseases that will be particularly useful for the comprehension of the next chapters.

There are considerable evidences that VEGF, in particular $VEGF_{165}$, is the main tumor angiogenesis factor. VEGF is overexpressed in a large number of human and animal carcinomas, sarcomas, hematological malignancies, and multiple myelomas [5,8,10]. A number of factors regulate low-level expression of VEGF in normal tissues and induce its overexpression in pathological conditions. One of these conditions, hypoxia, regulates both transcription and mRNA stability of VEGF during tumoral angiogenesis. VEGF transcription is under control of hypoxia-inducible factor 1 (HIF-1), a heterodimeric protein transcription factor. One HIF-1 peptide, HIF-1α, is rapidly degraded under normoxic conditions through the ubiquitin pathway; however, when stabilize by hypoxia, HIF-1α makes dimers with HIF-1β, and the complex binds and activates a hypoxia-responsible element in VEGF gene promoter, inducing the transcription of VEGF mRNA. Hypoxia regulation of VEGF has been characterized in many tumors even if many others express VEGF constitutively at high levels under normoxic condition. [5,8].

VEGF levels are elevated in the aqueous and vitreous humors of human eyes with proliferative retinopathy secondary to diabetes and other conditions [11]. Animal studies using several VEGF inhibitors have constitutively demonstrated the role of VEGF as key mediator of ischemia-induced intraocular neovascularization [12].

Angiogenesis and remodeling of liver vascular network have been related with progression of hepatic cirrhosis, which contribute to increase hepatic vascular resistance and portal hypertension. Established evidences clearly indicate that hepatic cirrhosis is characterized by intrahepatic vasculature development with formation of shunts, which lead to increased

hepatic resistance. Just this last feature, in turn, leads to portal hypertension, which is a major complication of cirrhosis and represents a leading cause of liver transplantation and death. Portal hypertension induces formation of collateral vessels that shunt the portal blood into the systemic circulation, causing high systemic concentration of several substances normally metabolized by the liver, such as drugs, toxins, hormones and bacteria. Traditionally, formation of collaterals was considered a mechanical consequence of the increased portal pressure that results in the opening of these vascular vessels. However, recent studies have proposed the involvement of neo-angiogenesis in the development of collateral vessels.

From a mechanistic point of view, intra and pre-hepatic angiogenesis may be interpreted by two main concepts. A first feature is the overexpression of several growth factors, cytokines and metalloproteases with pro-angiogenic function. Second, angiogenesis is stimulated by the progressive increase of tissue hypoxia. Recent studies have demonstrated that VEGF, the most important angiogenic factor, is overexpressed in splanchnic organs from portal hypertensive animals. The precise mechanism triggering VEGF-dependent angiogenesis in hepatic cirrhosis is not clear and remains speculative. Several factors, relevant for the progression of the pathology, such as hypoxia, cytokines, and mechanistic stress have been shown to promote VEGF expression in various cell types and tissues.

Understanding the molecular mechanism of VEGF gene regulation in hepatic cirrhosis-associated angiogenesis may lead to promising therapeutic strategies [13-16].

3. Models to study pathological angiogenesis in liver

As for all the pathological conditions, the use of animal models is of enormous importance to study the pathophysiology of hepatic cirrhosis and hepatic cirrhosis-associated portal hypertension, since they allow extensive study of questions that cannot be addressed in human studies.

In the present study, we used two animal models; the first, Common Bile Duct Ligation (CBDL), is a model of secondary biliary cirrhosis, commonly used to study hepatic cirrhosis and intrahepatic angiogenesis. The second, Partial Portal Vein Ligation (PPVL), is a pre-hepatic model largely used to study the pathophysiology of portal hypertension as consequence of liver cirrhosis.

Common Bile Duct Ligation (CBDL)

CBDL model has been used to study intrahepatic angiogenesis associated to hepatic cirrhosis. It's developed in rats, which are especially appropriate due to the lack of a gallbladder, isolating the common bile duct by a double ligature. This determines the retaining of the bile that, due to its toxicity, induces biliary fibrosis-cirrhosis [17,18] **(Figure 4)**.

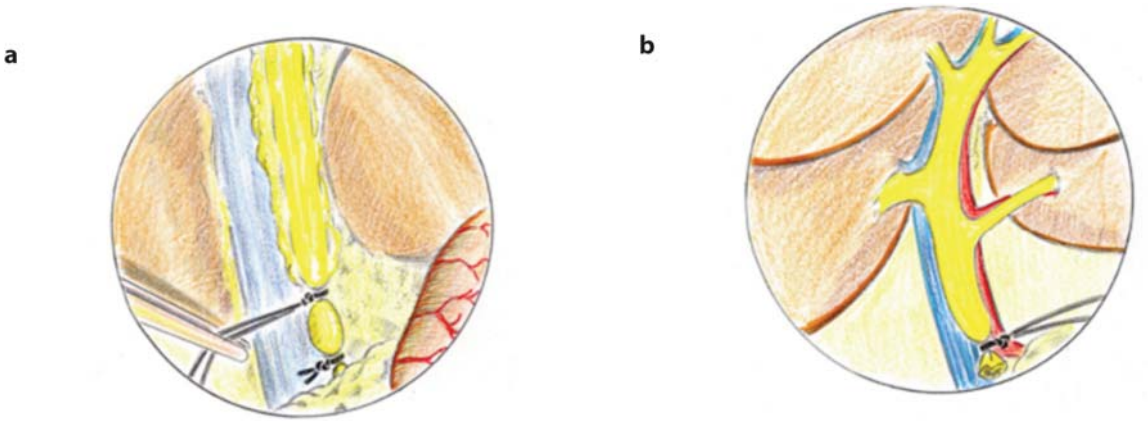

Figure 4. Schematic representation of Common Bile Duct Ligation procedure. The bile duct is isolated with a double ligation that causes the retaining of the bile into the duct. Modified from Maria-Angeles Aller et al, Protocol Exchange (2010) doi:10.1038/nprot.2010.56.

Partial Portal Vein Ligation (PPVL)

In this study, PPVL has been used for the analysis of angiogenesis associated with portal hypertension. It' has been developed in rats, freeing the portal vein from the surrounding tissues after a midline abdominal incision. A ligature has been placed around a blunt-tipped needle lying along the portal vein. Subsequent removal of the needle yields to a calibrated stenosis of the portal vein that has the diameter of the needle. The partial occlusion generates portal hypertension that, in turn, induces neo-vascularization of the mesentery, a vascular bed, we largely used for the study of angiogenesis [18,19] **(Figures 5 and 6)**.

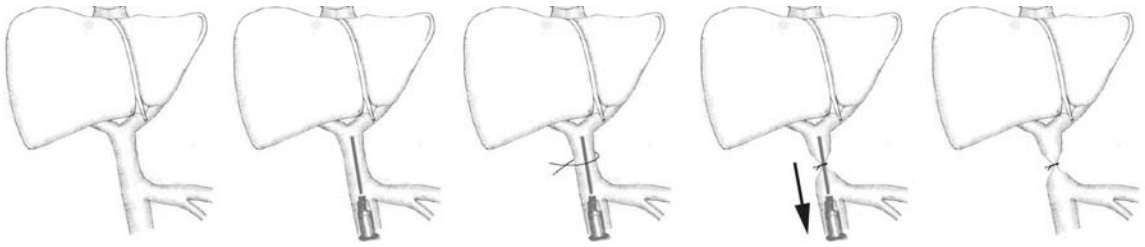

Figure 5. Schematic representation of Partial Portal Vein Ligation procedure. A ligature is placed around a blunt-tipped needle lying along the portal vein. After removal of the needle the portal vein has the diameter of the needle.

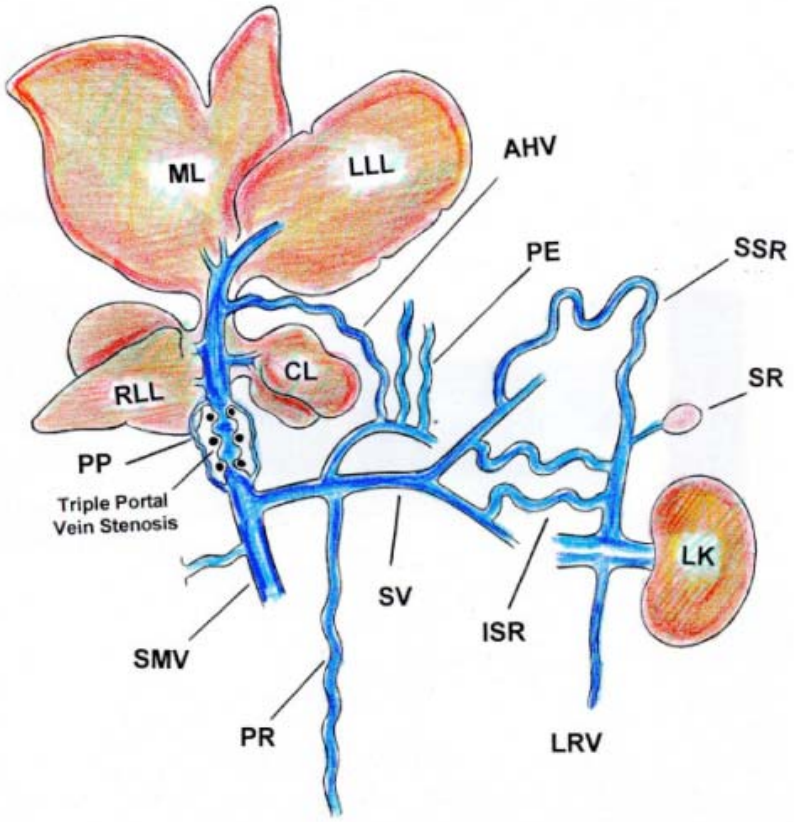

Figure 6. Collateral circulation in rats with partial portal vein ligation. ML: middle lobe; LLL: left lateral lobe; RLL: right lateral lobe; CL: caudate lobe; AHV: Accessory Hepatic Vein; PP: paraportal; SMV: superior mesenteric vein; PR: pararectal; SV: splenic vein; ISR: inferior splenorenal; SSR: superior splenorenal; PE: paraesophageal; LK: left kidney; SR: suprarenal gland; LRV: left renal vein. The development of the portal collateral venous system is not only due to the opening of preexisting vessels, but also to new vessel formation, which is a very active process. Particularly, it has been shown that portal hypertension in the rat is associated with vascular endothelial growth factor (VEGF) induced angiogenesis. Modified from María-Angeles Aller et al [20].

CHAPTER III: From pre-mRNA to mature mRNA

Gene expression is regulated at multiple levels, and emerging data suggest that the different processes involved in this regulation are integrated with each other. In this session of the study, the nuclear "life" of the mRNA will be described, with a focus on an important post-transcriptional modification called alternative polyadenylation.

1. Gene expression overview before 3'UTR processing

In the cell nucleus, the RNA polymerase II (pol II) initiation complex is recruited to the gene promoter to polymerize a pre-mRNA. After the eventual synthesis of proximal abortive transcripts, the pre-mRNA is properly elongated and it's immediately available for biochemical processing [21] [22]. Before a transcript can be exported from the nucleus to the cytoplasm in order to become available for the translation machinery, in fact, it has to undergo a series of processing steps. The first is the addition of an m^7G cap structure to the 5' end of the nascent RNA and takes place after the first 20-30 nucleotides have been synthetized [23]. In a three steps reaction, the nascent mRNA is hydrolyzed, the GMP portion of GTP is added to the first nucleotide of the transcript, and GMP is methylated at position N7. The so formed cap structure is important for mRNA stability and translation [24-26].
As the coding sequence of most mRNAs in eukaryotes is interrupted by introns, these non-coding sequences have to be spiced out from the pre-mRNA to generate a functional mRNA. Splicing needs specific consensus sequences that mark the exon-intron boundaries, and the spliceosome, the catalytic complex that carries out the reaction to remove the introns and ligate the flanking exons [27-29]. The alternative use of exons (alternative splicing) contributes to protein variety by allowing a single gene to produce multiple isoforms of mRNA [30].

2. 3'UTR cleavage and polyadenylation

In addition to the above mentioned pre-mRNA processing that takes place at level of 5' end and coding sequence, other important modifications occur in the 3'UTR. Stability, localization and translation of mature mRNAs are achieved by specific sequences in the 3' untranslated region, which recruit regulatory proteins and RNAs. Most mRNAs acquire an uncoded poly(A) tail at their 3' end in a process called polyadenylation [31,32]. The only known

protein-coding mRNAs lacking poly(A) tails codify for metazoan histones [30]. Polyadenylation involves two tightly coupled steps, in which the mRNAs are first cleaved at level of specific sequences, and then several adenosine (A) residues are added in a non-template dependent manner. In mammalian cells, the polyadenylation signal (PAS) contains the AAUAAA (or variants) hexamer motif, located between 10 and 35 nucleotides upstream of the cleavage and polyadenylation site. Furthermore, an U/GU rich element is localized between 14 and 70 nucleotide downstream of the PAS [33,34]. In addition to "in cis" RNA elements, different multi-subunit protein factors are required to make up the core mammalian cleavage and polyadenylation machinery: Cleavage and Polyadenylation Specificity Factor (CPSF) which binds the PAS, Cleavage Stimulation Factor (CStF) that binds to the U/GU rich element, Cleavage Factors I and II (CFI and CFII), Symplekin, and poly(A) polymerase (PAP) which mediated the synthesis of the poly(A) tail **(Figure 7)**. Whereas PAP and a sub-unit of the CPSF complex, CPSF73, are required for both cleavage and polyadenylation, CStF is required for the endonucleolytic cleavage and, together with CPSF, for recruitment of CFI and CFII [35-37]. The emerging poly(A) tail is bound by poly(A) binding protein nuclear I (PABPN1). PABPN1 directly starts to bind the poly(A) tail as the first 11-14 adenosines are added and the binding continues until the proper length of the poly(A) tail is reached (200-300 nucleotides in mammalian cells) [38,39]. In addition to help PAP in the polymerization of the poly(A) tail, PABPN1 protects the poly(A) tail from degradation by poly(A) nuclease (PAN) [40]. Moreover, PABPN1 is involved in nuclear export.

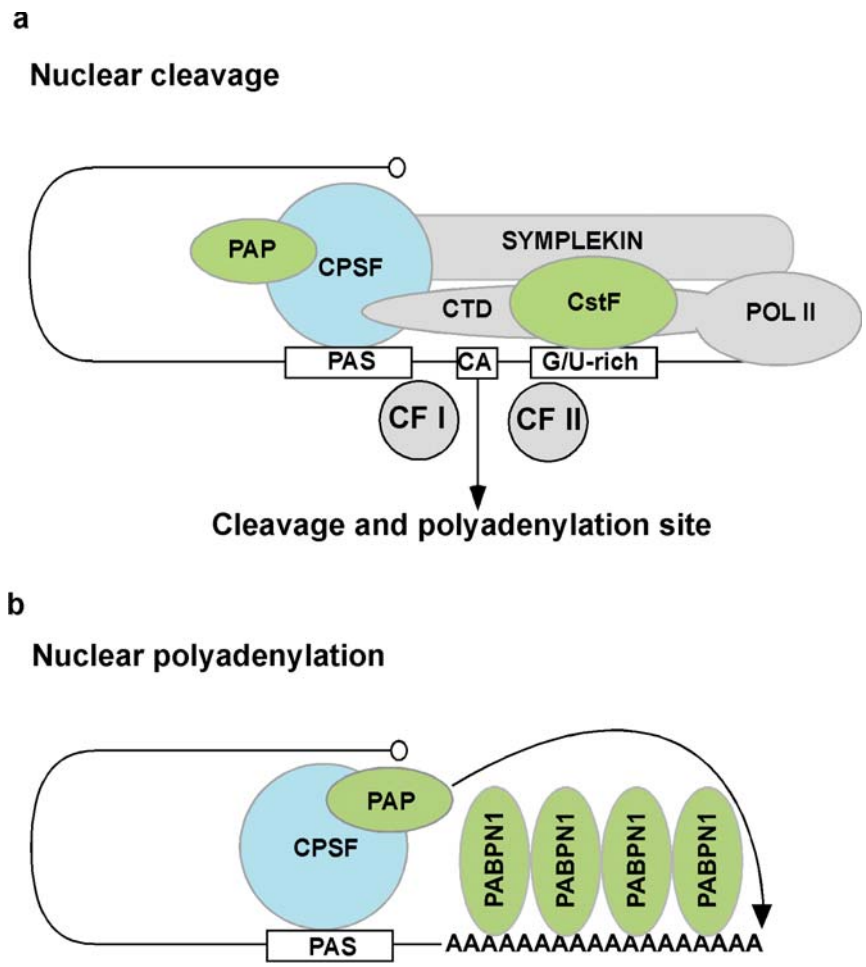

Figure 7. Nuclear cleavage and polyadenylation machineries. Representation of the protein complexes assembled at nuclear level for cleavage (a) and polyadenylation (b) of mRNA 3'UTRs. Modified from Alessio Bava's doctorate thesis, *CPEB1 coordinates alternative 3'UTR formation with translational regulation,* 2012.

In the simplest scenario, a single series of cleavage and polyadenylation events may occur on a pre-mRNA. However, last years of research on 3'UTR processing have proved that this simplest scenario is often not the rule. More than one PAS may be present in the mRNA 3'UTR. The choice between the utilization of one or the other PAS is exerted through a not completely understood mechanism called alternative polyadenylation (APA), and leads to the formation of a 3'UTR of different length, thus, different content of regulatory elements (RE), responsible for stability, transport and translation of the mRNA. When more than one PAS is present, usually, the proximal one (the nearest to the terminal exon) contains a sequence that differs a little from the canonical AAUAAA and that makes it "weaker", in

terms of cleavage and polyadenylation efficiency, compared with the "stronger" AAUAAA distal PAS (the nearest to the 3'end) that, for this reason, tends to be used by default. PAS with different nucleotide variants are relatively frequent, occurring in more than 30% of cases, as demonstrated by bioinformatics analysis [41] and are activated during APA [42,43] or tissue-specific polyadenylation [44]. Although it is not clear if the nucleotide sequence, alone, is sufficient to determine if PAS will be "weak" or "strong", it's now largely accepted the idea that, specific nucleotide sequences close to PAS, and their binding proteins can regulate APA, driving the cleavage and polyadenylation machinery in the selection of proximal or distal cleavage site. PABPN1, for example, binding to not consensus PAS, reduces its recognition by the cleavage and polyadenylation machinery [45,46]. An important biological concept is that APA, usually, results in shorter 3'UTR [41,47]. In general, longer 3'UTRs promote reduced translation, for example through regulation by micro RNA binding sites present in longer transcript and excluded in short variants [48]. Transformed cells and cells from highly proliferative tissues, like testis, express shortened 3'UTR for many mRNAs codifying for factors associated with proliferation and tumor progression. In contrast, non-proliferative tissues, such as brain, express mRNA with longer 3'UTR [49]. Moreover, 3'UTRs are shortened in response to extracellular stimuli, for example upon activation of neuronal cells [50], and during reprogramming of somatic cells into iPS cells [51]. Genome-wide analysis allowed to estimate how many transcripts can undergo through APA: 10%-15% of the transcriptome of *S. ceverisiae* [52], and almost 54% of the human transcriptome [41]. This last data underlines how important APA is for the global understanding of the regulation of gene expression.

3. mRNA nuclear export

Mature RNAs need to be exported from the nucleus to the cytoplasm for translation. These mRNAs are exported through the nuclear pore complex (NPC) as part of messenger ribonucleoprotein particles (mRNPs) that are assembled co-transcriptionally [53-55]. mRNPs contain the mRNA and the associated RNA binding proteins that bind the RNA during the different steps of processing [56,57]. In addition to the PABPN1, ribonucleopreotein particles may include serine/arginine rich (SR) proteins, and heterogeneous nuclear RNA (hnRNP) proteins, or the exon junction complex (EJC), which is a group of proteins loaded on the mRNA upstream of the exon-exon junctions as consequence of pre-mRNA splicing. Some of

these factors, important for association with the NPC and export into the cytoplasm, remain bound to the mRNA also once into the cytoplasm, whereas others are restricted to the nucleus [56,57].

CHAPTER IV: mRNA translation

1. Initiation

Translation can be divided in three steps: initiation, elongation, and termination. Translation initiation includes all the events that lead to the formation and the positioning of the elongation-competent 80S ribosome at level of the start codon of the mRNA. Several evidences indicate that initiation is the rate-limiting step for translation and that most of regulation occurs during this phase. The complexity and the importance of translation initiation compared to elongation and termination are further underlined by the fact that only few dedicated factors are needed to drive the latter two processes, whereas more then 25 proteins are required for proper translation initiation [58,59].

Translation initiation begins with the formation of the 43S preinitiation complex **(Figure 8)**. In the first step of this mechanism, the ternary complex, consisting in eIF2 (a hetero-trimer of α, β, and γ subunits), methionyl-initiator tRNA (Met-$tRNA_i^{Met}$), and GTP is assembled. This process is, furthermore, dependent on the guanine exchange factor eIF2B. GTP hydrolysis takes place after recognition of the AUG start codon, producing eIF2 bound to GDP, which has a tenfold-reduced affinity for Met-$tRNA_i^{Met}$. Binding of the ternary complex to the 40S ribosomal subunit is helped by eIF1, eIF1A, and eIF3. The 43S preinitiation complex is so ready to bind the 5' end of the mRNA. Recognition of the m^7G cap structure is mediated by eIF4F, which is composed by eIF4E, eIF4G, and eIF4A. eIF4E binds directly to the m^7G cap structure, eIF4A is a DEAD-box RNA helicase that unwinds secondary structures in the 5' UTR in the way that the 43S complex can scan along the mRNA, and eIF4G it's thought to act as scaffold protein [58]. The binding of the preinitiation complex to the mRNA involves the coordinated activity of eIF4F, eIF3, eIF4B, and poly(A) binding protein (PABP). The concerted binding of PABP and eIF4E to eIF4G pseudo-circularizes the mRNA [60], providing a possible framework through which 3' UTR binding proteins can regulate translation initiation. Despite translation starts at the 5' end of the mRNA, most of the known regulatory sequences and their binding factors act at level of the 3'UTR [59]. After proper assembly at the 5' end, the 43S preinitiation complex needs to scan along the mRNA to find the AUG start codon and bind it through interaction with the anticodon loop of the initiator tRNA. This stable complex is known as 48S initiation complex [61]. Several events take place in order for the 60S subunit to

join the 48S complex and form the 80S ribosome. eIF5 promotes the hydrolysis of GTP, and, as consequence, most of the initiation factors leave the small ribosome subunit, leaving the initiator tRNA bound to the start codon [59]. A second step of GTP hydrolysis is necessary to release the eIF5B. Thus, the 80S ribosome is competent for polypeptide elongation [62-64].

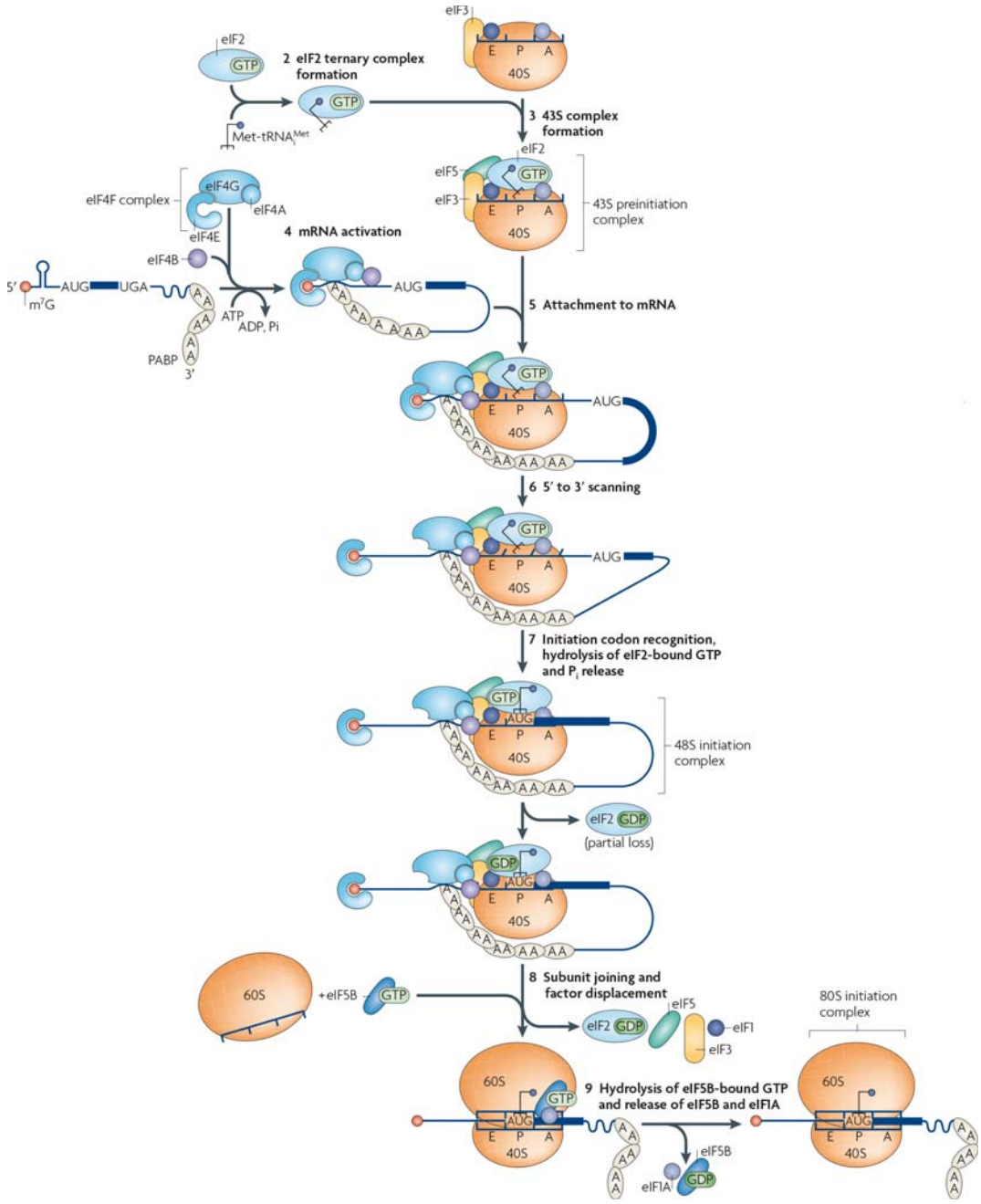

Figure 8. Model of eukaryotic translation initiation. Representation of the translation initiations steps from the 43S preinitiation complex formation to the positioning of the elongation-competent 80S ribosome at level of the start codon of the mRNA. Modified from Richard J. Jackson et al [65].

2. Elongation

When translation initiation finishes, and the 80S ribosome is formed, the methionyl-initiator tRNA is in the peptidyl site (P) of the ribosome while the ribosomal acceptor site (A) is empty. Elongation begins with the recruitment of an aa-tRNA at the site A and continues with the formation of a peptide bond between the incoming aa-tRNA and the former methionine carried by the initiator tRNA. At this point, the ribosome moves to the next codon, leaving the just formed bi-peptide in the site P and the deacetylated tRNA in the exit site (E). The deacetylated tRNA is then discarded [66,67]. This cycle is repeated until a stop codon appears and the process of termination starts.

Elongation factors eEF1 and eEF2 are required for proper elongation. eEF-1 has two subunits, α and βγ; α acts mediating the entry of the aminoacyl-tRNA into a free site of the ribosome. βγ acts serving as the guanine nucleotide exchange factor for α, catalyzing the release of GDP from α. eEF-2 catalyzes the translocation of the tRNA and mRNA down the ribosome at the end of each round of polypeptide elongation [67].

3. Termination and recycling

When one of the three stop codons (UAA, UGA, UAG) is recognized in the ribosomal A site, translation finishes. At this point, the completed polypeptide is released by the release factors (eRFs) after the hydrolysis of the ester bond that links the polypeptide chain to the tRNA in the P site. In Eukaryotes, two release factors are known, eRF1 and eRF3, which bind the ribosomal A site as a complex. The last event, after the polypeptide release, is the hydrolysis of a GTP molecule by eRF3 [68].

Since only free ribosomal subunits can initiate translation, it's important that post-termination ribosomes dissociates. In prokaryotes, this dissociation is achieved through a ribosome-recycling factor, which shows no known eukaryotic equivalent [69]. The eukaryotic initiation factors eIF3, eIF1, eIF1A, and eIF6 are thought to promote the dissociation in eukaryotes, but its mechanism is unknown. Recent data suggest that the activity of this factors is not sufficient to prevent the formation of the 80S ribosomes and that its dissociation is directly linked with 43S preinitiation complex formation [58].

CHAPTER V: Translational regulation of VEGF mRNA

1. 5'UTR-mediated regulation

For many years the above described cap-dependent or "scanning" mode was consider the only route through which translation initiation of eukaryotic mRNAs could take place. However, studies on viral gene expression in the late 1980s described an alternative translation initiation that bypasses the recruitment of the cap structure for the scanning of the mRNA and allows the 40S ribosome to be directed to the vicinity of the initiation codon [65,70,71]. The mRNA regions required for this direct recruitment of the 40S ribosomal subunit were termed Internal Ribosome Entry Sites (IRESs) to emphasize that the process is independent of the 5' end recognition **(Figure 9)** [65,70,71]. Analysis of the structure of viral IRESs elements has shown that they possess complex secondary and tertiary structures that are believed to direct non-canonical interactions between the IRESs and components of the canonical translation apparatus, thus allowing for 5' end independent initiation [71,72]. In certain cases the IRES-directed initiation can proceed without the involvement of any of the canonical initiation factors, relying exclusively on direct interactions between the IREs and the 40S ribosome [73].

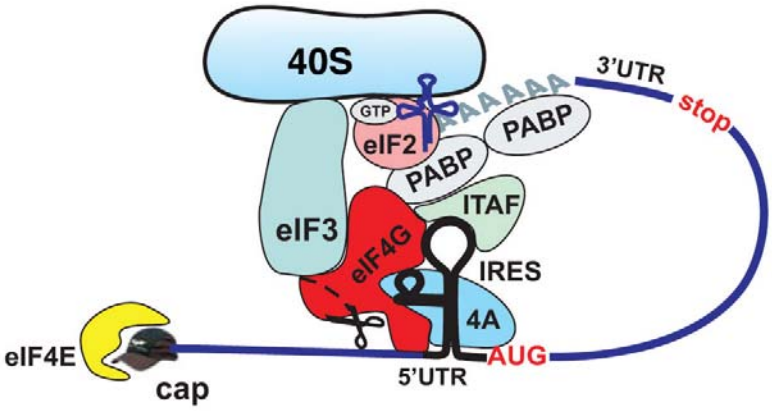

Figure 9. IRES-mediated mechanisms of translation initiation in eukaryotic cells. Cellular IRES-mediated translation generally does not require the cap-binding protein eIF4E and/or intact eIF4G, but may involve circularization of the mRNA. Modified from Anton A. Komar et al [74].

Although IRES-mediated translation of cellular transcripts has been less studied due to its reduced efficiency compared with the viral mechanism, it's now apparent that under condition of decreased cap-dependent initiation, cellular (viral-like) IRES-mediated initiation takes over [75,76].

The VEGF mRNA harbors two IRES-elements termed IRES-A and IRES-B **(Figure 10)**. IRES-A directs translation starting from the AUG located 1038 nucleotides downstream of the 5' end. IRES-B triggers translation starting from the upstream CUG codon located 499 nucleotides downstream of the 5' end of the mRNA [77]. Translation from the upstream CUG codon produces a 180 aminoacids longer VEGF isoform called L-VEGF. L-VEGF is further proteolytically processed to a N-terminal fragment, named N-VEGF and a C-terminal fragment of size similar to that of the AUG-initiated VEGF. N-terminal VEGF is intracellular, while C-terminal VEGF fragment of L-VEGF is a secreted VEGF isoform. Translation from the AUG codon generates secreted VEGF isoforms only. VEGF IRES-B- regulated initiation has been described in cellular stress condition such as hypoxia [78].

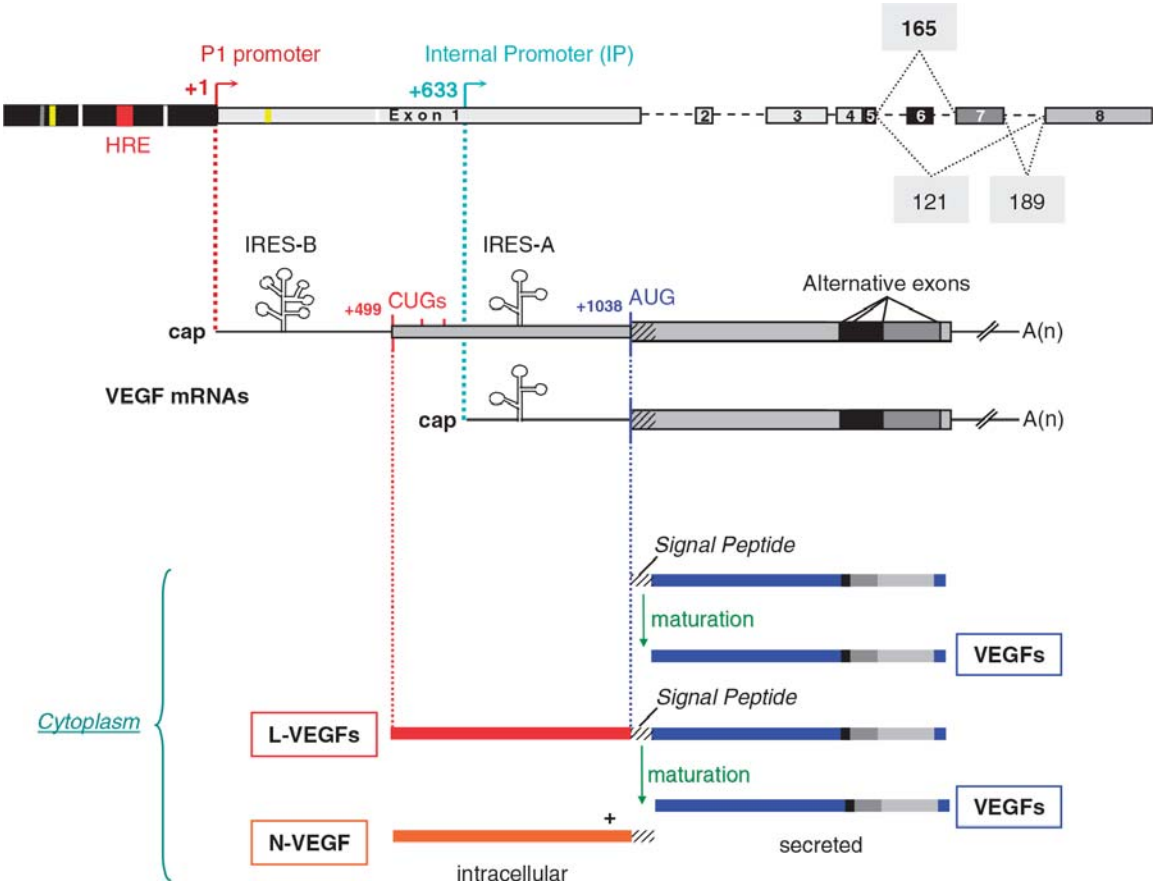

Figure 10. Schematic structure of VEGF gene. The 5'UTR of VEGF is represented containing: P1, TATA less promoter region including hypoxia responsive element (HRE); IP, internal promoter directs the transcription of a truncated mRNA. Three coding exons are alternatively spliced and give rise to several polypeptide, the most abundant are the 121, 165 and 189 amino acids isoforms. The 1038 nucleotides upstream from the AUG contain two IRESes (A and B) and in frame CUGs translation initiation codons that direct the synthesis of L-VEGF, which cleavage generates secreted-VEGF plus the intracellular N-VEGF. Modified from Amandine Bastide et al [77].

2. 3'UTR-mediated regulation

The 3'UTR of VEGF mRNA is long about 1900 nucleotides and contains several regulatory elements that, together with their protein binding factors are able to determine the translational fate of the mRNA.

Hu antigen R (HuR), belonging to the ELAV-like family of RNA binding proteins, binds to AU-rich elements (ARE) in the 3'UTR of VEGF, stabilizing the mRNA in tumor endothelial cells (TEC). HuR knockdown caused decreased VEGF mRNA and protein levels, shortening the half-life of the transcript [79]. HuR was also found to regulate VEGF mRNA stability in skeletal muscle [80].

The Poly(A)-binding Protein-interacting Protein 2 (PAIP2) was shown to interact with the VEGF 3'UTR both in vitro and in vivo, leading to VEGF mRNA stabilization, which correlated with increase in VEGF production. Co-immunoprecipitation experiments showed that PAIP2 interacts with HuR, suggesting cooperation of both proteins for VEGF mRNA stabilization [81].

The micro RNA miR-16 has been described as possible regulator of VEGF mRNA. The enhanced expression of $VEGF_{121}$ observed in prostate tumor cells might be due to loss of miR-16 translational control. Although the exact mechanism governing the effect of miR-16 on VEGF translation remains unknown, it may involve the hnRNP L protein, which binds within the VEGF 3'UTR at a site adjacent to the miR-16 binding site and may thereby alter the interaction of miR-16 with the mRNA [82].

Recent studies from Paul Fox group revealed a novel, negative regulatory mechanism of VEGF gene expression in which, VEGF mRNA, after induction by γ-interferon (IFN- γ), is translationally inhibited by binding of the heterotetrameric GAIT complex to a defined element in its 3'UTR [83].

CHAPTER VI: CPEB-mediated translational control

1. Cytoplasmic polyadenylation

Despite all mRNAs, with the exception of replication-dependent histone mRNAs, are polyadenylated into the nucleus, some of them may undergo elongation of their poly(A) tail in the cytoplasm, in a cleavage independent manner. This process, called cytoplasmic polyadenylation, was discovered 40 years ago and has been extensively studied during meiotic maturation in *Xenopus laevis* oocytes. Cytoplasmic polyadenylation plays important roles in mitotic cell cycle progression, cellular senescence and synaptic plasticity [84]. Cytoplasmic polyadenylation is guided by the same PAS used for nuclear polyadenylation (AAUAAA or variants), and it's binding protein CPSF, in coordination with cytoplasmic polyadenylation elements (CPE) present in the mRNA 3'UTR, and their binding proteins (CPEB) [85-87]. CPE-containing mRNAs are deadenylated during their transport to the cytoplasm, where they are stored in translationally repressed mRNPs, until when their poly(A) tails are elongated (80-250 residues) to allow the translation [88,89]. Cytoplasmic polyadenylation is driven by CPEB1 and CPSF that jointly recruit the poly(A) polymerase GLD2 that is responsible of the poly(A) tail elongation [90].

2. CPEB family of proteins

The CPEB family of proteins is composed by four paralogs (CPEB1-4) where CPEB2-4 are closely related each other while CPEB1 constitutes a distant branch of the family [91] **(Figure 11)**. CPEB orthologs are also present in other species: Orb1-2 in *Drosophila melanogaster* [92], Fog-1, and cpb1-3 in *Caenorhabditis elegans* [93], CPEB in *Aplysia californica* [94]. All CPEB proteins show similar structures, with a carboxy-terminal region composed by two RNA Recognition Motifs (RRMs) and two zinc-finger like motifs [95], and a regulatory N-terminal domain. The C-terminal domain is conserved in all CPEB1-4 proteins, while the N-terminal domain is highly variable, suggesting that different CPEBs may act in a different way in the regulation of the same mRNAs. CPEB binds the mRNA 3'UTR at level of specific sequences UUUUAAU or UUUUAU (consensus CPE) or variants (non-consensus CPE).

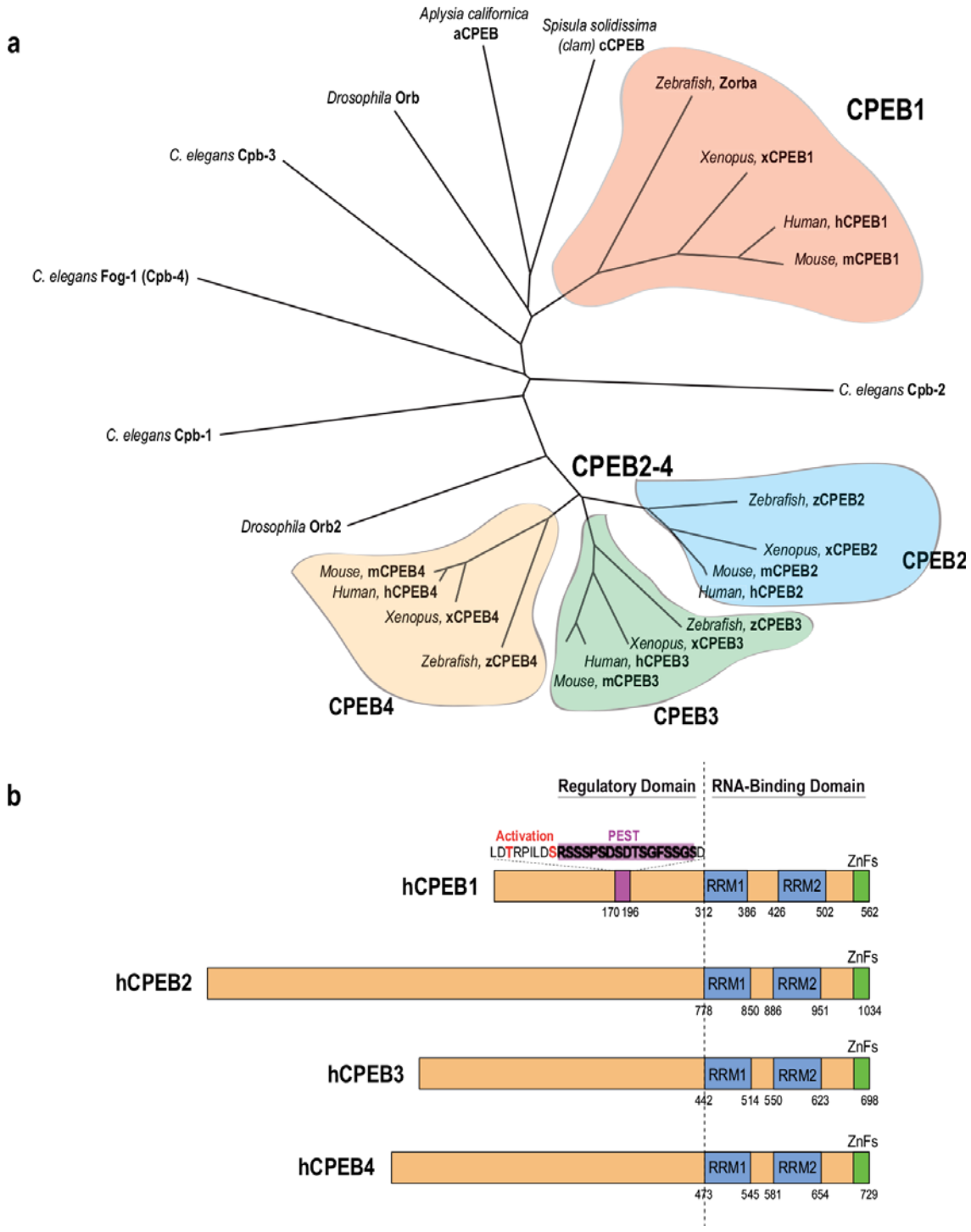

Figure 11. CPEB family of RNA-binding proteins. **a**. Unrooted phylogenetic tree of the most representative CPEB proteins performed by complete sequence alignment. **b**. Protein structure of human CPEBs. CPEBs share a conserved RNA-binding domain at the C-terminal part and a highly variable regulatory domain at the N-terminal part. The RNA-binding domain comprises two RNA recognition motifs (RRMs, in blue) and two zinc-fingers (ZnFs, in green). In the case of CPEB1, the regulatory domain contains two residues (in red) responsible for CPEB1 phosphorylated and activation by Aurora A, followed by a PEST-degradation motif (in purple). Modified from Gonzalo Fernández-Miranda et al [96].

3. CPEB-mediated repression and activation of translation

The mechanisms of translation repression and activation have been extensively studied in *Xenopus laevis* oocytes during meiotic progression, where CPEB plays a pivotal dual role. In stage VI arrested oocytes, CPEB is able to maintain several CPE-containing maternal mRNAs in a translational repressed state. On the other hand, upon progesterone stimulation, and consequent meiosis resumption, CPEB drives the activation of mRNA translation. CPEB-mediated translational repression requires a cluster of at least two CPEs, independently on their position along the 3'UTR, where the distance between the CPEs determines the repression extent with an optimal separation of 10-12 nucleotides [88]. CPEB recruits the poly(A) specific ribonuclease (PARN), that is a cap-interacting deadenylase [97-99], and GLD-2. PARN and GLD-2 are believed to be present in the repression complex of immature oocytes, where PARN shows a much stronger activity than GLD-2, resulting in the removal of the poly(A) tail as soon it is added by GLD-2 [100]. Since the presence of a short poly(A) tail is not sufficient to mediate the full translational repression, it has been proposed that Maskin, a member of the transforming acidic coiled-coil containing (TACC) family, associates with CPEB and binds to the cap-binding initiation factor eIF4E. This interaction, in turn, prevents the binding of eIF4E by eIF4G and the following recruitment of the 40S ribosomal subunit to the 5' end [85,86,101,102]. Although CPEB1 may recruit PARN to the mRNA, the deadenylase activity of PARN requires a 5' cap structure, partially discrediting the presence of Maskin and PARN in the same repression complex. Other authors proposed a different model of translation repression in which CPEB interacts with 4E-transporter (4E-T), which in turn binds an oocyte specific eIF4E isoform (4E1b). In this complex there are also present the RNA helicase RCK/Xp54 and Rap 55. Xp54 associates with CPEB and eIF4E, repressing the translation of the mRNAs [103] **(Figure 12)**. Further studies are needed to fully understand if just one of these two complexes is predominant in a given condition, if they may coexist, or they represent different steps of a unique translational repression pathway.

CPEB-mediated cytoplasmic polyadenylation and translational activation requires the presence of one consensus CPE, and the polyadenylation signal with an optimum distance of 25 nucleotides between them [88]. Progesterone stimulation and consequent meiosis resumption trigger to the activation of Aurora A kinase, that in turn activates CPEB by phosphorylation on Ser 174 (threonine 171/172 in mammals) [104,105]. The phosphorylation of

CPEB1 on Ser174 increases the affinity of the protein for CPSF and reduces the affinity for PARN that is excluded from the complex [100]. After phosphorylation by Cdc2 [90] or Aurora A [106], Maskin dissociates from eIF4E allowing the structured cap to get formed. In addition, embryonic Poly(A)-binding proteins (ePABP) bind both the newly polymerized poly(A) tail, and eIF4G with the formation of the pseudo-circularized mRNA [60,107,108]. The CPEB-CPSF-GLD-2 complex is further stabilized by Symplekin, the same scaffold protein found in cleavage and polyadenylation machinery.

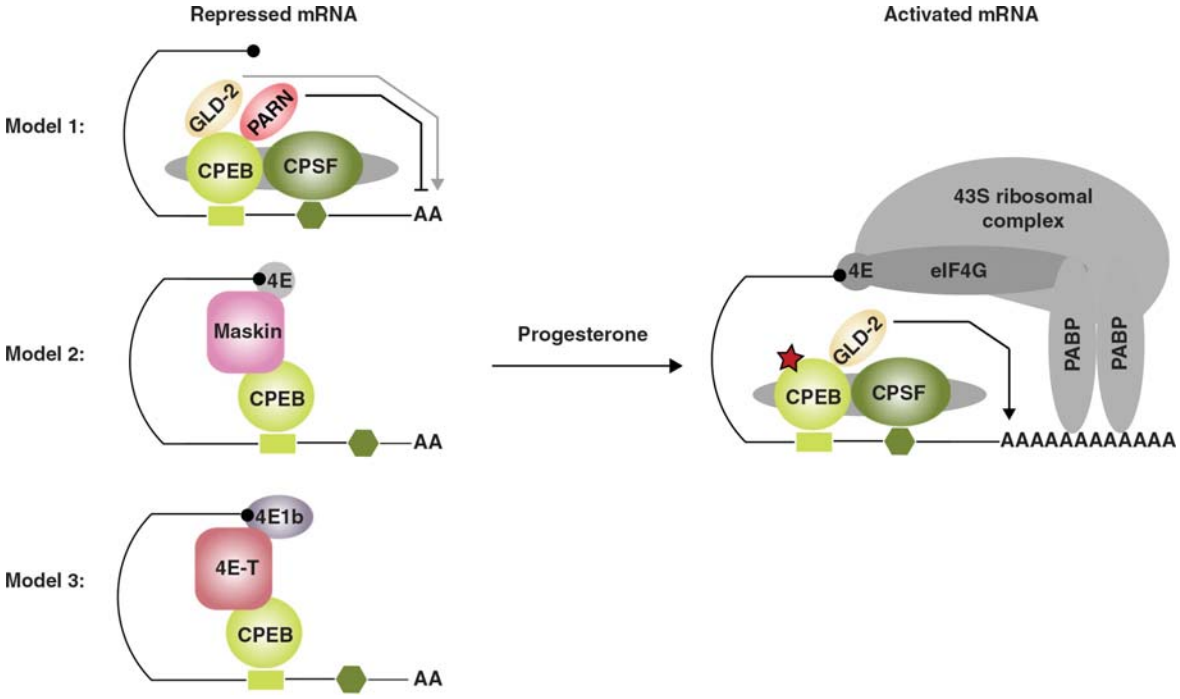

Figure 12. Models for CPE-mediated repression and cytoplasmic polyadenylation. The CPE and the Hex are indicated as a square and hexagon, respectively. Several models for CPEB-mediated repression in immature Xenopus oocytes have been described. Upon progesterone stimulation, CPEB is phosphorylated (red star) and polyadenylation is activated. The poly(A) tail recruits PABP, which establishes connections with the cap-binding complex for translation initiation.

4. CPEB in somatic cells

Although CPEBs were discovered and extensively studied in Xenopus Oocytes, last years of research in the field of cytoplasmic polyadenylation, focused also on the role of CPEB in

mammalian somatic cells. The four CPEBs are expressed in different tissues and show to have different functions:

mCPEB1 is highly expressed in brain and lowly in kidney, lung, hearth and oocytes [109,110]. It has been shown that CPEB1, in coordination with CPEB4, regulates phase-specific changes in the poly(A) tail length of hundreds mRNAs during the mitotic cell cycle of cancer-derived cells (HeLa). CPEB1 knockdown HeLa cells had a mitotic entry defect that leaded to block in G2 phase. This effect was even stronger in double CPEB1 and CPEB4 knockdown cells [111]. Another possible role of CPEB1 in non-germ cells mitosis derives from the observation of the protein at level of mitotic spindles, although it's not clear if it could play a role similar to which observed at spindles of Xenopus Oocytes [112].

mCPEB2 is abundantly expressed in testis and brain [113,114]; it has been proposed to mediate the repression of HIF-1α translation elongation, in hippocampal and cortical neurons [115].

mCPEB3 is strongly expressed in heart and brain where it has been proposed to have a role in episodic memory regulation [116];

mCPEB4 is expressed in brain, kidney, lung and heart [114]. It has been shown to have a function in the regulation of cancer progression [117].

Despite CPEBs were described to have a role in the regulation of cytoplasmic biological processes, as suggested by the name of the family (Cytoplasmic Polyadenyletion Element Binding protein), it has been recently reported their localization at nuclear level. CPEB1 is a nucleo-cytoplasmic shuttling protein that is blocked into the nucleus when the cells are treated with Leptomycin B [118]. CPEB1 KO MEFs show different splicing of the exon 34 of collagen 9a1, compared with WT MEFs, but it is not know if this effect is direct [119]. CPEB1 was recently found to regulate the nuclear 3'UTR formation of hundreds mRNAs, driving CPSF in the selection of proximal PAS [46]. CPEB3 was found moving to the nucleus and bind the transcription factor Stat5b in neurons, leading to the inhibition of Epidermal Growth Factor Receptor (EGFR) transcription [120]. CPEB4 was also described to move to the nucleus upon ischemia or endoplasmic reticulum calcium depletion, but its nuclear role is not known [121].

5. CPEB in angiogenesis and cancer

There are many evidences that allow us to claim CPEB1 and CPEB4 have a role in cell proliferation and senescence, suggesting a possible implication in cancer, and in related biological processes like angiogenesis.

In several tumors, such as breast and gastric cancer, colorectal cancer, and in myeloma cell lines, CPEB1 levels are decreased. In the specific case of gastric cancer, the promoter of CPEB1 is methylated, leading to reduction of gene transcription. Here, CPEB1 is supposed to repress the translation of mRNA encoding for proteins able to drive cancer progression, such HIF-1α, which induces the transcription of VEGF. Overexpression of CPEB1, in fact, results in decreased levels of VEGF [122].

The protein levels of the proto-oncogene myc are elevated two or three-fold in immortal CPEB1 KO MEFs, which have bypassed senescence, compared with immortal WT MEFs. In this model, CPEB1 represses the translation of myc mRNA [123].

CPEB1 controls the cytoplasmic polyadenylation of the tumor suppressor p53. In CPEB1 KD cells, p53 polyadenylation and translation are impaired with consequent reduction of protein production. Even though, immortal CPEB1 KO MEFs are not able to induce tumor formation when injected into mice. Surprisingly, when the same cells are transformed with Ras, before injection, bigger tumors appear, compared with WT MEFs transformed with Ras. CPEB1 depletion seams not to be able to promote tumor progression, but could somehow predispose to it [123,124].

As previously mentioned, CPEB4 is up regulated in Pancreatic Intraepithelial Neoplasia and in Pancreatic Ductal Adenocarcinoma (PDA), compared with healthy pancreas. In PDA, CPEB4 drives polyadenylation and translation of tissue plasminogen activator (tPA) mRNA. The depletion of CPEB4 in PDA cells resulted in reduced invasion *in vitro* and reduced tumor growth *in vivo*. Ectopic expression of tPA in CPEB4 knockdown cells, was able to recapitulate the tumoral phenotype after injection into mice.

OBJECTIVE

The aim of this study is to assess the role of CPEB1 and CPEB4 in angiogenesis, through the translational regulation of vascular endothelial growth factor (VEGF), and the contribution of these proteins to the vascular development in portal hypertension and hepatic cirrhosis.

RESULTS

CPEB1 and CPEB4 levels are increased in human cirrhotic liver

The histological characterization of healthy and cirrhotic human livers, by H&E staining, displayed pathological samples with diffuse fibrosis in the form of delicate bands and broad scars. These fibrotic formations, called "fibrous septa", presented a dense network of vascular ramifications that have been described to connect the vessels of the portal region with terminal hepatic veins, providing an alternative route of the blood flow along fibrous septa instead of through the acinar sinusoids, thus affecting the physiology of the hepatocytes. Fibrous septa replaced the normal lobular architecture and encompassed "regenerative nodules" which are formed through localized proliferation of hepatocytes and their entrapment by deposition of extracellular matrix **(Figure 13)**.

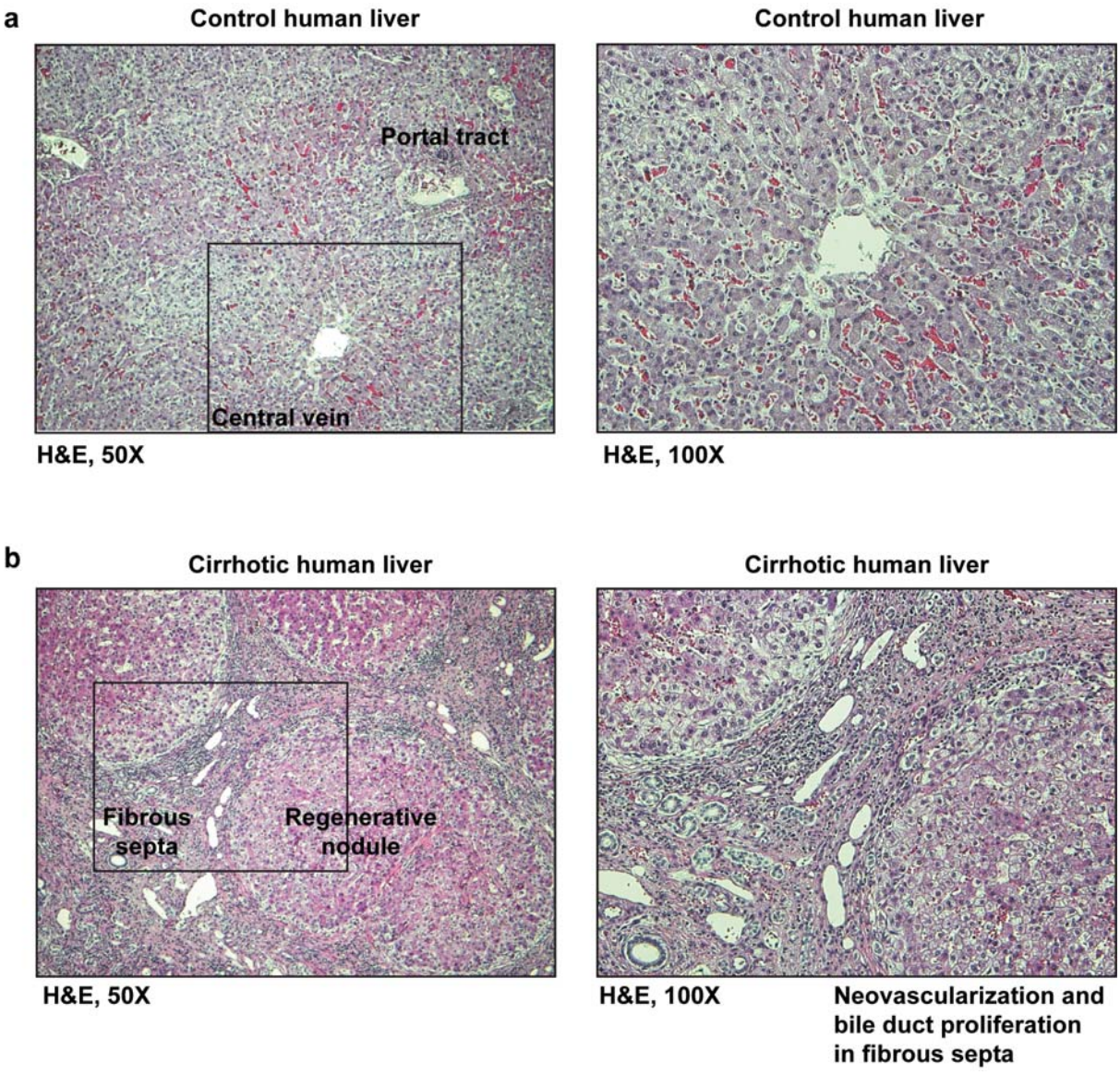

Figure 13. Histopathological characterization of human healthy and cirrhotic liver. Representative H&E staining of healthy and cirrhotic human livers. **a.** Parenchyma of a human healthy liver, with a portal tract and a central vein (left panel), and a higher magnification of the area defined by rectangle (right panel). It illustrates the arrangement of hepatocytes within the hepatic lobule, forming anastomosing plates between which sinusoidal blood passes to converge upon the central vein. **b.** In the left panel, micrographs of cirrhotic human liver displaying a robust disruption in architecture of the entire liver with loss of the normal central-portal relationships, and parenchymal nodules of regenerating hepatocytes surrounded by a dense scar of extracellular matrix (i.e., fibrous septa). Right panel shows a higher magnification of the area defined by rectangle in the left micrograph, focusing on the intense pathological neovasculature observed in fibrous septa (arrowheads). Scale bars: 200 µm for photographs a,b (left panels) and 100 µm for photographs a,b (right panels). **In collaboration with Mercedes Fernandez's group.**

Since hepatocytes of regenerative nodules have been described to produce angiogenic factors, such as VEGF, responsible of liver hyper-vascularization, we analyzed expression and localization of CPEB1, CPEB4 and VEGF in healthy and cirrhotic livers. Healthy hepatic parenchyma expressed basal levels of CPEB1, CPEB4 and VEGF **(Figure 14 a-c)**. In contrast, regenerative nodules of cirrhotic liver expressed increased levels of these proteins **(Figure 14 d-f)**. We also found that hepatocytes located at the interface between fibrous septa and liver parenchyma were highly positive for immunostaining of CPEBs and VEGF **(Figure 14 g-I, arrowheads)**. The localization of CPEBs correlated with areas markedly affected by neovascularization and, accordingly, with regions expressing high levels of VEGF **(Figure 14 j-l)**.

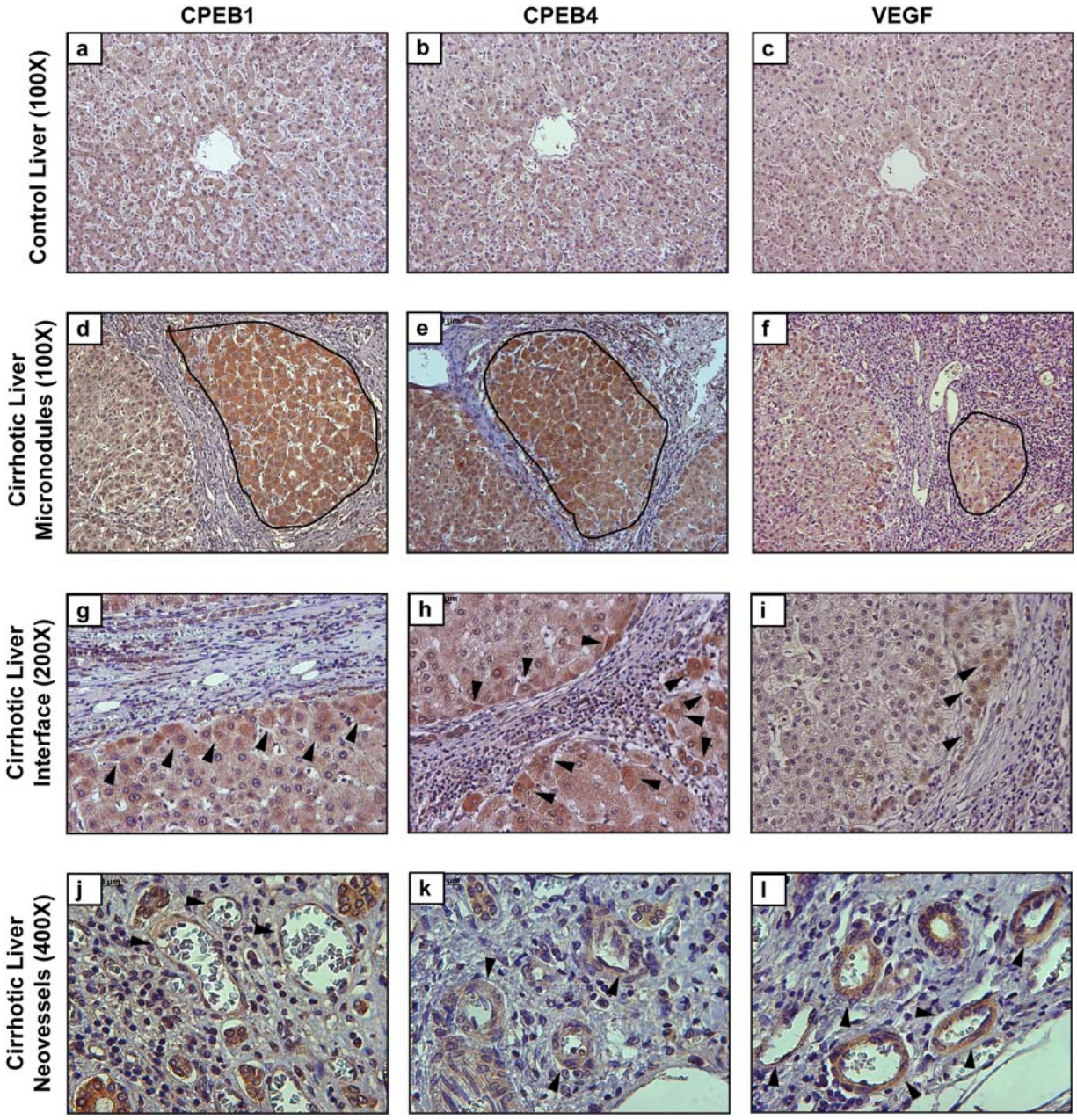

Figure 14. Expression of CPEB proteins in human cirrhotic liver. Representative photographs of CPEB1, CPEB4 and VEGF immunostainings in paraffin-embedded liver sections from healthy controls (n=5) and hepatitis C-related cirrhotic humans (n=12). Normal control liver specimens expressed low levels of CPEBs and VEGF, homogeneously distributed all over the hepatic parenchyma (**a-c**; scale bar: 100 µm). In cirrhotic liver specimens, CPEB1, CPEB4 and VEGF were strongly overexpressed, especially in hepatocytes within cirrhotic regenerative micronodules (**d-e**; arrowheads; scale bar: 100 µm), compared to normal liver. Arrowheads in photographs g-i point to cells with intense immunoreaction for CPEB1, CPEB4 and VEGF located at the interface between fibrous septa and liver parenchyma (**g-i**; scale bar 50 µm). The CPEB1, CPEB4 and VEGF immunostaining was also associated with the vascular wall of newly formed microvessels inside the fibrous septa (**j-l**; arrowheads; scale bar: 20 µm). These findings suggest a direct association of CPEBs proteins in the process of cirrhosis-mediated neovascularization. **In collaboration with Mercedes Fernandez's group.**

CPEB1 and CPEB4 expression correlates with VEGF-dependent intrahepatic angiogenesis

In order to confirm the interesting results obtained analyzing the correlation between histo-pathology of cirrhotic human liver and expression of CPEBs and VEGF, and with the aim of further investigate the role of CPEB1 and CPEB4 in the regulation of intrahepatic angiogenesis, we took advance of the secondary biliary cirrhosis model CBDL, developed in rats. Cirrhotic rat livers were characterized by high vascularization compared with control SHAM samples. Note that SHAM consisted in rats that underwent the surgical operation necessary to reach the common bile duct, without its ligation. The analysis of protein expression showed increased levels of CPEB1 and CPEB4 in CBDL condition. Interestingly, the levels of VEGF followed the trend shown by CPEB1 and CPEB4, revealing deep increase in protein expression after induction of hepatic cirrhosis. High VEGF protein levels were not generated in presence of increased amounts of mRNA, suggesting a post-transcriptional mechanism of regulation, possibly controlled by CPEB **(Figure 15)**.

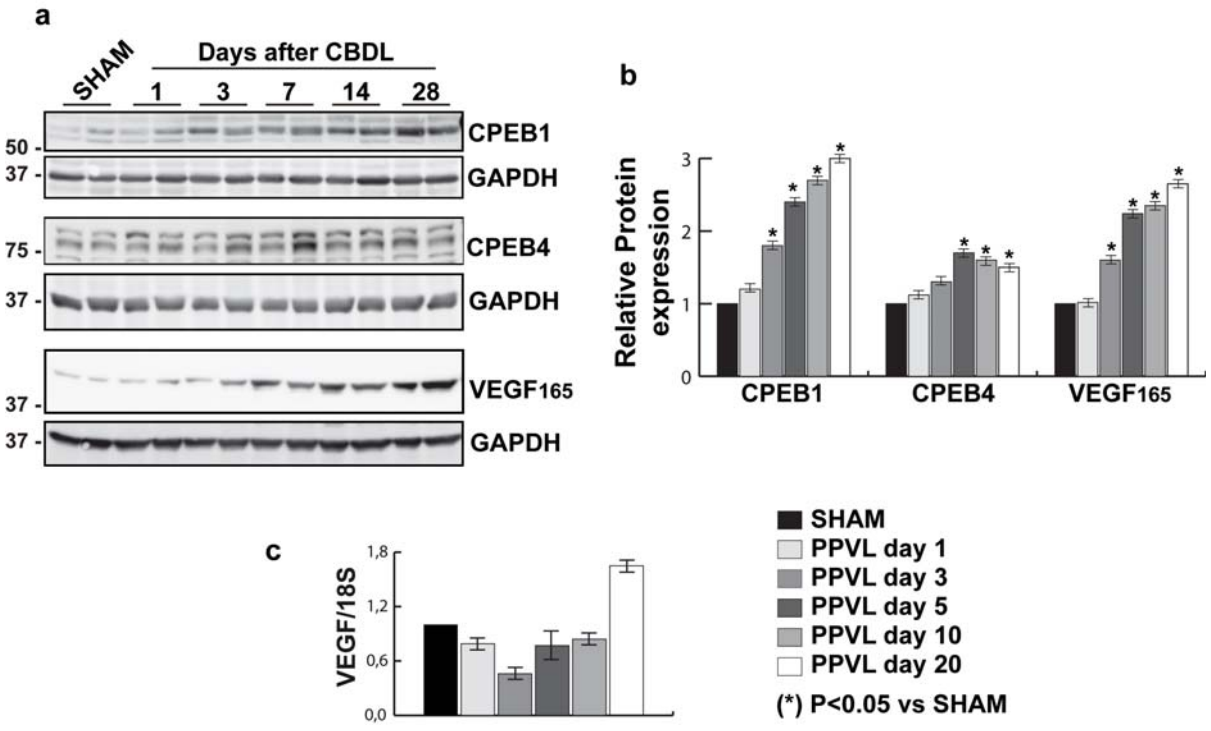

Figure 15. Expression of CPEB1, CPEB4 and VEGF proteins in rat cirrhotic liver. a. Western blotting of CPEB1, CPEB4 and $VEGF_{165}$ in the rat liver at different time points after inducing cirrhosis by common bile duct ligation (BDL) and in the liver from sham-operated control rats (SHAM). GAPDH is used as a loading control. **b.** Densitometric quantification of protein

expression relative to GADPH. Results are expressed as mean±S.E.M. *P<0.05 versus control rats. **(c)** Quantification of relative VEGF mRNA expression by RT-PCR showing that, at least at the initial stages of angiogenesis, VEGF overexpression in the cirrhotic liver did not correlate with parallel changes in VEGF mRNA. In advanced disease, at day 28 after BDL, both VEGF protein and mRNA were elevated. These results suggest that VEGF overexpression in cirrhotic rat liver is regulated at a post-transcriptional level during the first stages of the disease, but later on, in advanced cirrhosis, both transcriptional and post-transcriptional mechanisms may coordinately regulate VEGF expression. Results are expressed as mean±S.E.M. **In collaboration with Mercedes Fernandez's group.**

CPEB1, CPEB4 and VEGF localized at level of newly formed blood vessels that vascularized the cirrhotic liver **(Figure 16)**.

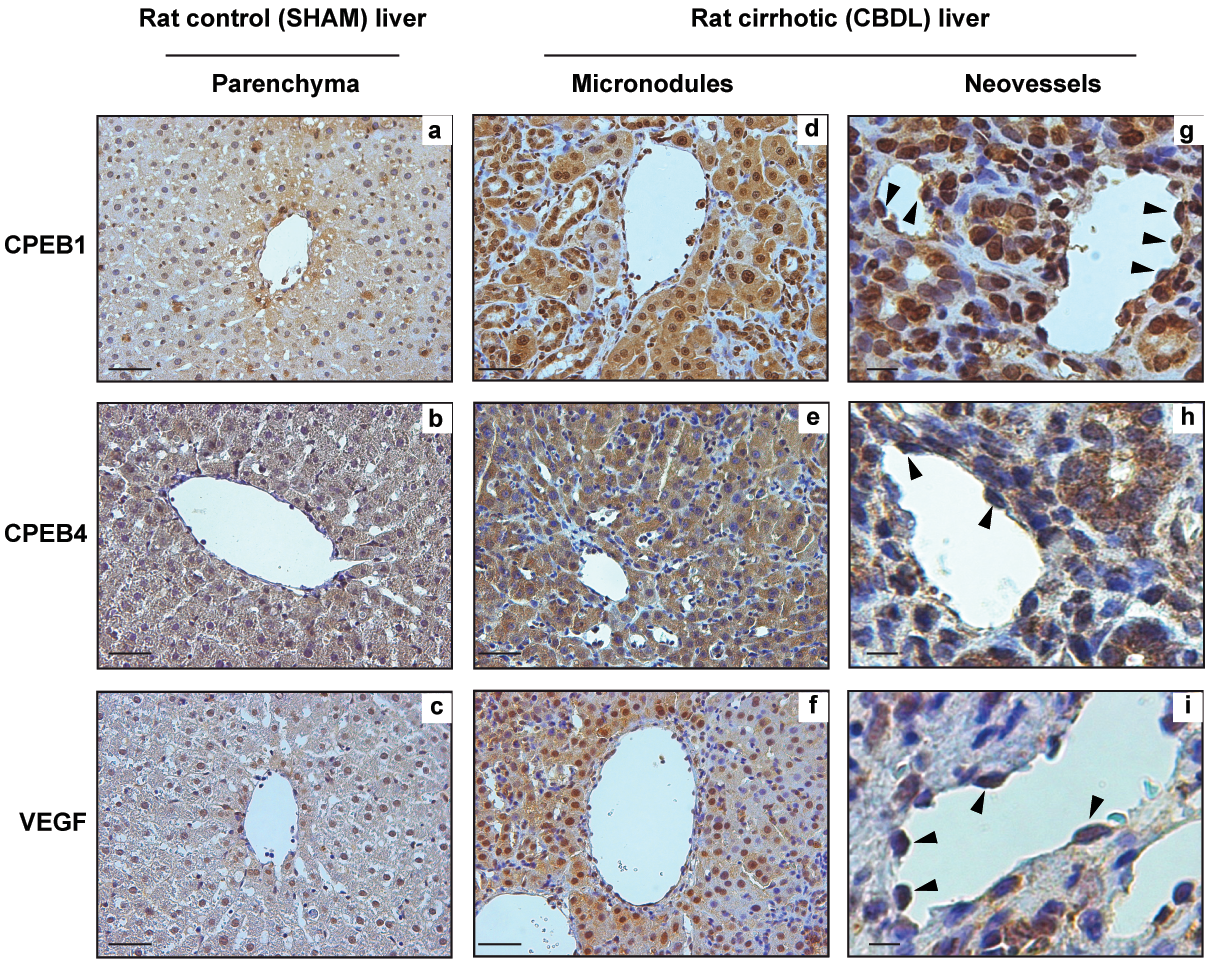

Figure 16. Localization of CPEB1, CPEB4 and VEGF proteins in rat cirrhotic liver. CPEB1, CPEB4 and VEGF immunohistochemistry in rat control (SHAM) liver and in liver from cirrhotic rats at day 28 after BDL. Micrographs **a-c** show the normal liver parenchyma, with plates of hepatocytes radially disposed in the hepatic lobule surrounding a central vein (scale bar: 50 µm). In the cirrhotic liver (**d-f**), numerous rounded micronodules of regenerating hepatocytes are detected, which strongly express CPEB1, CPEB4 and VEGF proteins.

Micrographs **g-i** illustrate new blood microvessels formed in the liver in response to cirrhosis induction, demonstrating expression of CPEB1, CPEB4 and VEGF in the endothelium of newly formed vessels (arrowheads; scale bar: 20 μm). **In collaboration with Mercedes Fernandez's group.**

CPEB1 and CPEB4 expression correlates with VEGF 3'UTR processing in portal hypertension

To investigate the function of CPEB1 and CPEB4 in the regulation of pre-hepatic angiogenesis, characteristic of liver cirrhosis and portal hypertension, we used PPVL model developed in rats. In PPVL rats, the ligation of the portal vein caused extensive increase of vasculature of the mesentery compared with control SHAM condition. The low levels of CPEB1 detected in SHAM rats strongly increased as consequence of the angiogenic induction. Moreover, in PPVL mesentery, CPEB1 was present in its activated form (P-CPEB1). Synthesis and phosphorylation of CPEB1 correlated with CPEB4 production and deep increase in $VEGF_{165}$ and $VEGF_{188}$ expression **(Figure 17 a,b)**, which was not due to changes of mRNA levels **(Figure 17 c)**. Increase of CPEB1-4 and VEGF was transient, as the levels of these proteins started to decline at days 10-20 after PPVL, when neovessels reached full maturation **(Figure 17 a)**.

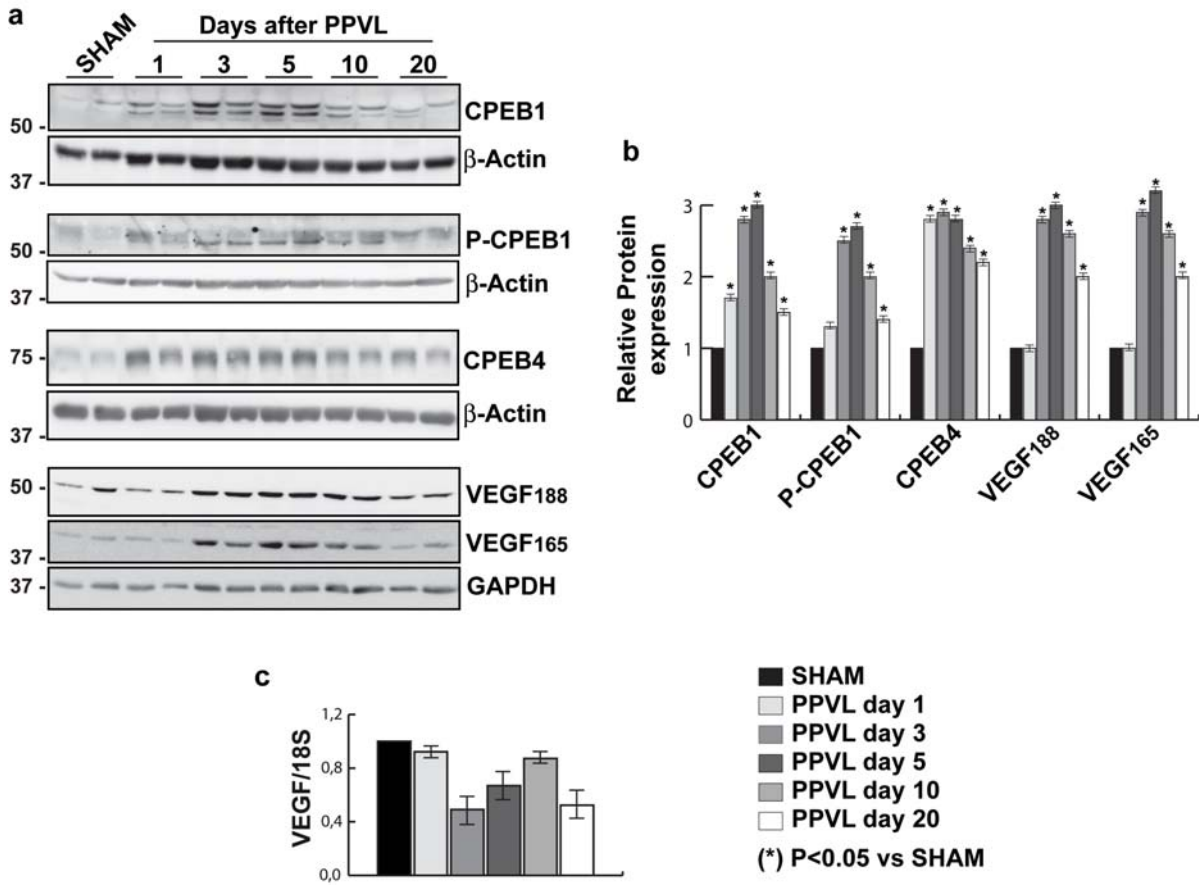

Figure 17. Expression of CPEB and VEGF proteins in portal hypertension-induced mesenteric angiogenesis in rats. a. Western blotting of CPEB proteins and the proangiogenic growth factor VEGF in the mesentery at different time points after inducing portal hypertension by partial portal vein ligation (PPVL) and in sham-operated control rats (SHAM). β-Actin and GAPDH are used as loading controls. **b.** Densitometric quantification of protein expression. Data are mean±S.E.M. **P*<0.05 versus control rats. **c.** Quantification of relative VEGF mRNA expression by RT-PCR showing that the increases in mesenteric VEGF protein observed during progression of portal hypertension did not correlate with parallel changes in VEGF mRNA, indicating that VEGF is not transcriptionally regulated. Results are expressed as mean±S.E.M. **In collaboration with Mercedes Fernandez's group.**

In comparison with control rats **(Figure 18 A-D)**, CPEB1, phospho-CPEB1, CPEB4 and VEGF were overexpressed in the vascular wall of preexisting mesenteric vessels in response to portal hypertension, particularly at the endothelium and peripheral adventitia, where active vessel growing occurs **(Figure 18 E-H)**.

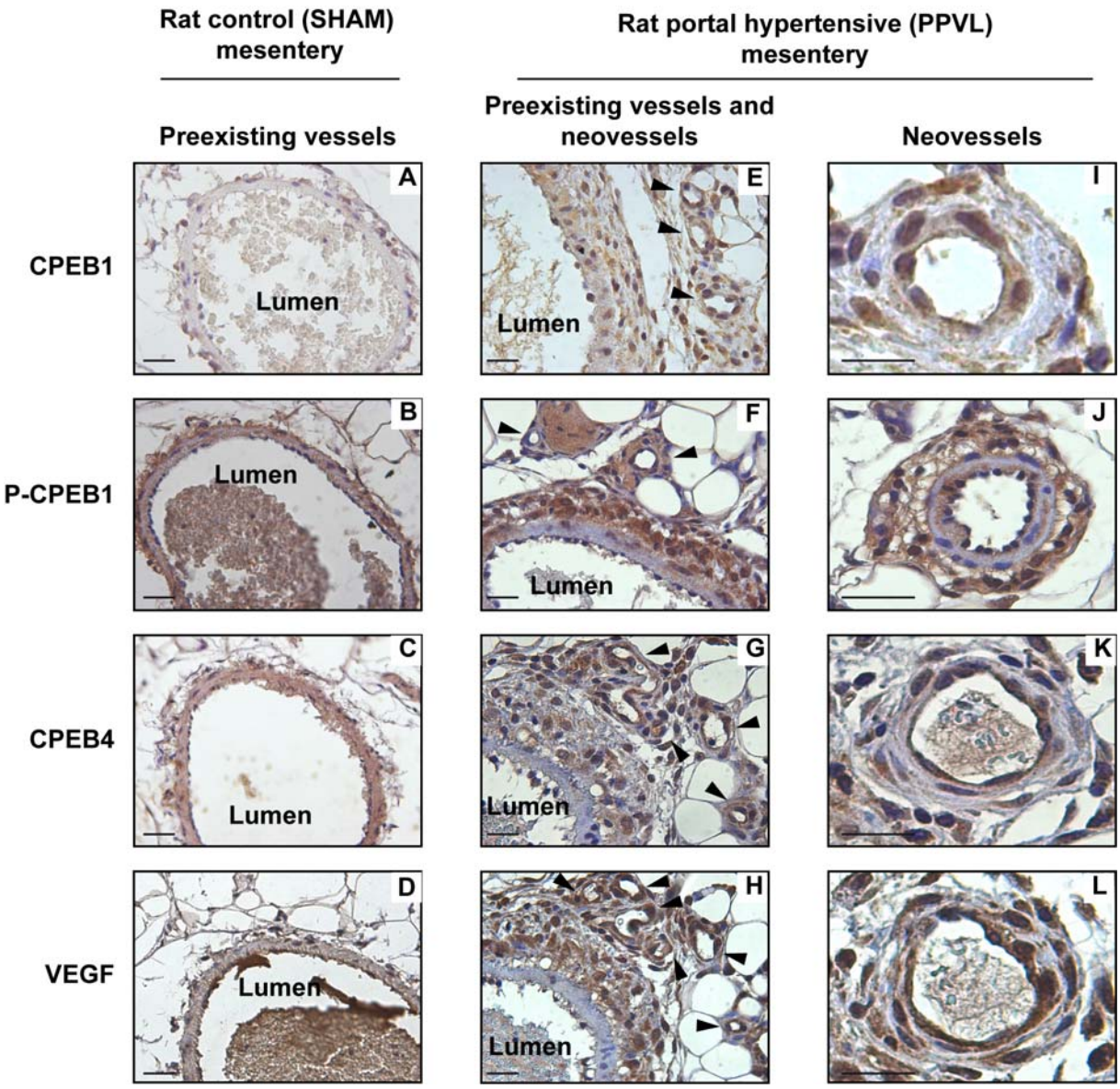

Figure 18. Localization of CPEB and VEGF proteins in portal hypertension-induced mesenteric angiogenesis in rats. Representative photomicrographs from immunohistochemical analyses in mesenteric sections from portal hypertensive rats (PPVL), showing overexpression of CPEB proteins and VEGF in the vascular wall of pre-existing mesenteric vessels (**E-H**), compared with control rats (SHAM) (**A-D**), as well as in the vascular wall of newly-formed mesenteric vessels (**I-L**). Scale bar: 20 µm. **In collaboration with Mercedes Fernandez's group.**

Co-localization of all CPEB proteins and VEGF was also observed in the vascular wall of newly formed mesenteric microvessels, as ascertained by immunohistochemistry and double-immunofluorescence **(Figure 18 I-L and Figure 19)**. These neo-vessels were indeed functional as shown by their vascular integrity and the presence of erythrocytes into their lumina

(Figure 18 I-L). Our findings, therefore, are rather consistent in different experimental models of cirrhosis and portal hypertension (i.e., bile duct ligation and portal vein stenosis), in two distinct scenarios of ongoing pathological angiogenesis (i.e., liver and mesenteric vascular bed), and in either rodent or human samples. In all cases, we observed a clear correlation between CPEB1 and 4 expression and VEGF synthesis in neovasculature, without changes in VEGF mRNA levels, thus suggesting a possible role of CPEB1 and CPEB4 in the posttranscriptional regulation of VEGF expression.

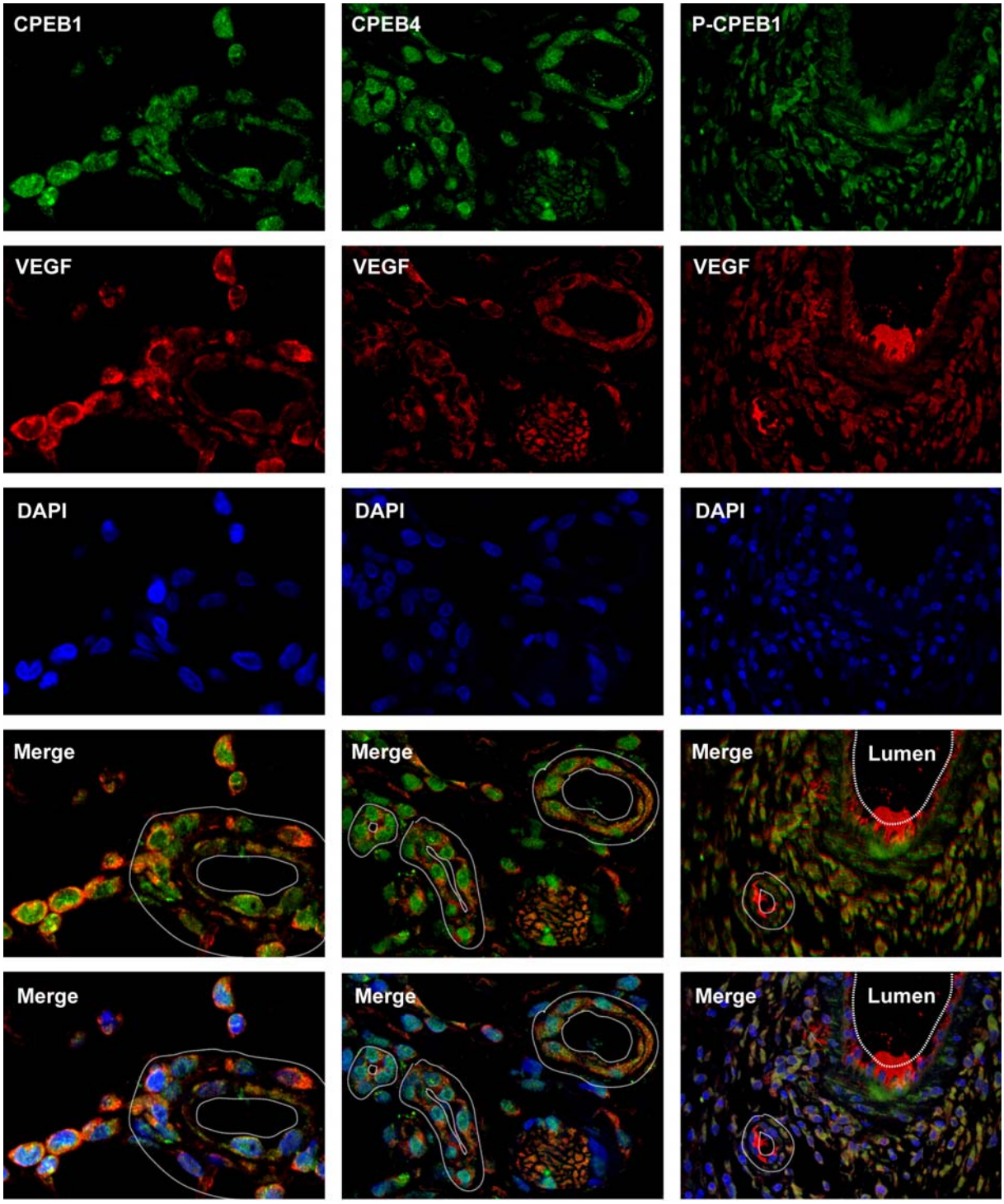

Figure 19. Expression of CPEB1, CPEB4 and VEGF in newly formed mesenteric vessels of portal hypertensive rats. Double-immunofluorescence and confocal microscopy showing cells double-expressing CPEB1 or CPEB4 proteins (green) and VEGF (red) in the vascular wall of newly formed vessels in the mesenteric vascular bed of portal hypertensive rats. Cell nuclei were visualized by Dapi (blue). Photographs at the bottom show the merge of CPEB1 or CPEB4 proteins with VEGF immunostainings, and the merge of CPEB1 or CPEB4 proteins with VEGF and DAPI stainings. These neovessels were indeed functional as shown by the lumen and vascular integrity, comprised of an endothelial layer stabilized by the presence of a supporting smooth muscle cell coverage (pericytes). Scale bar: 25 μm. **In collaboration with Mercedes Fernandez's group.**

To investigate the mechanism that could be regulating VEGF expression *in vivo*, we first analyzed VEGF mRNA processing and polyadenylation changes in mesentery upon portal hypertension induction, using as a control the intestinal mucosa, which is unaffected by VEGF changes during disease progression **(Supplementary Fig. 1)**. VEGF mRNA was indeed coimmunoprecipitated with CPEB1 in mesenteric samples of portal hypertensive rats **(Figure 20 a)**, but not in samples of intestinal mucosa, in which CPEB1 was not readily detectable **(Supplementary Figure 1 and data not shown)**. In intestinal mucosa, neither CPEB1, CPEB4 nor VEGF were overexpressed after PPVL **(Supplementary Fig. 1)**. Moreover, portal hypertension induction resulted in the preferential use of PAS1 over PAS2, generating the shorter VEGF 3'UTR variant, and the elongation of the poly(A) tail in mesentery, but not in intestinal mucosa **(Figure 20 b-d)**. These results show a good correlation between the VEGF 3´ end variants (both 3´UTR selection and polyadenylation state) detected in angiogenic mesentery in response to portal hypertension **(Figure 20 c,d)** and the pattern of CPEBs overexpression during portal hypertension **(Figure 18)** and cirrhosis **(Figure 14 and 16)**.

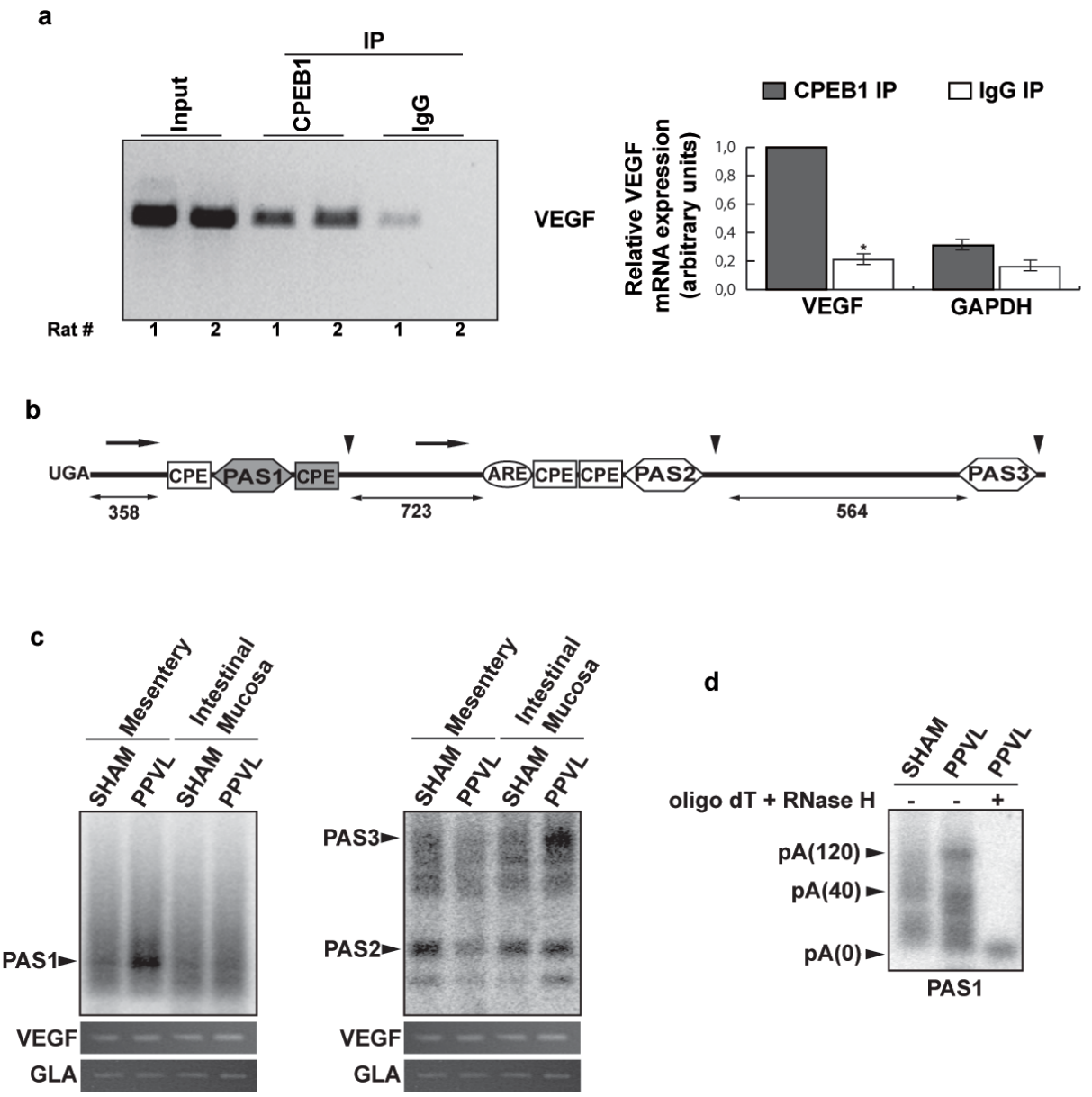

Figure 20. Rat VEGF 3'UTR processing. a. Semiquantitative (left panel) and quantitative (right panel) PCRs of VEGF performed using reversed transcribed immunoprecipitated mRNAs from rat PPVL mesentery extracts. GAPDH was used as a control. Quantitative RT-PCR showed a significant enrichment of VEGF mRNA in the anti-CPEB1 immunoprecipitate compared with the pre-immune IgG immunoprecipitate. **P*=0.03. **b.** Representation of rat VEGF 3'UTR. CPE (Cytoplasmic Polyadenylation Elements) and PAS (Poly Adenylation Signal) are indicated in white polygons (consensus sequences) or grey polygons (not consensus sequences). AU-rich elements (ARE) are also shown. Single headed arrows indicate the position of the primers used for 3'RACE analysis. Double headed arrows indicate the distance between different regulatory elements. PAS1 indicates proximal Poly Adenylation Signal while PAS2 and PAS3 indicate distal Poly Adenylation Signals. **c.** VEGF 3'UTR cleavage analysis performed by 3'RACE/southern blot in rat mesentery (in which VEGF is overexpressed during portal hypertension) and intestinal mucosa (in which VEGF expression is unaffected during portal hypertension progression), both in SHAM (control) and PPVL

conditions. Semiquantitative PCR of VEGF and GLA were used as control of total VEGF mRNA and general gene expressions of the cells. **d.** Polyadenylation analysis of short (PAS1) VEGF 3'UTR performed in SHAM and PPVL conditions of rat Mesentery. Poly(A) tail length is indicated. **In collaboration with Mercedes Fernandez's group.**

H5V cell line, a suitable model to study VEGF-dependent *in vitro* angiogenesis

To better define the mechanistic relevance of the correlation between CPEB expression and VEGF mRNA 3'UTR processing described in human cirrhotic liver, CBDL and PPVL models, we characterized the murine transformed endothelial cell line H5V [125]. Consistently with what found in human cirrhotic liver, in H5V cells CPEB1 had both nuclear and cytoplasmic localization, while CPEB4 was found in the cytoplasm only **(Figure 21)**.

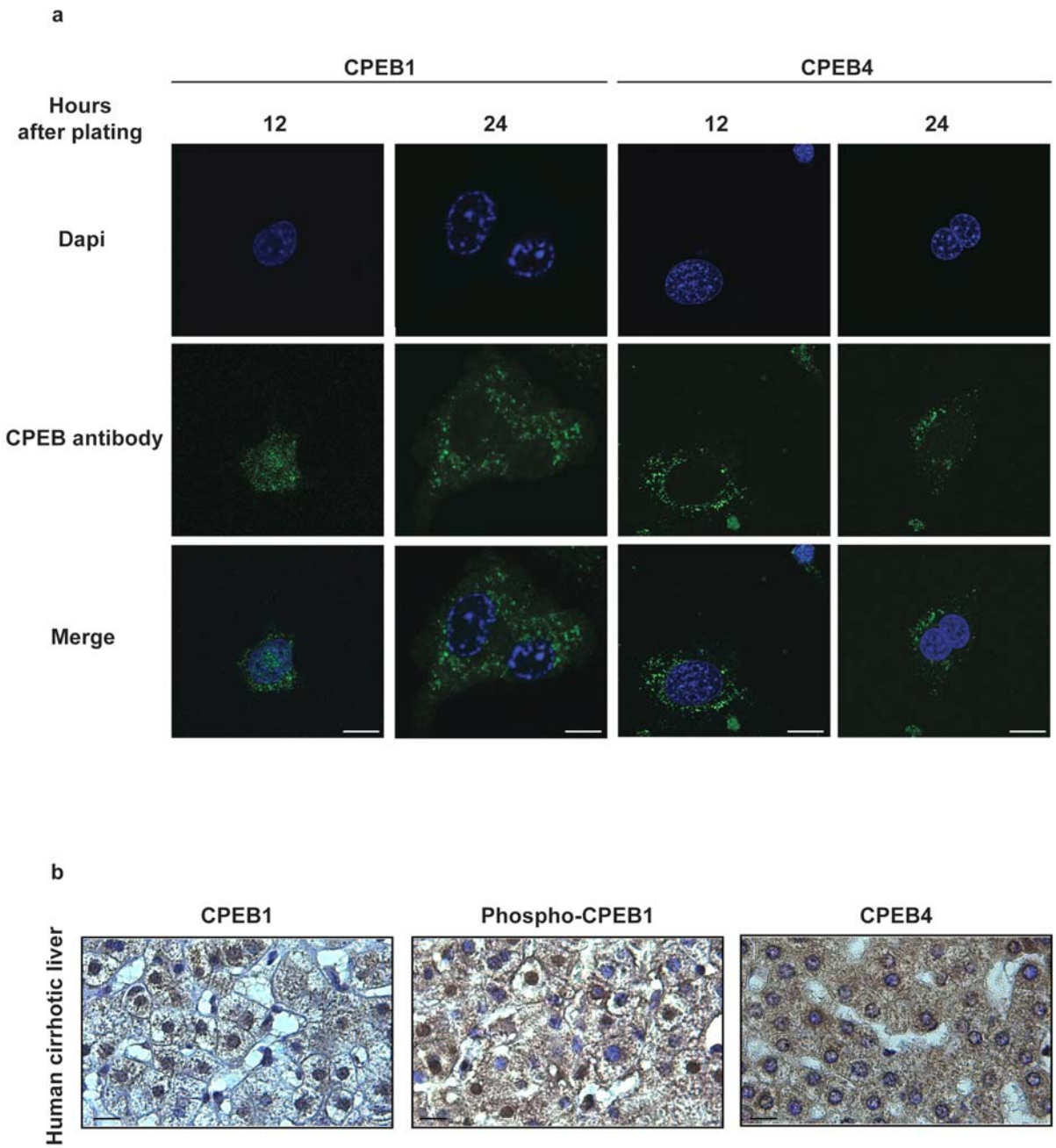

Figure 21. CPEB1 is a nucleocytoplasmic shuttling protein while CPEB4 localizes at cytoplasm. a. CPEB1 and CPEB4 immunofluorescence in H5V cells, 12 and 24 hour after plating. DNA staining (Dapi) in blue, CPEB1 or CPEB4 in green, and the merged signal are shown. CPEB1 shows both nuclear and cytoplasmic localization while CPEB4 is present only in the cytoplasm of the cells. Scale bar: 10 µm. **b.** Immunohistochemistry for CPEB1, phospho-CPEB1 and CPEB4 in human cirrhotic liver showing that CPEB1 and phospho-CPEB1 were present both in nuclear and cytoplasmic granules of hepatocytes, whereas CPEB4 localization was restricted to the cytoplasm. Scale bar: 20 µm. **In collaboration with Mercedes Fernandez's group.**

Moreover, H5V cells resulted to be a good model for studies of *in vitro* angiogenesis due to their ability to proliferate in plastic plates in presence of culture medium just supplemented with FBS (fetal bovine serum) and glutamine, and capacity to form blood vessel like structures when seeded in matrigel pre-coated plates [126] **(Figure 22)**.

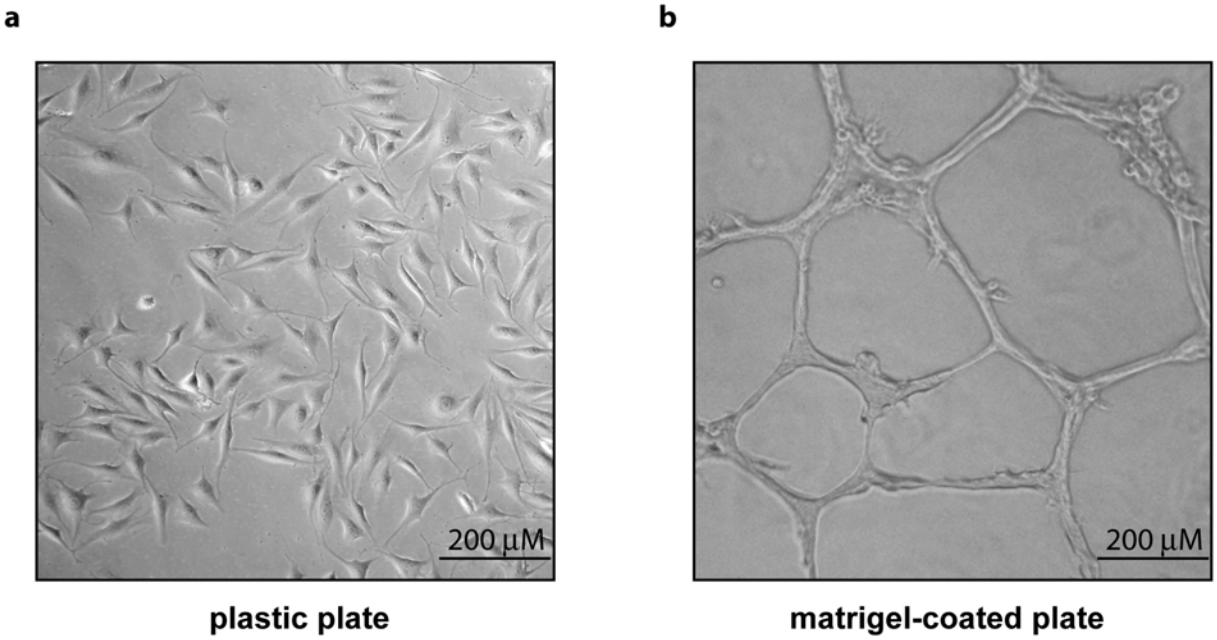

Figure 22. H5V cells. **a.** H5V cells cultured in plastic plate. **b.** *in vitro* angiogenesis assay performed using H5V cells and matrigel pre-coated plate.

CPEB1 and CPEB4 are required for *in vitro* angiogenesis

To investigate whether CPEB1 and CPEB4 have a role in the regulation of *in vitro* angiogenesis, through translational regulation of VEGF mRNA, we generated two H5V-derived cell lines expressing inducible shRNAs to target CPEB1 or CPEB4 mRNAs. In absence of CPEB1, we observed deep reduction of CPEB4 protein expression, a result that supports our previous data according to which CPEB1 drives CPEB4 mRNA processing and protein synthesis during meiosis. In addition to that, also VEGF protein levels were strongly reduced suggesting a cue of CPEB-mediated translational control of VEGF mRNA **(Figure 23 a)**. Quantitative PCR analysis revealed that the depletion of CPEB1 caused weak reduction of CPEB4 mRNA levels, which may partially explain the decrease of CPEB4 protein. For what concern VEGF, no variation of mRNA levels were detected in CPEB1 knockdown cells, pointing out that the reduction of the protein could not be attributed to changes in gene transcription and/or mRNA stability but had to be due to some alteration of the mechanism that governs VEGF gene expression at post-transcriptional level **(Figure 23 b)**. To further study the biological significance of CPEB1 depletion in H5V cells, we performed *in vitro* angiogenesis assay using growth factor reduced (GFR) matrigel pre-coated plates. Interestingly, CPEB1 knockdown cells were not able to form blood vessel like structures compared with control non-transfected or non-induced cells. To prove that the phenotype was due to the reduction of VEGF, the angiogenesis assay was performed incubating the cells in presence of culture medium conditioned by wild type H5V cells (thus supposed to be enriched with secreted angiogenic factors, VEGF included), or synthetic VEGF. Both conditioned medium and synthetic VEGF were able to rescue the angiogenic ability of CPEB1 knockdown cells **(Figure 23 c)**. To test if our strategy of targeting CPEB1 by expression of shRNAs was specific we generated another H5V-derived cell line, expressing a different shRNA which gave similar results **(Supplementary figure 2)**.

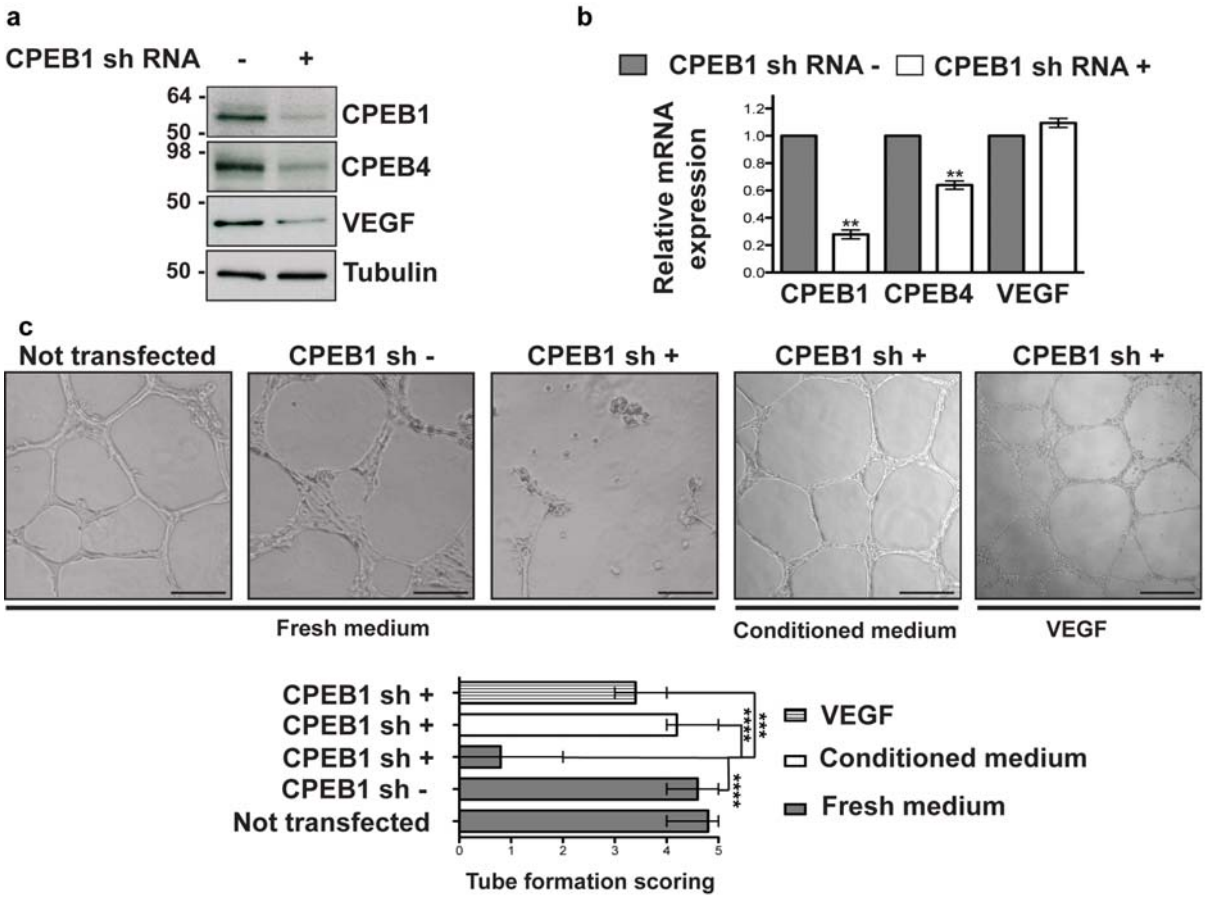

Figure 23. *In Vitro* characterization of the effects of CPEB1 depletion in H5V cells. The expression of CPEB1 shRNAs was induced treating the cells with IPTG, as described in "Materials and Methods". **a.** CPEB1, CPEB4 and VEGF protein concentrations in CPEB1 knockdown and control cells, analyzed by western blot. Tubulin is used as loading control. The results of a representative experiment (n=3) are shown. **b.** Relative CPEB1, CPEB4 and VEGF mRNA expression levels in CPEB1 knockdown and control cells. Data are mean ± S.D. *P* values (obtained by Student Test) are relative to not induced cells. ***P*≤ 0.005. Values correspond to three independent experiments. **c.** *In vitro* angiogenesis assay (top) and its quantification (bottom) performed seeding H5V cells on GFR (Grow Factor Reduced) Matrigel-coated dishes. Not transfected cells and not induced cells were used as control. Tube formation scoring was performed as described in "Materials and Methods". The results are representative of five independent experiments. Data are mean ± range. *P* values (obtained by Student Test) are relative to not induced cells. ****P*≤ 0.0005, *****P*≤ 0.00005. Scale bar 200 μm. VEGF concentration: 30 ng/ml.

As expected the depletion of CPEB4 by expression of shRNAs caused similar effects. In fact, in absence of CPEB4, deep reduction of VEGF protein, but not mRNA, was observed **(Figure 24 a,b)**, with consequent loss of *in vitro* angiogenic capacity of H5V cells. Also in this case, VEGF decrease was the cause of the severe phenotype as underlined by treatment with conditioned medium and synthetic VEGF **(Figure 24 c)**.

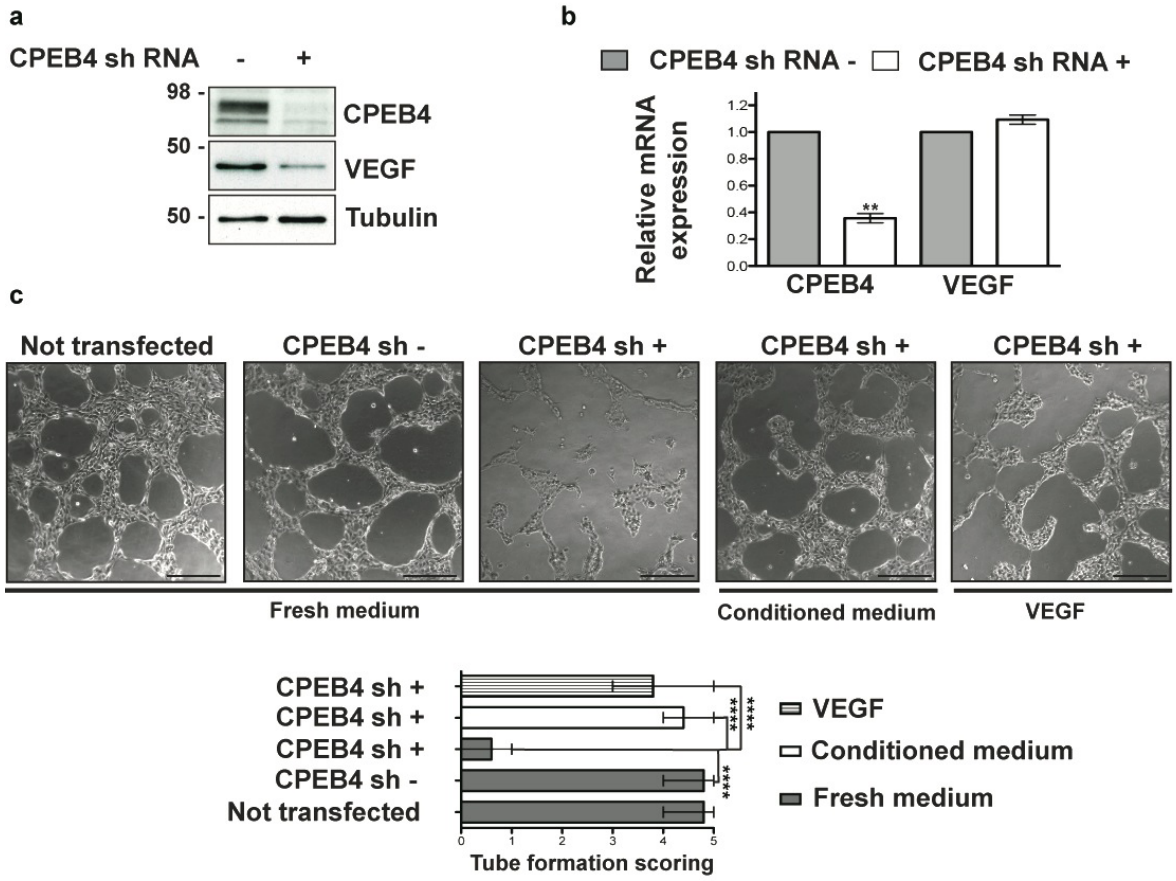

Figure 24. *In Vitro* characterization of the effects of CPEB1 depletion in H5V cells. **a.** CPEB4 and VEGF protein concentrations in CPEB4 knockdown and control cells, analyzed by western blot. Tubulin is used as loading control. The results of a representative experiment (n=3) are shown. **b.** Relative CPEB4 and VEGF mRNA expression levels in CPEB4 knockdown and control cells. Data are mean ± S.D. *P* values (obtained by Student Test) are relative to not induced cells. ***P*≤ 0.005. Values correspond to three independent experiments. **c.** *In vitro* angiogenesis assay (top) and its quantification (bottom) performed seeding H5V cells on GFR (Grow Factor Reduced) Matrigel-coated dishes. Not transfected cells and not induced cells were used as control. Tube formation scoring was performed as described in "Materials and Methods". The results are representative of five independent experiments. Data are mean ± range. *P* values (obtained by Student Test) are relative to not induced cells. *****P*≤ 0.00005. Scale bar 400 μm. VEGF concentration: 30 ng/ml.

In order to confirm the involvement of CPEB4 in the regulation of VEGF mRNA translation during angiogenesis, we transfected CPEB4 knockdown cells with a vector triggering the coding domain sequence of CPEB4. The sequence of the shRNA binding site of ectopic CPEB4 was mutated in order to attenuate the efficacy of the shRNA. As expected, expression of mutated CPEB4 mitigated the reduction of VEGF protein in CPEB4 knockdown **(Figure 25 a)**

and permitted to prevent the negative effects that the depletion of endogenous CPEB4 had had on the angiogenic ability of the cells **(Figure 25 b)**.

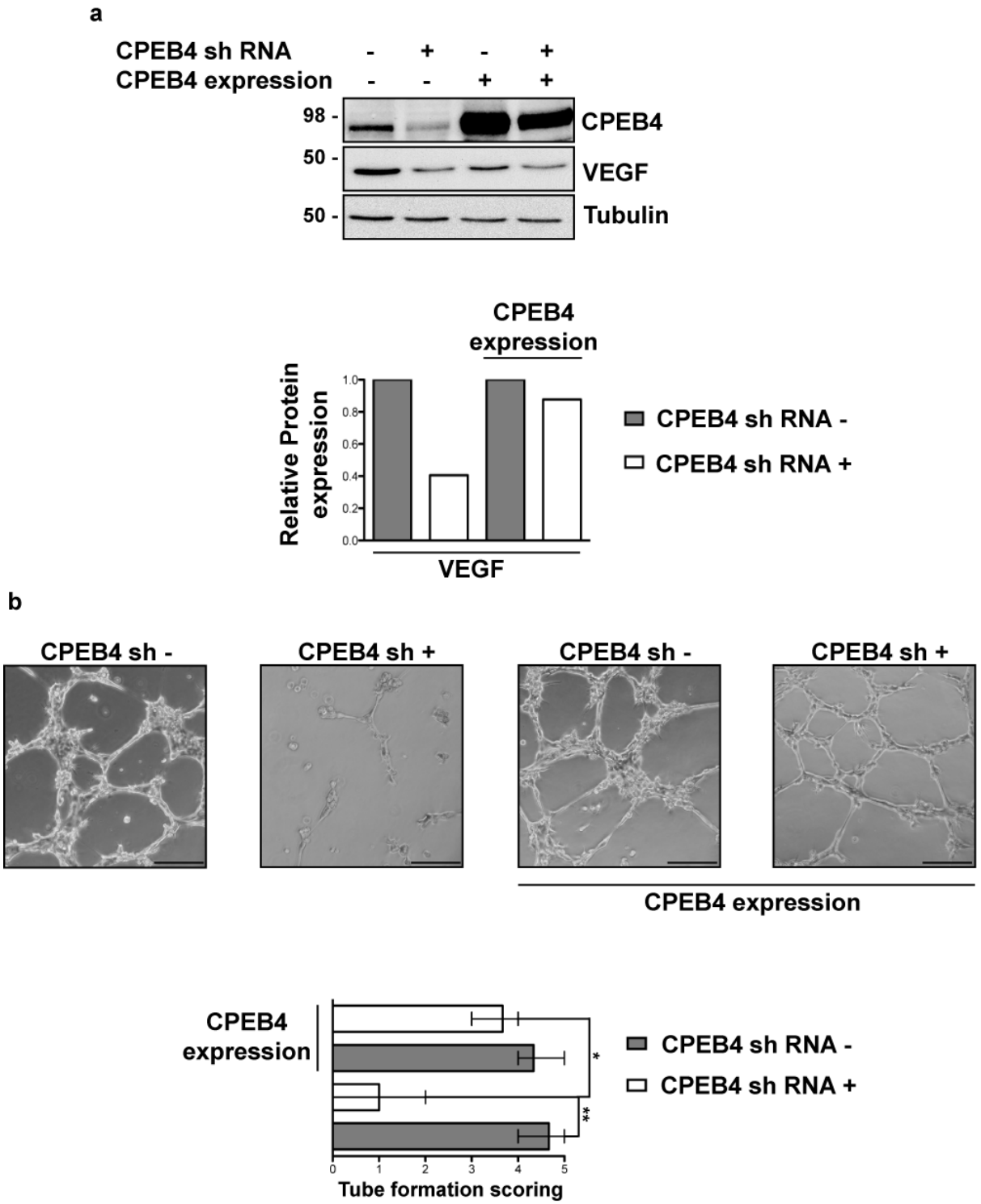

Figure 25. *In Vitro* characterization of the effects of mutated-CPEB4 expression in CPEB4 knockdown H5V cells. a. CPEB4 and VEGF protein expression (top) and relative quantification (bottom) in control and CPEB4 knockdown H5V cells. Tubulin was used as

loading control. **b.** *In vitro* angiogenesis assay (top) and its quantification (bottom) performed seeding H5V cells on GFR (Grow Factor Reduced) Matrigel-coated dishes. Not induced cells were used as control. Tube formation scoring was performed as described in "Materials and Methods". The results are representative of three independent experiments. Data are mean ± range. *P* values (obtained by Student Test) are relative to not induced cells. **P*≤ 0.05, ***P*≤ 0.005. Scale bar 200 μm

CPEB1 and CPEB4 directly interact with VEGF mRNA

After the characterization of the effects that CPEB1 and CPEB4 depletion had on VEGF production and in vitro angiogenic capability of H5V cells, we addressed the hypothesis that CPEB1 and CPEB4 directly interacted with the 3'UTR of VEGF mRNA. First of all, we proved to be able to specifically immunoprecipitate CPEB1 and CPEB4 by IP-western blot. Then, we proceeded with the immunoprecipitation of ribonucleoprotein (RNP) complexes containing CPEB1 or CPEB4, and the characterization of their ribonucleic composition. Both CPEB1 and CPEB4 were found to specifically interact with VEGF and CPEB4 mRNAs **(Figure 26)**.

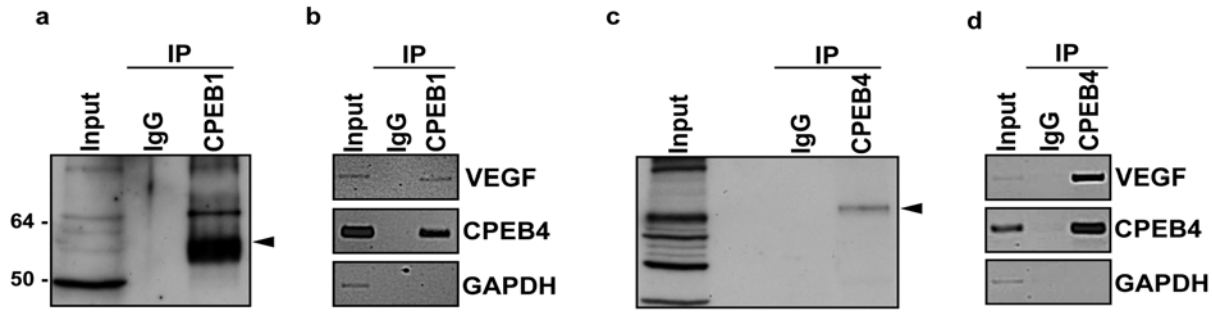

Figure 26. CPEB1 and CPEB interaction with VEGF mRNA a,c. CPEB1 and CPEB4 Immunoprecipitation analyzed by western blot. IgGs were used to show the specificity of CPEB1 and CPEB4 antibodies. **b,d.** Semiquantitative PCR of VEGF and CPEB4 performed using reversed transcribed immunoprecipitated mRNAs. GAPDH was used as control.

CPEB1 and CPEB4 regulate VEGF 3'UTR processing in H5V cells

The presence of CPEB1 and CPEB4 bound to VEGF mRNA, and the consequences that the depletion of these two proteins had on molecular and cellular biology of H5V cells induced us to further investigate on the function of CPEB1 and CPEB4 in the regulation of VEGF 3'UTR

processing. In addition to the very well understood role of both CPEB1 and CPEB4 in the regulation of cytoplasmic polyadenylation in somatic and germ cells, *A. Bava* and collaborators recently described CPEB1 involved in alternative 3'UTR formation of CPE-containing mRNAs [46]. For this reason, we studied the role of CPEB1 in APA of VEGF mRNA, which results in three possible 3'UTRs, generated by use of three different PAS. Note that PAS1 is a not consensus, "weak" polyadenylation signal, since its sequence UAUAAA differs from the canonical AUUAAA, while PAS2 is a consensus, "strong" polyadenylation signal **(Figure 27 a)**. To confirm VEGF alternative 3'UTR regulation mediated by CPEB1 and to evaluate possible changes in PAS selection, we analyze the different 3'UTRs generated in control non-induced H5V cells or after CPEB1 knockdown. For this purpose, total RNA from both conditions was extracted, and VEGF 3'UTRs were amplified by 3'RACE. The resulting PCR products were then resolved by electrophoresis and visualized by Southern blot (more technical details are available in Materials and Methods). In control H5V cells, CPEB1 increased the affinity of the nuclear cleavage machinery for the "weak" polyadenylation signal PAS1, thus preferentially used for VEGF 3'UTR processing. An important consideration is that, in wild type condition, the 3'UTR of VEGF was cleaved at level of PAS1 even if the "strong" PAS2 could be used also. A possible explanation of the PAS1 choice is that the alternative polyadenylation process takes place co-transcriptionally. The cleavage machinery components, bound to the C-terminal domain of Pol II were loaded on PAS1 and the neighbor CPE as soon as the first portion of VEGF 3'UTR was transcribed. The result of the cleavage complex activity was the generation of VEGF transcript with short 3'UTR. In CPEB1 knockdown H5V, the "weak" PAS1 was not able, alone, to recruit the cleavage machinery that was therefore loaded at level of the stronger and downstream PAS2, with consequent formation of VEGF transcript with a longer 3'UTR. Thus, CPEB1 depletion had important effects on VEGF 3'UTR processing inducing a switch from short to long 3'UTR **(Figure 27 b, left panel)**. VEGF 3'UTR generated using PAS3 was never detected. The amplification of constitutive VEGF and GLA exons, by PCR, allowed us to show that CPEB1 depletion didn't have any effect neither on specific nor on general gene expression. As expected, the depletion of CPEB4 in H5V cells, didn't affect the nuclear 3'UTR processing of VEGF mRNA **(Figure 27 b, right panel)**, corroborating the idea that CPEB4 is involved in cytoplasmic events of translational regulation.

In order to understand if the switch from short to long 3'UTR detected in CPEB1 knockdown reflected in a different translational behavior of VEGF mRNA, we performed a luciferase reporter assay, transfecting H5V cells with synthetic chimeric mRNAs containing the firefly luciferase coding sequence fused upstream to short or long VEGF 3'UTR. The RNA containing long 3'UTR showed an about 50% reduced luciferase activity compared with the short 3'UTR-containing partner, suggesting that the longer 3'UTR made the mRNA less competent for translation than the short one **(Figure 27 c)**. The long 3'UTR of VEGF, in fact, contains several translation regulatory elements, such as ARE, that may negatively regulate the translation of the mRNA and are excluded when the short 3'UTR is generated.

To address the hypothesis that CPEB1 and CPEB4 played a role in cytoplasmic polyadenylation, we analyzed the length of VEGF poly(A) tail in CPEB1 and CPEB4 knockdown H5V cells. Since in CPEB1 knockdown cells, the expression of VEGF mRNA with short 3'UTR was so low as to be considered negligible, we tested the polyadenylation of the mRNA with long 3'UTR only. The depletion of CPEB1 didn't cause any change in VEGF poly(A) tail length (Figure d, left panels). In addition to that, we also observed that in both wild type and CPEB1 knockdown conditions, the poly(A) tail of VEGF contained about 40 adenosines, a length that is known to be not sufficient to mediate robust mRNA translation. Interestingly and coherently with our work model, the 40 adenosines long poly(A) tail may be the result of the antagonistic activity between the cytoplasmic polyadenylation machinery, that elongates the poly(A) tail, and the ARE-recruited deadenylase complex that tends to remove it. All together, these results suggested that the main role of CPEB1 was mediating the "shortening" of VEGF 3'UTR and that there was another element responsible for the strong polyadenylation that it's required for efficient mRNA translation. To understand whether CPEB4 was the factor involved in the polyadenylation of VEGF mRNA, we measured the poly(A) tail in wild type and knockdown H5V cells. This time, since CPEB4 knockdown cells expressed VEGF mRNA with the two version of the 3'UTR (short and long), we performed polyadenylation assay using both the substrates. The depletion of CPEB4 completely abrogated the polyadenylation of VEGF mRNA **(Figure 27 d, right panels)**. VEGF mRNA with short 3'UTR presented a poly(A) tail long about 120 adenosines which is the optimal condition for efficient RNA translation. Also the weak polyadenylation of the long 3'UTR was lost in CPEB4 knockdown cells. These results allowed us to claim that CPEB1 drives the

nuclear cleavage of VEGF 3'UTR while CPEB4 is responsible of its cytoplasmic polyadenylation.

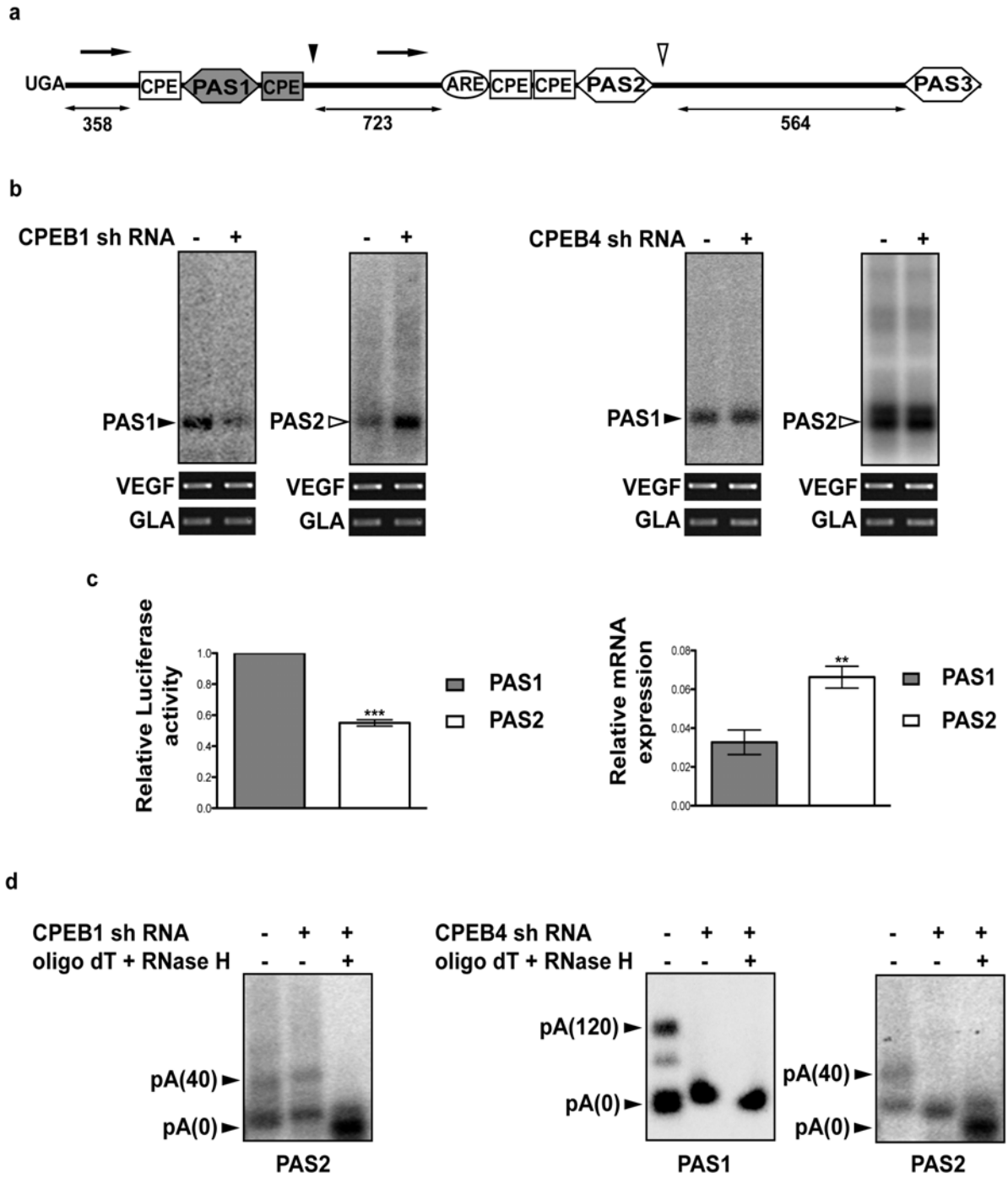

Figure 27. CPEBs-mediated VEGF 3'UTR processing in H5V cells. **a.** Representation of mouse VEGF 3'UTR. CPE (Cytoplasmic Polyadenylation Elements) and PAS (Poly Adenylation Signal) are indicated in white polygons (consensus sequences) or grey polygons (not consensus sequences). AU-rich elements (ARE) are also shown. Single headed arrows indicate the

position of the primers used for 3'RACE analysis. Arrowheads are used to indicate the cleavage sites. Double headed arrows indicate the distance between different regulatory elements. **b.** VEGF 3'UTR cleavage analysis performed by 3'RACE/southern blot in CPEB1 knockdown cells (left panel) and CPEB4 knockdown cells (right panel). Semiquantitative PCR of VEGF and GLA were used as control of total VEGF mRNA and general gene expressions of the cells. **c.** Analysis of translational activity performed using H5V cells transfected with synthetic chimeric mRNAs containing the firefly luciferase coding sequence fused upstream to short or long VEGF 3'UTR obtained by usage of PAS1 or PAS2 respectively. The activity of Renilla luciferase was used for normalization. Data are mean ± S.D. *P* values (obtained by Student Test) are relative to PAS1 (short VEGF 3'UTR). ***$P \leq 0.0005$. Translational activity results were normalized against relative mRNA levels of Firefly and Renilla construct transfected into the cells (right panel). Data are mean ± S.D. **$P \leq 0.005$. Values correspond to three independent experiments. **d.** Polyadenylation analysis of short (PAS1) and long (PAS2) VEGF 3'UTR performed in CPEB1 knockdown cells (left panel) and CPEB4 knockdown cells (right panel). Poly(A) tail length is indicated.

Once elucidated how CPEB1 and CPEB4 regulate VEGF mRNA processing and intrigued by the fact that in absence of CPEB1, also the levels of CPEB4 mRNA and protein were reduced, we focused on the possible CPEB1-mediated alternative formation of CPEB4 3'UTR. Due to the presence of several CPEs and PASs, this 3'UTR was supposed to undergo APA **(Supplementary figure 3 a)**. An initial indication about the validity of this assumption was suggested by a study conducted in our group by *A. Bava* and collaborators, in which the depletion of CPEB1 in H.D My-Z cells determined a switch from short to long CPEB4 3'UTR **(Supplementary figure 3 c)**. In support of these results, the analysis of 3'UTR formation, performed by quantitative PCR in H5V cells, showed increased expression of CPEB4 transcripts with long 3'UTR in CPEB1 knockdown **(Supplementary figure 3 b, right panel)**. In absence of CPEB1, the lengthening of CPEB4 3'UTR was accompanied by decrease of total CPEB4 mRNA levels **(Supplementary figure 3 b, left panel)**. The effect may be attributed to regulatory elements, present in the long 3'UTR and excluded in the short one, which reduced mRNA stability and translation. This concept is supported by recent findings from *AF. Muro* and collaborators, which described and functionally validated two micro RNA binding sites, miR-26 and miR-92 present in the last part of CPEB4 3'UTR [127].

CPEB1 and CPEB4 are required for *in vivo* angiogenesis

The analysis of CBDL and PPVL models developed in rats allowed us to propose a exhaustive description of CPEBs expression during hepatic and pre-hepatic angiogenesis and its

contribution to VEGF 3'UTR formation and polyadenylation. Moreover, in vitro experiments performed using the H5V model, enabled to further elucidate the molecular mechanism of VEGF translational regulation. To more precisely determine the *in vivo* requirement of CPEB1 and CPEB4 to sustain pathological angiogenesis, we generated tamoxifen-inducible murine models for CPEB1 or CPEB4 gene inactivation, and subjected them to PPVL to induce portal hypertension (**Supplementary Figures 4 and 5)**. We confirmed that the expression of CPEB1 and CPEB4 proteins was almost absent in the CPEB1 and CPEB4 induced knockout (iKO) mice **(Figure 28 a,b and Supplementary Figure 6 a,b)**. Both CPEB1 and CPEB4 downregulation correlated with a robust and significant reduction (85% for CPEB1 iKO and 89% for CPEB4 iKO) in the vascular density of newly formed mesenteric microvessels **(Figure 28 c-e)**, without affecting preexisting vasculature density **(Supplementary Figure 6 c)**. Such a dramatic prevention of mesenteric neovascularization should likely translate into improvement of the portal hypertensive syndrome, with reduction of splanchnic blood flow and portosystemic collateral vessel formation [128]. In fact, CPEB1 and CPEB4 iKOs presented a marked attenuation of the splenomegaly, which is a commonly encountered consequence of portal hypertension that correlates with the increase in portal pressure [129], without changes in body weight **(Supplementary Figure 6 e)**. VEGF expression in the mesentery was also reduced when comparing CPEB4 KO and the WT mice after portal hypertension induction **(Supplementary Figure 6 d)**. As a whole, these results demonstrate that CPEB1 and CPEB4-mediated translation is an essential regulatory mechanism governing the control of angiogenesis during portal hypertension.

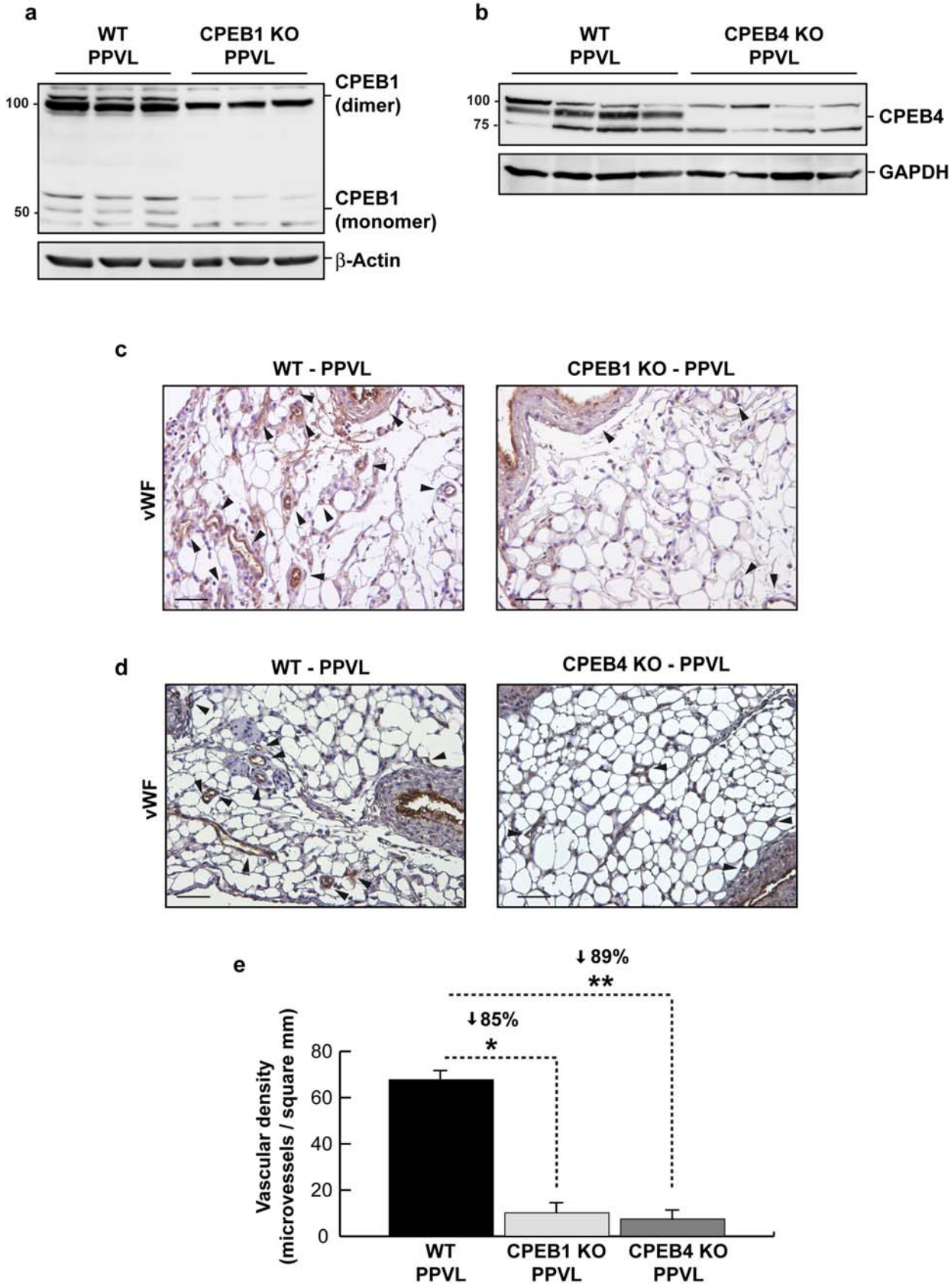

Figure 28. Studies in CPEB1 and CPEB4 inducible knockout mice. Tamoxifen-treated CPEB1 or CPEB4 inducible knockout mice (CPEB1 iKO, n=5; CPEB4 iKO n=9) and wild type (WT, n=8) mice were subjected to partial portal vein ligation (PPVL) to induce portal hypertension. **a.**

Western blotting of CPEB1 protein in testicles from WT mice and CPEB1 iKO mice, 8 days after inducing portal hypertension by PPVL. Results demonstrate effective depletion of CPEB1, both dimeric and monomeric forms of the protein, in the CPEB1 iKO mice. **b.** Western blotting of CPEB4 protein in mesentery from WT mice and CPEB4 iKO mice, 8 days after PPVL, showing effective depletion of CPEB4 protein in the CPEB4 iKO mice. **c.** Photomicrographs of mesentery sections immunostained for the endothelial cell marker von Willebrand factor (vWF), from WT mice and CPEB1 iKO mice, 8 days after PPVL. Scale bar: 50 µm. **d.** Photomicrographs of vWF immunostained mesentery sections from WT mice and CPEB4 iKO mice, 8 days after PPVL. Scale bar: 50 µm. **e.** Quantification of the vascular density (vWF-positive microvessels per square millimeter) in the mesentery of WT mice and the CPEB1 and CPEB iKO mice after PPVL. Results are expressed as mean±S.E.M. **P*=0.00003, ***P*=0.000002. **In collaboration with Mercedes Fernandez's group, Gonzalo Fernandez-Miranda and Carlos Maillo.**

DISCUSSION

Hepatic cirrhosis is a largely diffused pathology caused by alcohol abuse and hepatitis C in developed countries, whereas hepatitis B is the cause in most parts of Asia and sub-Saharan Africa. It's characterized by development of regenerative nodules delimited by fibrous tissue in form of delicate bands and broad scars. These formations, called fibrous septa, replace normal hepatic parenchyma during the development of the pathology. Regenerative nodules are composed by proliferating hepatocytes, entrapped by deposition of extracellular matrix, and have been shown to be involved in growth factor production, in particular VEGF. Regenerative nodules-produced VEGF is responsible of angiogenic induction that culminates with formation of a dense network of blood vessels into fibrous septa. The newly formed blood vessels of fibrous septa connect the vessels of the portal region with terminal hepatic veins, determining an alternative route of the blood flow that, in this way, is redirected into the systemic circulation bypassing the liver. In addition, the dense network of blood vessels, representing an obstruction for the blood flow, generates portal blood hypertension. At pre-hepatic level, portal hypertension induces development of new blood vessels that shunt the portal blood into the systemic circulation. As consequence of both intrahepatic and pre-hepatic angiogenesis, the liver cannot metabolize several blood components such as drugs, nutrients, toxins, and bacteria, with obvious deleterious effects. Despite angiogenesis is one of the main complications of liver cirrhosis and VEGF has a pivotal role in the control of blood vessels formation, the molecular mechanisms that govern VEGF expression during angiogenesis and hepatic cirrhosis are poorly understood.

In order to address whether CPEB family of proteins may have a function in the regulation of angiogenesis in liver diseases, we analyzed the expression of CPEB1 and CPEB4 in liver of patients affected by hepatic cirrhosis. The expression of CPEB1 and CPEB4 was increased in regenerative nodules, compared with basal levels of expression detected in healthy hepatic parenchyma. Interestingly, also VEGF expression was higher in regenerative nodules. The numerous fibrous septa that characterized cirrhotic livers resulted highly vascularized, and the endothelium of newly formed blood vessels expressed high levels of CPEB1, CPEB4 and VEGF. Also the healthy parenchymal hepatocytes close to fibrous septa showed increased expression of CPEBs and VEGF. The description of CPEB1, CPEB4 and VEGF expression in healthy and cirrhotic conditions represented a first cue of CPEB-mediated translational regulation of VEGF mRNA during angiogenesis. Regenerative nodules and, partially,

parenchyma hepatocytes expressed increased levels of CPEB1 and CPEB4, which were "suspected" to drive VEGF mRNA translation.

To prove the accuracy of this hypothesis we implemented two animal models that allowed us to study intrahepatic and prehepatic angiogenesis correlated with liver cirrhosis. CBDL experiments performed in rats enabled to recapitulate the histopathological conditions observed in human hepatic cirrhosis. Cirrhotic rat livers showed deep histological perturbations, with high proliferation of blood vessels and biliary ducts. Compared with control healthy samples, the expression of CPEB1, CPEB4 and VEGF in pathological liver was strongly increased. These proteins localized at level of both, blood vessels and biliary ducts. The possibility that CPEB1 and CPEB4 were involved in the regulation of VEGF mRNA at post-transcriptional level was further suggested by the analysis of VEGF mRNA levels. VEGF protein increase was not due to augmentation of VEGF mRNA transcription or stability, even better, messenger levels were lower in CBDL samples, compared with healthy ones. The reason resides in the fact that, paradoxically, many mRNAs are present at lower level when highly translated, because less stable and exposed to the action of ribonucleases. In contrast, when the translation is repressed, some mRNAs are stabilized and accumulated into the cytoplasm, thus present at higher concentrations.

Partial portal vein ligation (PPVL) experiments performed in rats enabled to show an important correlation between CPEB1 and CPEB4 expression with VEGF synthesis and consequent high vascularization of mesentery. In angiogenic condition, both pre-existing and newly formed blood vessels expressed CPEB1, CPEB4 and VEGF at level of endothelium, smooth muscle and adventitia, tissues that play a pivotal role in the development of the vascular net. 3'RACE assays conduced using RNA extracted from SHAM and PPVL mesentery showed interesting changes in VEGF 3'UTR length comparing control versus angiogenic samples. In PPVL animals, VEGF mRNA harboured a shorter 3'UTR than in SHAM condition. The same experiment, performed using RNA extracts from the intestinal mucosa, where CPEB1 and CPEB4 are not expressed, showed the presence of VEGF mRNA with long 3'UTR, giving evidence that CPEB1 production and phosphorylation, and VEGF 3'UTR shortening was not a mere coincidence but a clear clue of CPEB1-mediated APA of VEGF mRNA. The 3'UTR formation of VEGF mRNA was not the only important change detected comparing PPVL with SHAM conditions. Only after induction of angiogenesis, and consequent synthesis of CPEB4, VEGF mRNA was strongly polyadenylated. Thus, during angiogenesis we described a loop of

correlations that started with CPEB1 production and activation, and CPEB4 synthesis, triggered to VEGF 3'UTR cleavage and polyadenylation, and culminated with deep vascularization of rat mesentery.

To better define the mechanistic relevance of these correlations, we characterized the endothelial cell line H5V. In this in vitro model we modulated the levels of CPEB1 and CPEB4, and showed a direct involvement of this two proteins in the translational regulation of VEGF mRNA. Taking advance of the ability of H5V cells to form blood vessel like structure in an in vitro angiogenesis assay, we were able to show that CPEB1 and CPEB4 are required for VEGF synthesis and secretion, which in turn are essential to create the correct microenvironment necessary to activate the cells and induce them to form a dense network of vascular structures on Matrigel. It's more than possible that the culture medium conditioned by H5V cells presented a variegated composition of growth factors that, in addition to VEGF, contribute to confer the angiogenic ability to the cells. However, rescue experiments conduced using VEGF recombinant protein allowed claiming that this protein had a privileged role in angiogenesis, and underlined the importance of CPEB-mediate translational control of its mRNA. CPEB1 is an RNA binding protein found to shuttle from the nucleus to the cytoplasm, and coordinate nuclear 3'UTR formation with cytoplasm function, in genome wide manner [46]. VEGF mRNA resulted to be a nice example of CPEB1-mediate APA. VEGF 3'UTR in fact, harbouring two polyadenylation signals PAS1 and PAS2, resulted differently regulated depending on the activity of CPEB1. While PAS2 is a "strong", consensus polyadenylation signal, able to drive, alone, efficient cleavage of VEGF 3'UTR, PAS1 is a "weak", non-consensus polyadenylation signal, since its sequence differs from the canonical AAUAAA and AUUAAA sequences. However, in wild type H5V cells, CPEB1, binding to CPE sequence present in the proximity of VEGF PAS1, allowed it to behave as a strong polyadenylation signal, able to mediate efficient cleavage of the 3'UTR which resulted in a shorter version. Depletion of CPEB1 in H5V cells completely overturned the scenario. In absence of this protein, in fact, the 3'UTR of VEGF was cleaved only at level of PAS2, with consequent formation of longer version. VEGF translation was strongly dependent on the length of the mRNA 3'UTR. By luciferase assay we showed that, a reporter RNA presenting the long 3'UTR of VEGF (obtained using PAS2), was translated with about 50% less efficiency than another one expressing the short version of VEGF 3'UTR. Thus, long VEGF 3'UTR presented some *in cis* elements that, together with their trans-acting factors, were able to

attenuate the translation of the mRNA, and that were not included in the short version of the 3'UTR. Our attention fell on the AU-rich elements present in the vicinity of PAS2 and peculiar of long VEGF 3'UTR. These elements were thought to recruit a deadenylase complex that, establishing a competition with the polyadenylation machinery, reduced mRNA translation. As expected, CPEB4 didn't have any role in VEGF 3'UTR formation. CPEB4 exerted, in fact, its function regulating the polyadenylation of VEGF mRNA. In H5V cells depleted of CPEB4, the polyadenylation of VEGF mRNA was completely impaired, an effect that caused deep reduction of both protein synthesis and angiogenic cell activation. Our in vitro model permitted to definitively claim that CPEB1 regulates nuclear formation of VEGF 3'UTR, while CPEB4 is responsible of cytoplasmic polyadenylation of the mRNA. A further level of complexity was added by the evidence that CPEB1 regulated also CPEB4 3'UTR formation. As happened to VEGF, also CPEB4 mRNA presented longer 3'UTR in H5V cells depleted of CPEB1. It's interesting to notice that CPEB4 is one of the mRNA with highest number of predicted miRNA binding sites in the 3'UTR. Some of them, miR-26 and miR-92, are present in the most 3' portion of the 3'UTR and have been functionally validated as negative regulators of translation [127]. The weak decrease on CPEB4 mRNA levels observed in CPEB1 knockdown H5V may be explained by the activity of miR-26 and miR-92.

The obvious technical and conceptual limitations that human and rat models presented, and the fact that H5V cells, even being a great system for molecular studies, represented only the endothelial component of the vasculature, induced us to analyze the effects of *in vivo* depletion of CPEB1 and CPEB4 on the vascular network development. PPVL experiments performed in CPEB1 or CPEB4 KO mice showed that, in absence of the protein, the vascularization of mesentery was deeply impaired.

All together, our results are consistent with the following model **(Figure 29)**. In non-angiogenic tissues, where activated CPEB1 is absent, VEGF and CPEB4 pre-mRNAs are processed using the "default" distal polyadenylation site (PAS), with consequent formation of the longest possible 3'UTR variant, which, in turn, harbours multiple AREs and miRNA binding sites. These regulatory sequences and their binding factors inhibit their translation and/or shorten the half-life of the mature transcripts in the cytoplasm. Upon stimulation of the angiogenic process associated with portal hypertension and cirrhosis, CPEB1 would become overexpressed and activated by phosphorylation, while shuttling between the nucleus and the cytoplasm. Nuclear CPEB1 will promote the use of more 5' alternative

polyadenylation site, therefore shortening the 3'UTRs of CPEB4 and VEGF mRNAs and excluding the AREs and miRNA binding sites from the mature transcripts. For CPEB4, elimination of these elements triggers transcript stabilization and translational activation. The resulting CPEB4 would bind to its own transcript generating an amplification loop that further increases CPEB4 levels. CPEB4, now present at high concentration, binds to VEGF mRNA promoting its cytoplasmic polyadenylation. Thus, CPEB1 is required for nuclear APA of VEGF and CPEB4 mRNAs, while CPEB4 is required for subsequent translational activation through cytoplasmic polyadenylation. Both functions are coordinated through the pre-mRNA processing and cytoplasmic polyadenylation loops connecting CPEB1 and CPEB4.

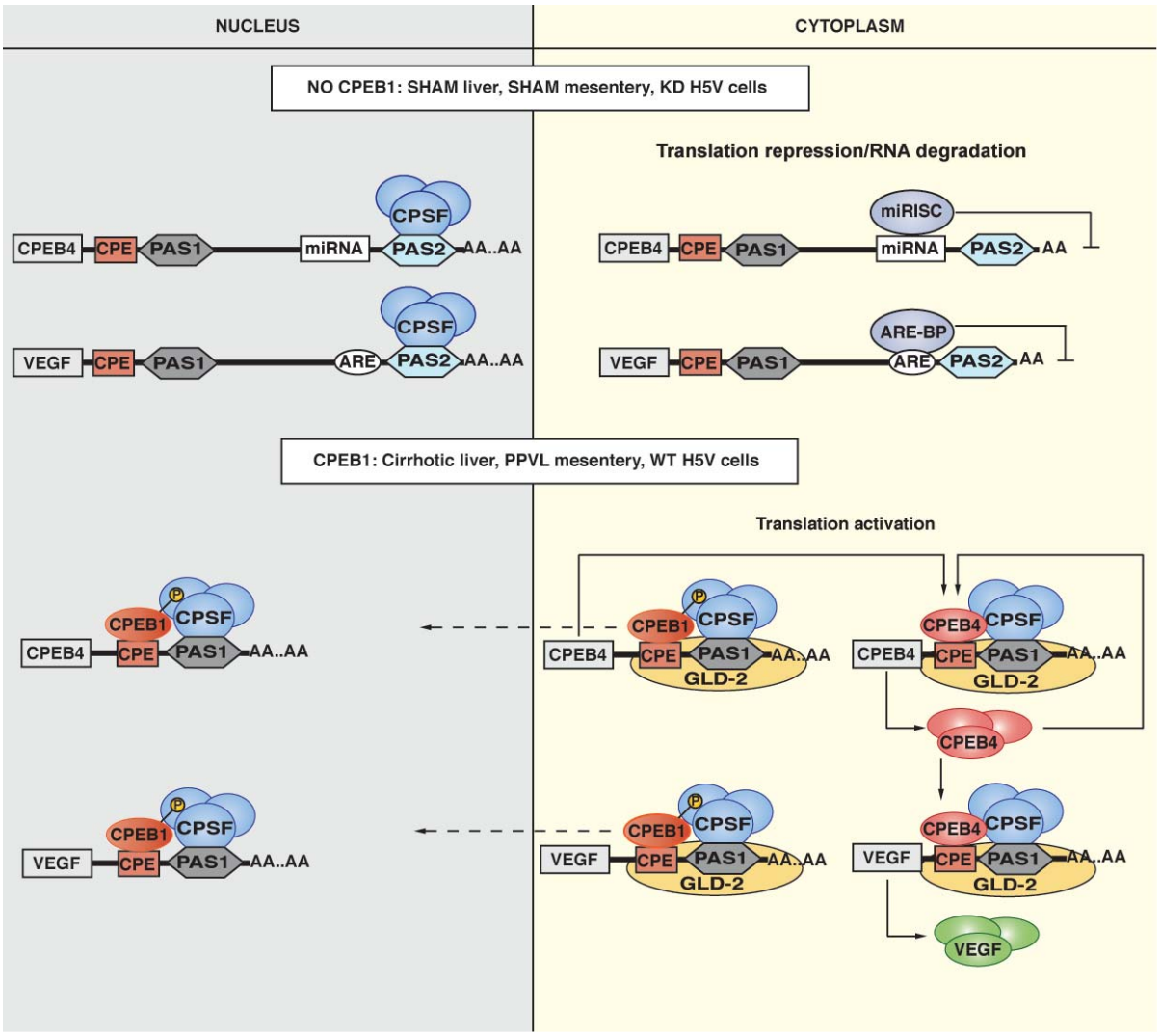

Figure 29. CPEB1 and CPEB4 sequentially regulate nuclear and cytoplasmic VEGF mRNA processing. Schematic representation of alternative polyadenylation (left) and cytoplasmic polyadenylation (right), in absence (top) and in presence (bottom) of Phosphor-CPEB1.

Abbreviations: CPE, Cytoplasmic Polyadenylation Element; CPEB, Cytoplasmic Polyadenylation Element Binding protein; PAS, Polyadenylation Signal; CPSF, Cleavage and Polyadenylation Specificity Factor; GLD-2, Defective in Germline Development-2; VEGF, Vascular Endothelial Growth Factor.

It's highly probable that *in vivo*, CPEBs regulate not only VEGF translation, but also that of several other mRNAs encoding for proteins involved in angiogenesis. Interestingly, some important integral membrane proteins that act in VEGF signaling pathway, such as Notch and Dll4, present CPE and APA signals in their 3'UTR. Moreover, IL-6, that has been described involved in angiogenesis associated with gastric carcinoma and cervical tumor [130,131] and that has a role in post stroke angiogenesis, is regulated by CPEB1 [132]. Although in our study we didn't find substantial changes in VEGF mRNA transcription, it's not possible to exclude that, at least in certain condition, VEGF gene expression is regulated also at that level. Nevertheless, CPEB has been shown to indirectly regulate VEGF mRNA transcription. The translation of Hypoxia Inducible Factor (HIF-1α) mRNA, in fact, is regulated by CPEB1 and CPEB2 while the Signal Transducer and Activation of Transcription 3 (STAT3) is regulated by CPEB1 [133,134]. Several other proteins encoded by CPE-containing mRNAs may be involved in the regulation of angiogenesis.

It's clear that a so complex biological process requires anatomo-functional changes that are regulated at all levels of gene expression. However, finding that VEGF synthesis can be regulated at translational level by CPEB opens new exiting perspectives of therapeutical strategies based on the specific inhibition of CPEB proteins. Our findings unveil, in fact, a new mechanism of regulation of angiogenesis during cirrhosis and portal hypertension, highlighting that the posttranscriptional regulation of VEGF expression by sequential functions of CPEB1 and CPEB4 could constitute a potential therapeutical target for patients suffering from chronic liver disease. Because healthy liver and splanchnic organs express negligible CPEB levels, putative treatments could have the additional advantage of being selective for the neovasculature generated during pathological conditions, not affecting the pre-existing vessels that are not involved in ongoing angiogenic process, which makes CPEB attractive as a therapeutic target. This is of particular significance, since the management of patients with chronic liver disease continues to be a critical and prevalent clinical problem, for which the clinical armamentarium is not so abundant [135]. Although VEGF inhibition has

been shown to improve chronic liver disease symptoms, it has severe collateral effects on "normal" vasculature. On the contrary, targeting CPEBs would impact in the pathological overexpression of VEGF while maintaining the basal levels required for normal vascular homeostasis, as clearly evidenced in the normal vasculature and embryonic angiogenesis of constitutive CPEB1 or CPEB4 Kos. Therefore CPEBs constitute highly specific targets for chronic liver disease associated angiogenesis. In addition, because pathological neovascularization also plays an essential role in many other diseases, including inflammatory diseases, diabetic retinopathy, hemangiomas, and cancer, our findings could be beneficial also for a wide spectrum of pathological situations. Accordingly we have found that CPEB4 depletion in xenographted pancreatic ductal adenocarcinoma cells results, not only is significant reduction of tumoral growth, but also in impaired angiogenesis [117]. In this regard, our finding that CPEBs are highly expressed in regenerative micronodules of human and rat cirrhotic livers could have important implications supporting a role of CPEB in the pathogenesis of hepatocellular carcinoma as well, which is a highly vascularized tumor that needs an intense angiogenic activity to develop and progress [136]. Thus, formation of regenerative nodules in cirrhotic liver might be the first step of hepatocarcinogenesis, making it plausible to hypothesize that early interference with CPEB and angiogenesis signaling may prevent the transition from hepatic dysplasia to hepatocellular carcinoma.

CONCLUSIONS

The present study allowed claiming a new mechanism of angiogenesis regulation through CPEB-mediated translational control. The main points of the mechanism and its biological relevance are resumed below.

1. As consequence of angiogenesis induction, CPEB1 is expressed in its activated form (phosphor-CPEB1) and drives APA of CPEB4 and VEGF mRNAs, thus expressed with a shorter 3'UTR.

2. CPEB4 and VEGF mRNAs, expressing short 3'UTRs, are exported to the cytoplasm, where CPEB4 mRNA is translated at basal level under translational control of phosphor-CPEB1. The so produced CPEB4 activates a positive feedback loop of translation of its own mRNA that culminates with synthesis of high amounts of protein. CPEB4 is then responsible of robust polyadenylation of VEGF mRNA, which translation is essential for the development of a dense network of blood vessels *in vivo,* and blood vessel-like structure *in vitro.*

3. CPEB1 and CPEB4, over-expressed at level of newly formed blood vessels in cirrhotic livers (both human and murine) and in mesentery may be used as hallmark of pathological angiogenesis associated with hepatic cirrhosis and related portal hypertension.
4. CPEB1 and CPEB4, being expressed at low levels in pre-existing blood vessels and strongly increased in newly formed vascular structures, may represent an attractive target for putative treatment of diseases whose establishment and progression depend on the development of a pathological network of blood vessels.

MATERIALS AND METHODS

Cirrhotic patients. Human samples of hepatitis C virus-related cirrhotic liver (n=5) were obtained from transjugular liver biopsies or from the explanted organ at the time of liver transplantation. Liver samples were fixed in 10% neutral buffered formalin and paraffined for immunohistochemistry. Clinical data of the patients at the moment of liver sampling were as follow: three patients had compensated cirrhosis, and two decompensated cirrhosis. All had severe portal hypertension (hepatic venous pressure gradient, HVPG = 15, 18.5 and 20 mmHg, respectively). All research protocols regarding human samples have been approved by the Clinical Review Board and Ethics Committee at the Hospital Clinic of Barcelona (protocol number: 2011/6723). All patients participating in these studies have been thoroughly informed about the studies and have signed both their consent information and the suitability of the information received.

Animals. Male Sprague-Dawley rats (Charles River Laboratories, Cambridge, Massachusetts, US) weighing 300-350 g body weight (b.w.) and C57BL6 or mixed C57BL6/129 mice were used in this study. All animal experiments were approved by the Laboratory Animal Care and Use Committees of the University of Barcelona and the Barcelona Scientific Park, and were carried out in accordance with the Guide for the Care and Use of Laboratory Animals (NIH publications no. 85-23, revised 1996).

Antibodies. Rabbit polyclonal CPEB4 serum (prepared in R. Mendez laboratory as described in [111]), rabbit polyclonal CPEB4 (ab83009, Abcam, Cambridge, UK), rabbit polyclonal CPEB1 (Protein Tech 13274-1-AP and ab15917, Abcam), rabbit polyclonal vWF (Dako, Glostrup, Denmark), rabbit polyclonal VEGF (ab46154, Abcam), mouse monoclonal VEGF (ab1316 and ab46154, Abcam), mouse monoclonal alpha-tubulin (T9026, Sigma, St Louis, Missouri, US), and mouse monoclonal GAPDH (sc-32233, Santa Cruz Biotechnology, Santa Cruz, California, US). Antibody against phosphorylated CPEB1 was from Abyntek Biopharma (Derio, Bizkaia, Spain).

Oligonucleotides. For semiquantitative PCR: mouse CPEB4, 5'-TTGTTTCCGATGGAAGATGG-3' (sense) and 5'-TCAATATCAGGAGGCAATCCA-3' (antisense); mouse VEGF, 5'-GGTTCCAGAAGGGAGAGGAG-3' (sense) and 5'-GCATTCACATCTGCTGTGCT-3' (antisense); mouse GAPDH, 5'-CCCTTCATTGACCTCAACTAC-3' (sense) and 5'-AAGGCCATGCCAGTGAG-3'

(antisense); mouse GLA, 5'-ACCAGCAGGTGACACAGATG-3' (sense) and 5'-GAAACAGTAGCCCTGCTTGC-3' (antisense), rat VEGF 5'-GGCCTCTGAAACCATGAACT-3' (sense) and 5'-CGTACTAGACGTATCACTGC (antisense). For quantitative PCR: mouse CPEB1, 5'-CCTCCTCTGCCCTTTCTTTC-3' (sense) and, 5'-TCCAAGAAGGTCCCAAGATG-3' (antisense); mouse CPEB4, 5'-TTGTTTCCGATGGAAGATGG-3' (sense) and 5'-TCAATATCAGGAGGCAATCCA-3' (antisense); mouse VEGF, 5'-CATGCGGATCAAACCTCAC-3' (sense) and 5'-GCATTCACATCTGCTGTGCT-3' (antisense); mouse GLA, 5'-ACCAGCAGGTGACACAGATG-3' (sense) and 5'-GAAACAGTAGCCCTGCTTGC-3' (antisense); mouse CPEB4 3'UTR PAS1, 5'-CTCTCGTGTCACTGCAAACAG-3' (sense) and 5'- TTAGATCCTCTTGGCCTCCA-3' (antisense); mouse CPEB4 3'UTR PAS2, 5'-AAAGTCATTTTCACGTTAAGTTCC-3' (sense) and 5'-TCCACTAGCACTTCAACAAATGA-3' (antisense); firefly luciferase, 5'-TGATTTTTCTTGCGTCGAGTT-3' (sense) and 5'-GTTTTGGAGCACGGAAAGAC-3' (antisense); renilla luciferase, 5'-GATAACTGGTCCGCAGTGGT-3' (sense) and 5'-ACCAGATTTGCCTGATTTGC-3' (antisense). For 3'RACE: 3'RACE, 5'-TAATACGACTCACTATAGGGCGGATCCTTTTTTTTTTTTTTTTTTTTTTT
TVN-3' (antisense); PAS1 of mouse VEGF 3'UTR, 5'-CCTCAGGGTTTCGGGAACC-3' (sense), PAS2 of mouse VEGF 3'UTR, 5'-AAGAAGAGGCCTGGTAATGG-3' (sense), T7, 5'-GTAATACGACTCACTATAGGGC-3' (antisense); PAS1 of human CPEB4 5'-GATTCTTGTGTCACTGCAAAC-3' (sense), PAS2 of human CPEB4 5'-CATCACTTCAATTCACCAAGC (sense). For Poly(A) tail assay: SP2, 5'-P-GGTCACCTCTGATCTGGAAGCGAC-NH2-3' (sense), ASP2, 5'-GTCGCTTCCAGATCAGAGGTGACCTTTTT-3' (antisense), APAS1 of mouse VEGF 3'UTR, 5'-AAGATTAGGGTTGTTTCTGG-3' (sense), APAS2 of mouse VEGF 3'UTR, 5'-AAGAAGAGGCCTGGTAATGG-3' (sense). For southern blotting probes of 3'RACE: PAS1 of mouse VEGF 3'UTR, 5'-AGTCCTTAATCCAGAAAGCC-3' (sense), PAS2 of mouse VEGF 3'UTR, 5'-GGTACAGCCCAGGAGGACCT-3' (sense); PAS1 of human CPEB4 5'-GGAAGTTTGGATCCTCTTGG-3' (sense), PAS2 of human CPEB4 5'-GCACTTCAACAAATGAACTC-3'. For southern blotting probes of Poly(A) tail assay: PAS1 of mouse VEGF 3'UTR, 5'-GATTCCTGTAGACACACCCACC-3' (sense), PAS2 of mouse VEGF 3'UTR, 5'-GGTACAGCCCAGGAGGACCT-3' (sense).

Plasmid construction. The plasmid pFlag-hCPEB4-CMV2, previously described [111], was used to subclone the DNA corresponding to the CDS (coding domain sequence) of CPEB4 into pLV plasmid. The nucleotide sequence of CPEB4 sh binding site 5'-GCTGCAGCATGGAGAGATAGA-3' was mutated to 5'-GCCGCAGCGTGGAGGGATAGG-3' using QuikChange II XL Site-Directed Mutagenesis Kit (200521 Stratagene). The mutagenesis affected neither the CDS frame nor the amino acid sequence. This new construct is called pLV-mutated-CPEB4. The sequence corresponding to the first 1213 nucleotides of mouse VEGF mRNA 3'UTR was subcloned downstream of the firefly luciferase CDS in PLuc cassette plasmid. Using this first clone we generated, by PCR, another construct carrying the first 416 nucleotides of mouse VEGF mRNA 3'UTR subcloned downstream of the firefly luciferase CDS in PLuc cassette plasmid. The previously described pBSK-Renilla plasmid was used for normalization [111].

CPEB knockdown cell lines. CPEB4 inducible knockdown H5V (murine heart-derived ECs) cell line was generated using reagents and protocol previously described [111]. CPEB4 inducible knockdown H5V cells were cultured during 5 days in DMEM (Dulbecco's Modified Eagle Medium, Gibco BRL, Grand Island, NY) supplemented with 10% FBS (Foetal Bovine Serum, Gibco), 2 mM L-glutamine, 1% penicillin/streptomycin, in the presence of PBS (5 µl/ml of medium) or doxycycline (5 µg/ml of medium) in order to induce the expression of shRNAs directed against the sequence 5'-GCTGCAGCATGGAGAGATAGA-3' and then used for RNA and protein extractions and Matrigel tube formation assay. CPEB1 inducible knockdown H5V cell line was generated as previously described [111], with some modifications: H5V cells were transduced with pLKO IPTG Lac0 lentivector carrying sequence for CPEB1 shRNAs expression (Sigma). Virus production was performed as indicated in http://tronolab.epfl.ch/. CPEB1 inducible knockdown H5V cells were cultured during 4 days in DMEM supplemented with 10% FBS, 2 mM L-glutamine, 1% penicillin/streptomycin, in presence of PBS (1 µl/ml of medium) or IPTG (5 µM isopropyl-β-D-thio-galactoside) in order to induce the expression of shRNAs directed against the sequence 5'- AGGCGTTCCTTGGGATATTAC-3' and then used for RNA and protein extractions and Matrigel tube formation assay. CPEB4 inducible knockdown H5V cells were transduced with pLV-mutated-CPEB4 lentivector for stable expression of CPEB4 mRNA not target of shRNAs. Virus production was performed as indicated in http://tronolab.epfl.ch/.

H5V cells were transduced with pLKO1 lentivector carrying sequence for constitutive expression of CPEB1 shRNAs or control shRNAs (Sigma). CPEB1 sh RNAs targeted the sequence 5'- CCATCTTGAATGACCTATTTG-3'. The cells were cultured in DMEM supplemented with 10% FBS, 2mM L-glutamine, 1% penicillin/streptomycin and used for RNA and protein extraction and Matrigel tube formation assay. H.D. MyZ cells were produced as previously described [137].

Conditioned medium. CPEB1 inducible knockdown H5V cells and CPEB4 inducible knockdown H5V cells were cultured in absence of doxycycline and IPTG, in DMEM supplemented with 10% FBS, 2 mM L-glutamine, 1% penicillin/streptomycin, during 48 h in order to obtain conditioned medium. Conditioned medium was collected and centrifuged 2 min at 300 xG; supernatant was used in Matrigel Tube Formation Assay.

Generation of CPEB1 and CPEB4 conditional knockout mice

CPEB1-targeted mice. The conditional targeting vector was assembled by flanking exon 4 of the murine Cpeb1 locus with loxP sequences (**Supplementary Fig. 12**). The vector was electroporated in mouse W4 ES cells derived from a 129S6/Sv strain. The positive recombinant ES cells were identified by Southern Blot and microinjected in developing blastocysts. The resulting chimeric mice were crossed with C57BL6/J mice and the mouse colony maintained in a mixed (129/Sv x C57Bl/6J) background.

CPEB4-targeted mice. Mouse ES cells carrying a bgeo [b-galactosidase gene fused to the neomycin resistance gene] cassette in Cpeb4 intron 1 (clone EPD0060_4_E10; Sanger Institute) were microinjected in developing blastocysts (**Supplementary Fig. 13**). The resulting chimeric mice were crossed with C57BL6/J mice and the mouse colony maintained in a pure C57BL6 background.

Conditional mice for CPEB1 and CPEB4 were generated upon expression of FlpO recombinase in recombinant ES cells [138] or by mating with Tg. pCAG-Flp mice [139]. To obtain a tamoxifen-inducible mouse line the conditional mice were crossed with the Tg.Ubc-CreERT2 mice [140]. For systemic deletion, 4 weeks old conditional mice were fed with tamoxifen-enriched food (Harlan Laboratories Models) during 30 days. Oligonucleotides and genotyping protocols of both mouse models are available upon request.

Animal model of prehepatic portal hypertension. Portal hypertension was induced in rats and mice by partial portal vein ligation (PPVL), as previously described. Briefly, rats were anesthetized with a ketamine (100 mg/kg) plus midazolam (5 mg/kg) mixture, and mice with isofluorane, and a midline abdominal incision was made. The portal vein was dissected free of surrounding tissue, and a loose ligature of silk suture (size 3-0 for rats and 5-0 for mice) was guided around it. A blunt-end needle (20-gauge for rats and 27-gauge for mice) was placed alongside the portal vein, and the suture was tied snugly around the portal vein and needle. The needle was subsequently removed to yield a calibrated constriction of the portal vein. Sham-operated (SHAM) control rats and mice were operated in the same manner as the portal hypertensive animals, except that the portal vein was not ligated.

Animal model of secondary biliary cirrhosis and intrahepatic portal hypertension. Secondary biliary cirrhosis was induced in rats by common bile duct ligation (CBDL), as previously described. Briefly, the animals were anesthetized with a ketamine (100 mg/kg) plus midazolam (5 mg/kg) mixture, and a midline abdominal incision was made. The common bile duct was isolated and doubly ligated with 5-0 silk. The first ligature was made below the junction of the hepatic ducts and the second ligature was made above the entrance of the pancreatic ducts. The portion of the bile duct between the two ligatures was resected to avoid repermeabilization. Sham operation (SHAM) was performed similarly, with the exception of ligating and transecting the bile duct.

Histological analyses and immunohistochemistry. Tissues were harvested, fixed by submersion in 10% buffered formalin solution, and embedded in paraffin. Successive 2-µm sections were then obtained and prepared for H&E staining, using standard histological protocols. For immunostaining, the 2-µm paraffin sections were deparaffinized in xylol and rehydrated in graded alcohol series. Endogenous peroxidase was inhibited using 3% H_2O_2 (10 min, RT). Sections were then washed in distilled water and heated in a pressure cooker for epitope retrieval (in 10 mM citrate buffer, pH 6.0, 5 min). Slides were blocked with 5% normal goat serum for 1 hour, and then incubated (1 hour, RT, or overnight, 4ºC) with the following primary antibodies: polyclonal antibodies against VEGF (1:500 dilution), CPEB1 (1:500 dilution), CPEB4 (1:500 dilution) and vWF (1:1000 dilution); and monoclonal antibody against P-CPEB1 (1:50 dilution). Sections were then washed with TBS containing 0.05%

Tween 20, and incubated with Dako Real EnVision Detection System (HRP mouse/rabbit secondary antibody; 30 min, RT). Antibody binding was revealed using H_2O_2 as a substrate, and diaminobenzidine as a chromogen. Hematoxylin was used as a counterstain. For negative control, primary antibody was omitted and then sections were incubated with corresponding secondary antibodies and detection systems. Stained sections were visualized with a Zeiss microscope. Images from several regions of the tissue sections were then acquired using an AxioCam camera (Carl Zeiss Vision, Germany). Analysis of the digitalized images was performed with computerized imaging system (AxioVision and Image J).

Immunofluorescence and confocal laser microscopy. Tissue sections (2 mm) were deparaffinized, and antigen retrieval and blocking were performed as described above for immunohistochemistry. The following primary antibodies were used: Polyclonal antibodies against CPEB1 (1:100 dilution), and CPEB4 (1:200 dilution), and monoclonal antibody against VEGF (1:50 dilution). For fluorescence visualization of antibody reactions, primary antibodies were detected using secondary antibodies labeled with the fluorochromes Alexa Fluor (Alexa anti-mouse A555 and Alexa anti-rabbit A647) from Invitrogen. To detect cell nuclei, paraffin-embedded tissues were deparaffined and mounted on Vectashield mounting medium for fluorescence with DAPI (H-1200; Vector). Negative controls were run omitting the primary antibody and incubating with secondary antibodies labeled with the fluorochromes Alexa Fluor. Confocal microscopy was performed at the Advanced Light Microscopy Unit (Scientific and Technological Centers) from the University of Barcelona. Confocal images were acquired using a Leica TCS SP5 laser scanning confocal microscope (Leica Microsystems Heidelberg GmbH, Manheim, Germany) equipped with a DMI6000 inverted microscope. DAPI, Alexa Fluor 555 and Alexa Fluor 647 images were acquired sequentially using 405, 561 and 633 laser lines, AOBS (Acoustic Optical Beam Splitter) as beam splitter and emission detection ranges 415-525 nm, 570-650 nm and 650-750 nm, respectively, and the confocal pinhole set at 1 Airy units. All images were acquired with an APO 63x oil (NA 1.4) immersion objective lenses, digitized into TIFF format of 1024 ×1024 pixels and 12 bit depth (4096 fluorescence intensity levels of information). Electronic zoom (x3) was used for stronger magnification and better image resolution. Images were taken in the X-Y plane and/or the Z axis. Stacks of 1 micrometer-thick serial optical slices were taken in Z axis.

Immunofluorescence analysis on H5V cells. Immunofluorescence analysis was performed on H5V cells as previously described [137].

Quantification of tissue vascularization. To quantify vascularization on mice tissue sections, blood vessels were first detected by immunostaining for the endothelial cell marker vWF. Digital images of an average of 40 different microscopic fields (at x200 final magnification) of each mesenteric tissue, obtained from five individual mice per group, were then acquired using a Zeiss microscope and an AxioCam colour digital camera (Carl Zeiss Vision, Germany). Zeiss Axio Vision image analysis system (Zeiss) and IPLab software (BioVision Technologies) were used for computerized quantification of immunostained vascular structures. Results were expressed as number of vessels per square millimeter. Vascularization quantification was conducted by two independent investigators who were blinded to the samples´ profiles.

Analysis of protein expression by Western blotting. Animal tissue samples were homogenized using an all-glass homogenizer in ice-cold lysis buffer (20 mM Tris, pH 7.5, 150 mM NaCl, 10 µg/ml aprotinin, 10 µg/ml leupeptin, 10 µg/ml pepstatin, 40 µg/ml phenylmethylsulfonyl fluoride, 10 µM sodium pyrophosphate, 20 µM sodium fluoride, 1% Triton X-100, 1 mM sodium orthovanadate, and 0.1 µM okadaic acid). Cellular debris were pelleted (15,700*g*, 15 min, 4°C) and protein concentration was determined by the Bradford Protein assay (BioRad). Equal amounts of proteins were heated (95°C, 5 min) in SDS- and ß-mercaptoethanol-containing sample buffer and separated by SDS-polyacrylamide gel electrophoresis. After transfer onto a nitrocellulose or PVDF membrane, specific proteins were labeled with the corresponding primary antibodies against CPEB1 (1:500 dilution), phospho-CPEB1 (1:10 dilution), CPEB4 (1:500 dilution), and VEGF (1:1000 dilution). Loading accuracy was evaluated by membrane rehybridization with antibodies against GAPDH (1:1000 dilution) or beta-actin (1:000 dilution). Proteins were then detected using horseradish peroxidase-conjugated secondary antibodies (Stressgen; Sidney, Canada) and an enhanced chemiluminescence detection system. Quantification of protein signals was performed using computer-assisted densitometry.

For Western blot analysis in H5V cells, cell lysis was performed by scraping, using RIPA buffer [25 mM Tris-Cl, pH 7.6, 1% Nonidet P-40 (NP-40), 1% sodium deoxycholate, 0.1% SDS, 150 mM NaCl] containing protease inhibitors (complete EDTA-free protease inhibitor

cocktail, one tablet for 50 ml of lysis buffer, 12715300, Roche Molecular Biochemicals), 100 mM PMSF (phenylmethylsulfonyl fluoride) and 1 mM DTT (dithiothreitol). The lysates were sonicated 5 min at medium intensity with Standard Bioruptor Diagenode. After 10 min of centrifugation at 4ºC and max speed, the supernatants were collected and the pellets discarded. Supernatants were quantified, boiled with Laemmli buffer, resolved by 10% SDS-PAGE and proteins transferred onto a PVDF membrane (Immobilon-P, Millipore) 2 h at 250 mA for CPEB1, VEGF and Tubulin analysis or Nitrocellulose (Whatman, GE Healthcare) 1 h at 100 V for CPEB4 and Tubulin analysis. Membranes were incubated under constant mixing in TBS, 0.05% Tween-20, 5% dry milk for 30 min at room temperature and incubated over night at 4ºC under constant mixing with antibodies directed against CPEB1 (1:200 dilution), VEGF (1:500 dilution) and Tubulin (1:3000 dilution) in TBS, 0.05% Tween-20, 5% dry milk or over night at 4ºC with rabbit polyclonal CPEB4 serum (1:2000 dilution) in TBS, 0.05% Tween-20, 5% dry milk. Membranes were rinsed four times during 7 min with TBS, 0.05% Tween-20 at room temperature and further incubated with horseradish peroxydase-coupled anti-rabbit (1:3000 dilution, GE-Healthcare NA934V) or anti-mouse (1:3000 dilution, GE-Healthcare NXA931) 1 h at room temperature in TBS, 0.05% Tween-20, 5% dry milk under constant mixing. Membranes were rinsed four times during 7 min with TBS, 0.05% Tween-20 at room temperature and immunocomplexes were revealed using ECL western blotting detection reagents (GE-Healthcare RPN 2106) after exposure to Hyperfilm ECL (GE-Healthcare 28-9068-40).

RNA extraction and RT (Reverse Transcription). Total RNA from H5V cells was extracted using RNAspin Mini Kit (GE Healthcare 25-0500-72) and additionally treated with TURBO DNA-free Kit (Ambion inc). Reverse transcription-PCR was performed using RevertAid™ First Strand cDNA Synthesis Kit (K1622 Fermentas), according to manufacturer's instructions.

qPCR. Reverse transcription was performed as indicated in "RNA extraction and RT (Reverse Transcription)" starting with 1 µg of total RNA. qPCR was carried out in a LightCycler 480 (Roche) using SYBRGreen I Master (Roche), 50 ng cDNA per sample and the primers indicated in "oligonucleotides". All the quantifications were normalized to the endogenous control (GLA) using Light Cycler 480 Software.

RNA processing and Real-Time TaqMan polymerase chain reaction (PCR) analysis. Total RNA from rat tissue was isolated and purified using RNAspin Mini Kit (GE Healthcare 25-0500-72), according to the manufacturer's instructions. RNA quality was verified using Agilent's 2100 Bioanalyzer. RNA was reverse-transcribed to complementary DNA (cDNA) using the QuantiTect Reverse Transcription kit (Qiagen). cDNA templates were amplified by real-time TaqMan PCR on an ABI Prism 7900 sequence Detection System (Applied Biosystems, Foster City, CA). Expression of VEGF was analyzed using predesigned gene expression assays obtained from Applied Biosystems, according to the manufacturer's protocol, and reported relative to endogenous control 18S. All PCR reactions were performed in duplicate and using nuclease-free water as no template control.

3'RACE (Rapid Amplification of cDNA ends). Reverse transcription was performed as indicated in "RNA extraction and RT (Reverse Transcription)" starting with 1 µg of total RNA and the 3'RACE antisense primer. 3'RACE was performed using sense primers that specifically amplified VEGF 3'UTR obtained by usage of PAS1 or PAS2 and the T7 antisense primer. PCR products were resolved in 1.8% agarose gel and underwent to southern blotting.

Poly(A) tail assay (RNA-ligation-coupled RT–PCR). Poly(A) tail assay was performed as previously described [141], with some modifications. Total RNA from H5V cells and rats was extracted using RNAspin Mini Kit, additionally treated with TURBO DNA-free Kit and precipitated with Lithium Chloride at final concentration of 2.5 M. 6 µg of total RNA were incubated 30 min at 37ºC in presence of 0.2 µl of oligo (dT) 20 µM and 0.2 U of RNase H (M0297S, New England Biolabs) or H2O. Phenol/Chloroform extraction was performed to purify the RNA. 4 µg of RNA were ligated to 0.4 µg SP2 anchor primer in a 10 µl reaction using T4 RNA ligase (New England Biolabs M0204L) according to the manufacturer's instructions. The whole 10 µl RNA ligation product was used in a 50 µl reverse transcription performed with RevertAid™ First Strand cDNA Synthesis Kit using 0.4µg ASP2T antisense primer. 1 µl of cDNA was used to perform 50 µl PCR reactions using BioTaq Polimerase (Bio21040, Bioline). PCR products were resolved in 2% agarose gel and underwent to southern blotting.

Southern blotting. Agarose gels used in 3'RACE analysis or Poly(A) tail assay were incubated in denaturation solution (1,5 M NaCl, 0,5 M NaOH) during 30' under constant soft agitation and neutralized by incubating with neutralization solution (1 M Tris, 1,5 M NaCl pH 7.4) for 30 min under soft agitation. After over night transfer, DNA was cross-linked (254 nm; 0.12 J) to nylon membrane (0.45 µm, Pall Corporation). The membrane was pre-hybridized with Church buffer during 3 h, hybridized with 32P-labelled probe (indicated in "Oligonucleotides") for 12 h, rinsed with washing buffer (SSC 1X, 0.1% SDS) until background signal removal and exposed to Phosphorimager screen.

RIP (RNA immunoprecipitation) RT-PCR. RIP was performed as described before [142] with some modifications. Briefly, H5V cells were cultured in DMEM supplemented with 10% FBS up to 90% confluence, rinsed twice with 10 ml of PBS and incubated with FBS free DMEM, 1% Formaldehyde 10 min at room temperature under constant soft agitation to crosslink RNA-binding proteins to the target RNAs. Cross-linking reaction was quenched adding Glycine to final concentration of 0.25M and incubating the cells at room temperature for 5 min under constant soft agitation. The cells were washed twice with 10 ml of PBS and lysated with scraper and RIPA buffer (25 mM Tris-Cl, pH 7.6, 1% Nonidet P-40 (NP-40), 1% sodium deoxycholate, 0.1% SDS, 100 mM EDTA, 150 mM NaCl) containing protease inhibitors (complete EDTA-free protease inhibitor cocktail, one tablet for 50 ml of lysis buffer), RNase inhibitors (200 U/ml EO0281 Termo Scientific), sonicated 10 min at low intensity with Standard Bioruptor Diagenode. After 10 min of centrifugation max speed at 4ºC, the supernatants were collected and the pellet discarded. Supernatants were precleared and immunoprecipitated with 10 µg of anti-CPEB4 antibody (Abcam) or anti-CPEB1 antibody (ProTein Tech) or with 10 µg of rabbit IgG (15006 Sigma) bound to 50 µl of Dynabeads Protein A (100-02D Invitrogen) for 4h at 4ºC on rotation. Beads-immunoprecipitated complexes were washed 10 times with cold RIPA buffer supplemented with RNase inhibitors. Beads-immunoprecipitated complexes were resuspended in 200 µl of proteinase K buffer, 70 µg of proteinase K (3115852001 Roche) and incubated 40 min at 30ºC. RNA was extracted using RNA microextraction kit (74004 Qiagen) according to manufacturer's instructions and retrotranscribed as indicated in (RNA extraction and RT (Reverse Transcription)" using random primers (Roche). After PCR, amplification products were resolved in 2% agarose gel.

To perform RIP RT-PCR in rat tissues, samples were homogenized using an all-glass homogenizer in ice-cold lysis buffer containing 10 mM HEPES, pH 7.0, 100 mM KCl, 5 mM $MgCl_2$, 250 mM sacarose, 0.5% NP-40, 1 mM DTT, protease inhibitor cocktail (Roche), 100 U/ml RNase inhibitor (Fermentas) and 2 mM vanadyl rybonucleoside complexes solution (Sigma). Cellular debris were pelleted (15,700*g*, 15 min, 4°C) and protein concentration was determined by the Bradford Protein assay (BioRad). Supernatants were precleared and immunoprecipitated with 2 mg of anti-CPEB1 antibody (Abcam) or with 2 mg of rabbit IgG (15006 Sigma) bound to 20 ml of protein G PLUS (Santa Cruz), overnight, at 4ºC on rotation. Beads-immunoprecipitated complexes were washed 10 times with cold lysis buffer buffer supplemented with RNase inhibitors, treated with DNase I-RNase-free (Roche) 10 min at 37ºC, resuspended in 200 µl of proteinase K buffer, 35 µg of proteinase K (3115852001 Roche), and incubated 30 min at 50ºC. The protein-bound RNAs were purified by phenol–chloroform extraction. The RNA extracted was used for the retrotranscription, performed with the 3' Race primer with the MLuV reverse transcriptase from Fermentas, following the manufacturer's instructions. After PCR, amplification products were resolved in 2% agarose gel. Quantification of RNA immunoprecipitation was performed by Real-Time TaqMan Polymerase Chain Reaction (PCR). The fold enrichment of target sequences in the immunoprecipitated (IP) compared with input fractions was calculated using the comparative Ct (the number of cycles required to reach a threshold concentration) method with the equation 2Ct(IP)_Ct(Ref) and normalized with GAPDH. Then, we considered 1 the value obtained for VEGF immunoprecipitated with CPEB1.

Matrigel tube formation assay. Twenty-four hours before performing tube formation assay, GFR (Grow Factor Reduced) Matrigel (356231 BD Biosciences) was incubated at 4ºC for slow thawing. Liquid Matrigel was added to a 24 wells plate (300 µl/well) previously chilled at -20ºC. The plate was then incubated at 37ºC during 1h to allow the Matrigel to solidify. H5V cells (10^5/well) were plated in presence of fresh medium (DMEM + 10% FBS, 2mM L-glutammine, 1% penicillin/streptomycin) only or fresh medium supplemented with either conditioned medium (ratio 1:1) or 40 ng/ml VEGFA (V4512-5UG Sigma), incubated at 37ºC and 5% CO2 during 15h. Medium was removed, endotubes rinsed twice with PBS and fixed with 4% paraformaldehyde. Endotubes formation was evaluated by inverted microscopy (X100) and scored as previously described [143]: 0, individual cells, well separated; 1, cells

begin to migrate and align themselves; 2, capillary tubes visible, no sprouting; 3, sprouting of new capillary tubes visible; 4, closed polygons begin to form; 5, complex mesh-like structures develop.

Translation of luciferase reporters in H5V cells. For RNA synthesis, plasmids were linearized by restriction enzyme digestion and transcription reaction was performed using mMACHINE® T7 Kit (AM1344 Ambion). Firefly and Renilla mRNAs were co-transfected (Ratio 5:1) into H5V cells using Metafectene Pro (TO40-1.0 Biontex), according to manufacturer's instructions. Luciferase activity was measured using the Dual-Luciferase reporter assay system (E1960 Promega) and normalized against mRNA levels quantified by quantitative PCR.

Statistical analysis. Data are presented as mean±S.E.M., mean±S.D., or mean±Range, as indicated in the corresponding Figure Legends. Results that were normally distributed were compared with parametric statistical procedures (two-tailed Student *t* test and two-way analysis of variance (ANOVA) followed by the Bonferroni´s test for multiple comparisons). For non-parametric data, we used the Kruskall-Wallis one-way analysis of variance and the Mann-Whitney U test. *P* values of less than 0.05 were considered statistically significant.

Table 1: Clinical data of the patients at the moment of liver sampling. Liver samples were obtained from three patients with HCV-related cirrhosis and portal hypertension. The following table summarizes the main characteristics of the patients:

Gender and age	Source of the liver sample	Stage of the disease and Child-Pugh score	HVPG	Histology description
Female, 62 y/o	Liver biopsy	Compensated cirrhosis; no varices; Child A5	7.5 mmHg	Micronodular cirrhosis with mild parenchymal and periseptal necroinflammatory activity
Male, 63 y/o	Explanted liver on transplantation	Decompensated cirrhosis; large esophageal varices; Child B9	18.5 mmHg	Micronodular cirrhosis without parenchymal necroinflammatory activity; marked perinodular biliary duct proliferation
Male, 50 y/o	Explanted liver on transplantation	Decompensated cirrhosis; small esophageal varices; Child C10	20.5 mmHg	Cirrhosis predominantly micronodular without parenchymal necroinflammatory activity; moderate linfocitary periseptal infiltrate

SUPPLEMENTARY FIGURES

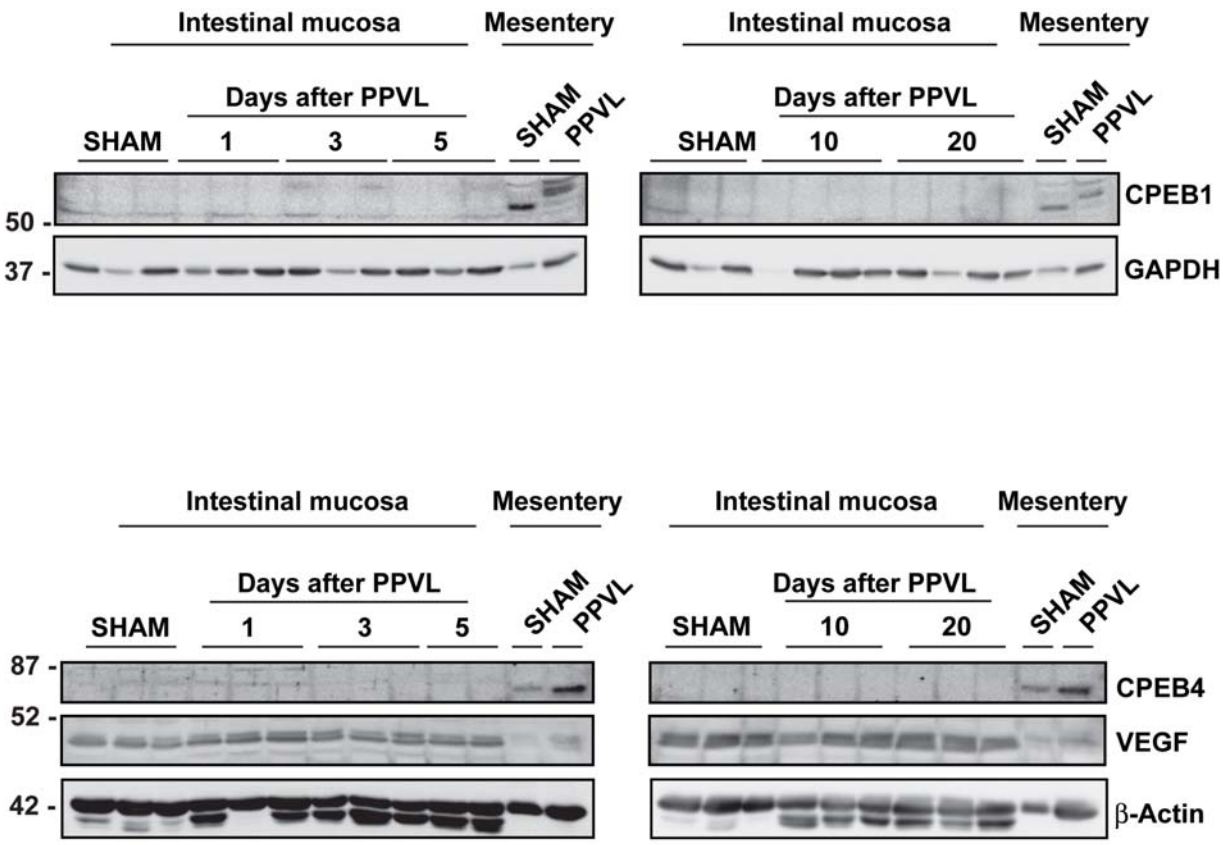

Supplementary figure 1. Expression of CPEB and VEGF proteins in the intestinal mucosa of portal hypertensive rats. (a) Western blotting of CPEB1 (*top*), and CPEB4 and VEGF proteins (*bottom*) in the intestinal mucosa at different time points after inducing portal hypertension by partial portal vein ligation (PPVL) and in sham-operated control rats (SHAM). Protein expression in the mesentery of PPVL and SHAM control rats is also shown. β-Actin and GAPDH are used as loading controls. Results demonstrate that CPEB1 and CPEB4 proteins are almost undetected in the intestinal mucosa of PPVL and SHAM rats, and that VEGF expression in the intestinal mucosa does not change during progression of portal hypertension. **In collaboration with Mercedes Fernandez's group.**

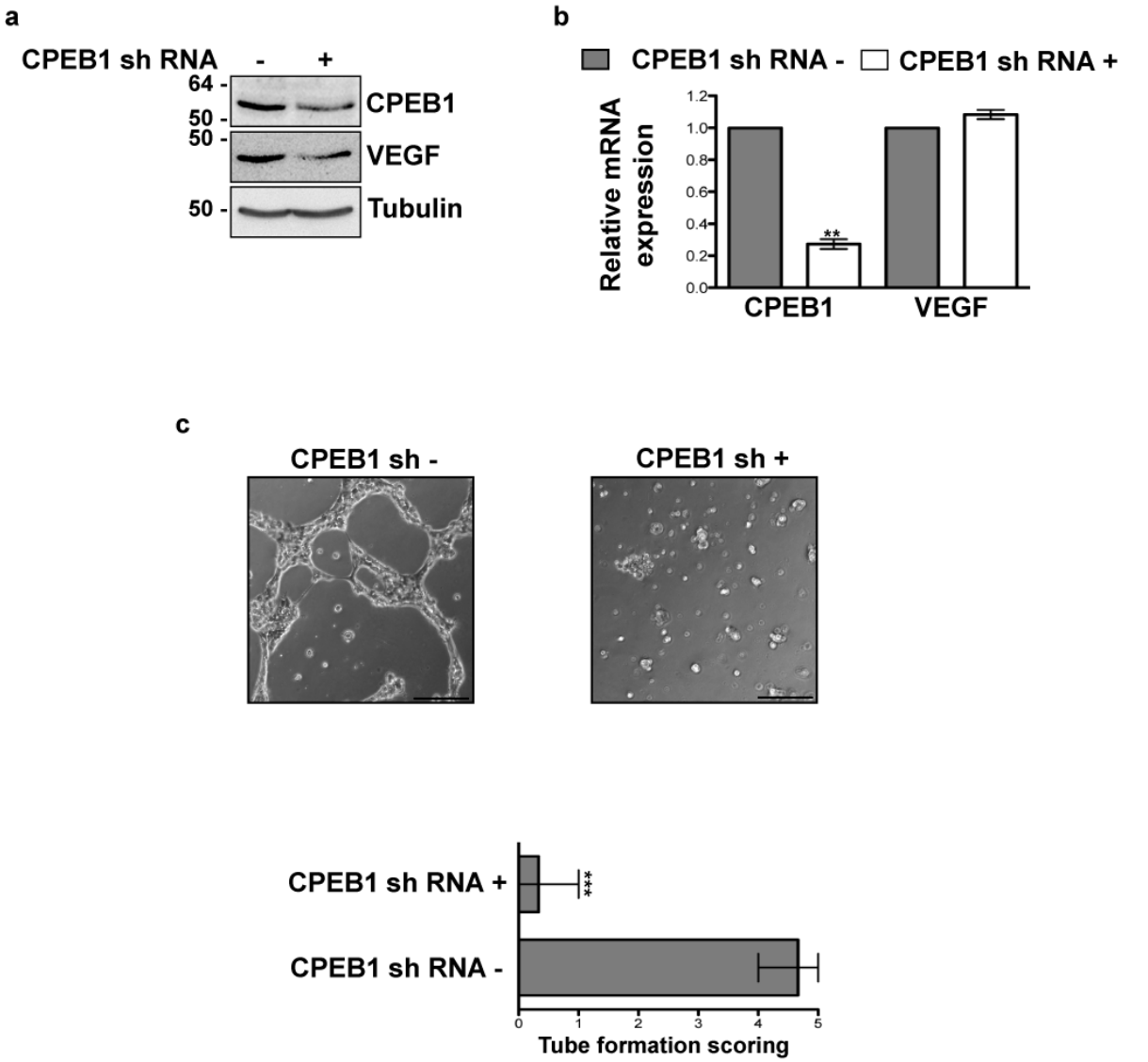

Supplementary figure 2. *In Vitro* characterization of the effects of CPEB1 depletion in H5V cells. H5V cells constitutively expressing control shRNA or CPEB1 shRNA were generated as described in "Materials and Methods". **a.** CPEB1 and VEGF protein concentrations in CPEB1 knockdown and control cells, analyzed by western blot. Tubulin is used as loading control. The results of a representative experiment (n=3) are shown. **b.** CPEB1 and VEGF mRNA expression levels measured in CPEB1 knockdown and control cells. Data are mean ± S.D. *P* values (obtained by Student Test) are relative to control shRNA. ***$P \leq 0.0005$. Values correspond to three independent experiments. **c.** *In vitro* angiogenesis assay (top) and its quantification (bottom) performed seeding H5V cells on GFR (Grow Factor Reduced) Matrigel-coated dishes. Cells transfected with control shRNAs were used as control. Tube formation scoring was performed as described in "Materials and Methods". The results are representative of three independent experiments. Data are mean ± range. *P* values (obtained by Student Test) are relative to cells transfected with control shRNA. ***$P \leq 0.0005$. Scale bar 200 μm.

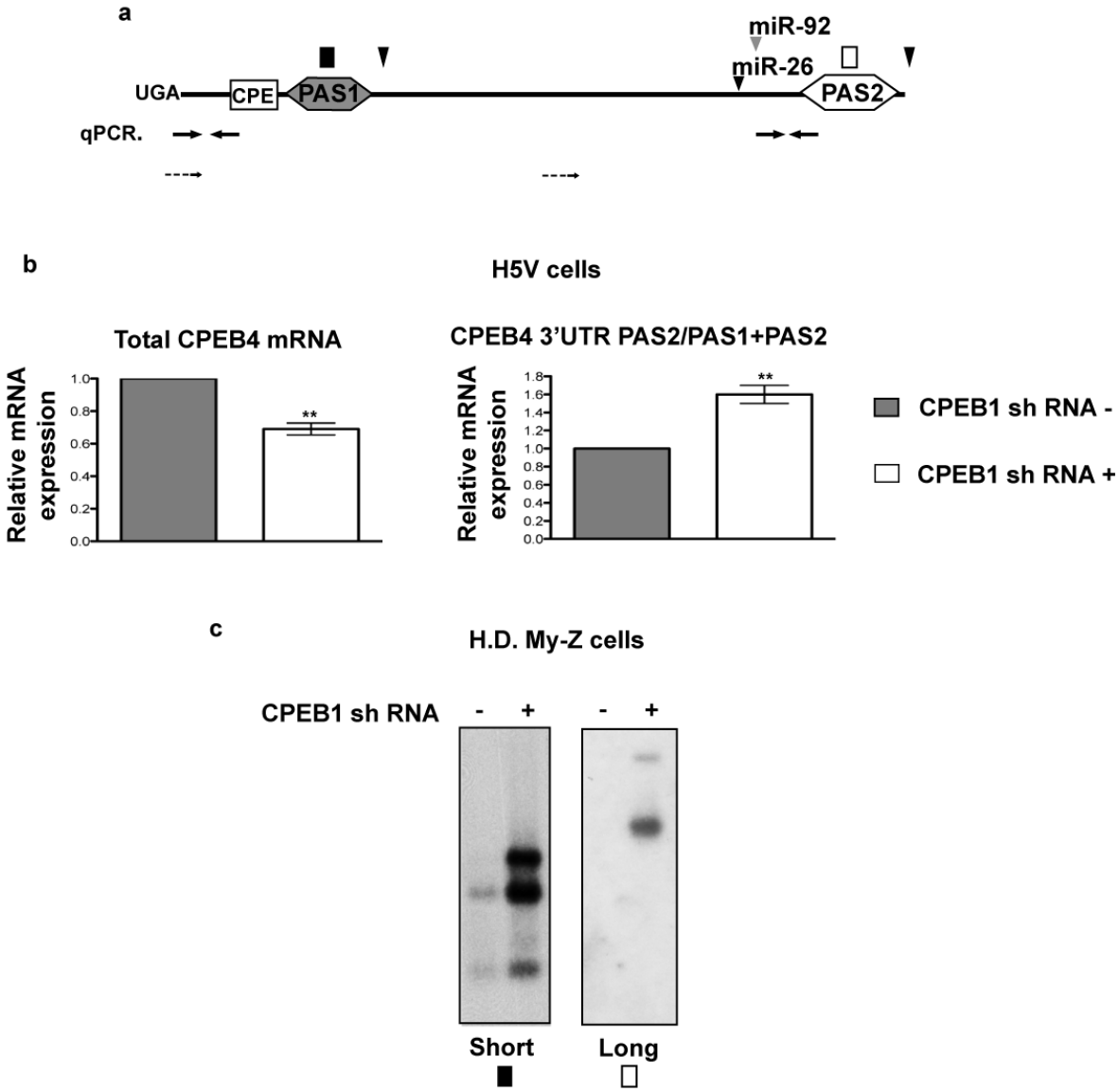

Supplementary figure 3. Analysis of the effects of CPEB1 depletion on CPEB4 3'UTR formation in H5V and H.D. My-Z cells. (a) Simplified representation of CPEB4 3'UTR. CPE (Cytoplasmic Polyadenylation Elements) and PAS (Poly Adenylation Signal) are indicated in white polygons (consensus sequences) or grey polygons (not consensus sequences). miR-26 and miR-92 binding sites are indicated with arrowheads. Single headed arrows indicate the position of the primers used for quantitative PCR analysis. (b) The relative expression levels of CPEB4 mRNA are measured in control and CPEB1 knockdown H5V cells (left panel). The relative expression levels of long CPEB4 3'UTR (obtained using PAS2) normalized by total CPEB4 mRNA levels are shown in the right panel. Data are mean ± S.D. *P* values (obtained by Student Test) are relative to not induced cells. ***P*≤ 0.005. Values correspond to three independent experiments. (c) CPEB4 3'UTR cleavage analysis performed by 3'RACE/southern blot in CPEB1 knockdown H.D. My-Z cells. **In collaboration with Alessio Bava.**

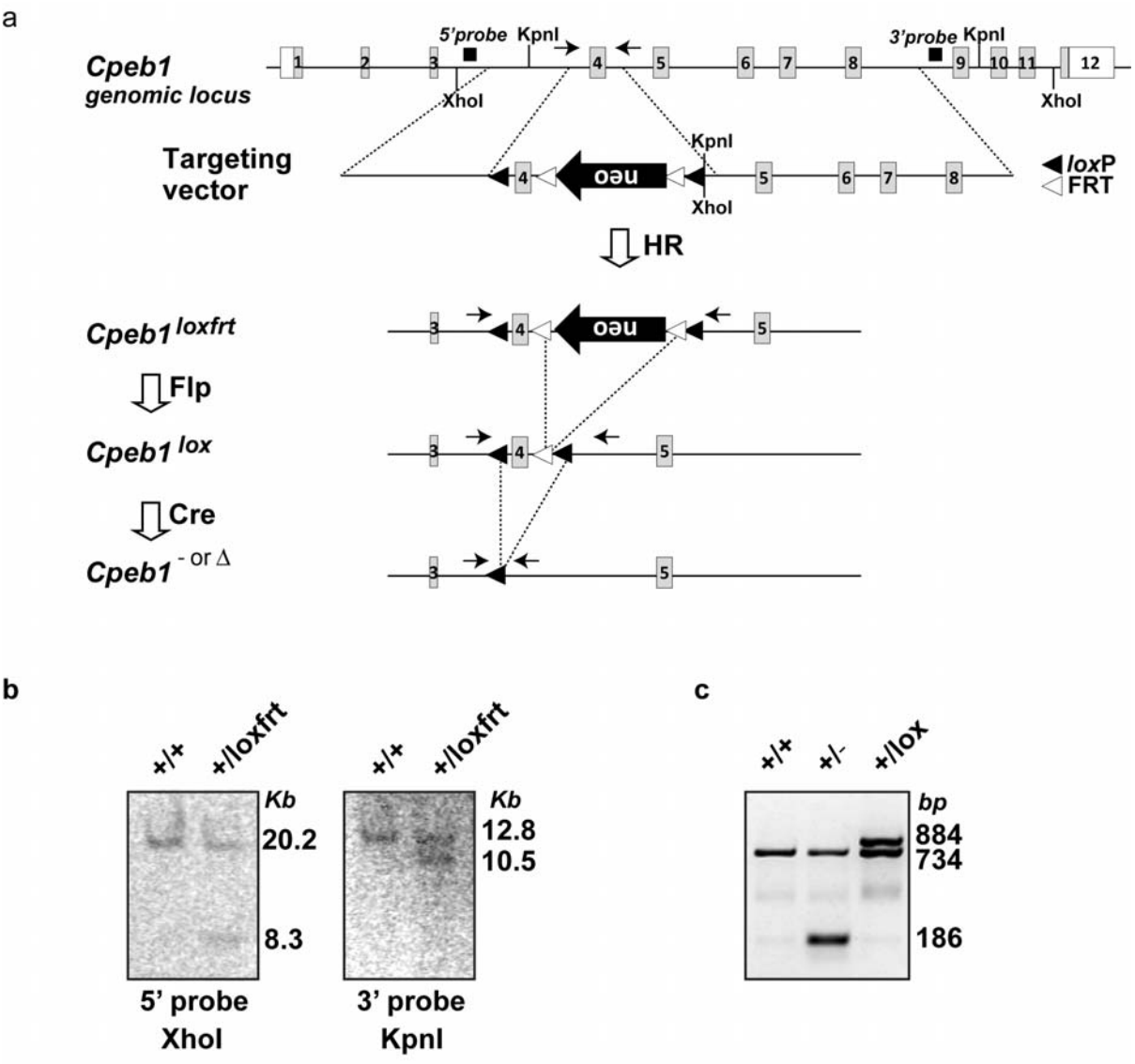

Supplementary figure 4. Generation of CPEB1-deficient mice. a. Schematic representation of the Cpeb1 alleles used in this study. The mouse Cpeb1 locus encoding CPEB1 contains 12 exons (boxes) including non-coding (open boxes) or protein-coding (grey boxes) sequences. *lox*P (black triangles) and FRT (white triangles) sites were used to flank exon4 or the neo-resistance cassette (black). The neo cassette was deleted by expressing FlpO in the recombinant ES cells [138]. Further excision of exon4 was achieved by Cre mediated DNA recombination leading to a frame-shift and loss of function Cpeb1^{--} allele. Inducible activation of Cre by tamoxifen turns the conditional Cpeb1^{lox} allele into the deleted Cpeb1Δ allele. HR, homologous recombination. **b.** Southern blot analysis of recombinant embryonic stem (ES) cells showing a clone that underwent HR. DNA was digested with XhoI and KpnI and hybridized with the 5' and 3' probes, respectively. The position of both probes is shown in panel a. **c.** PCR amplification of wild-type (+), conditional (lox) and null (-) Cpeb1 alleles using the oligonucleotides represented by arrows in panel a. **In collaboration with Carlos Maillo and Gonzalo Fernandez-Miranda.**

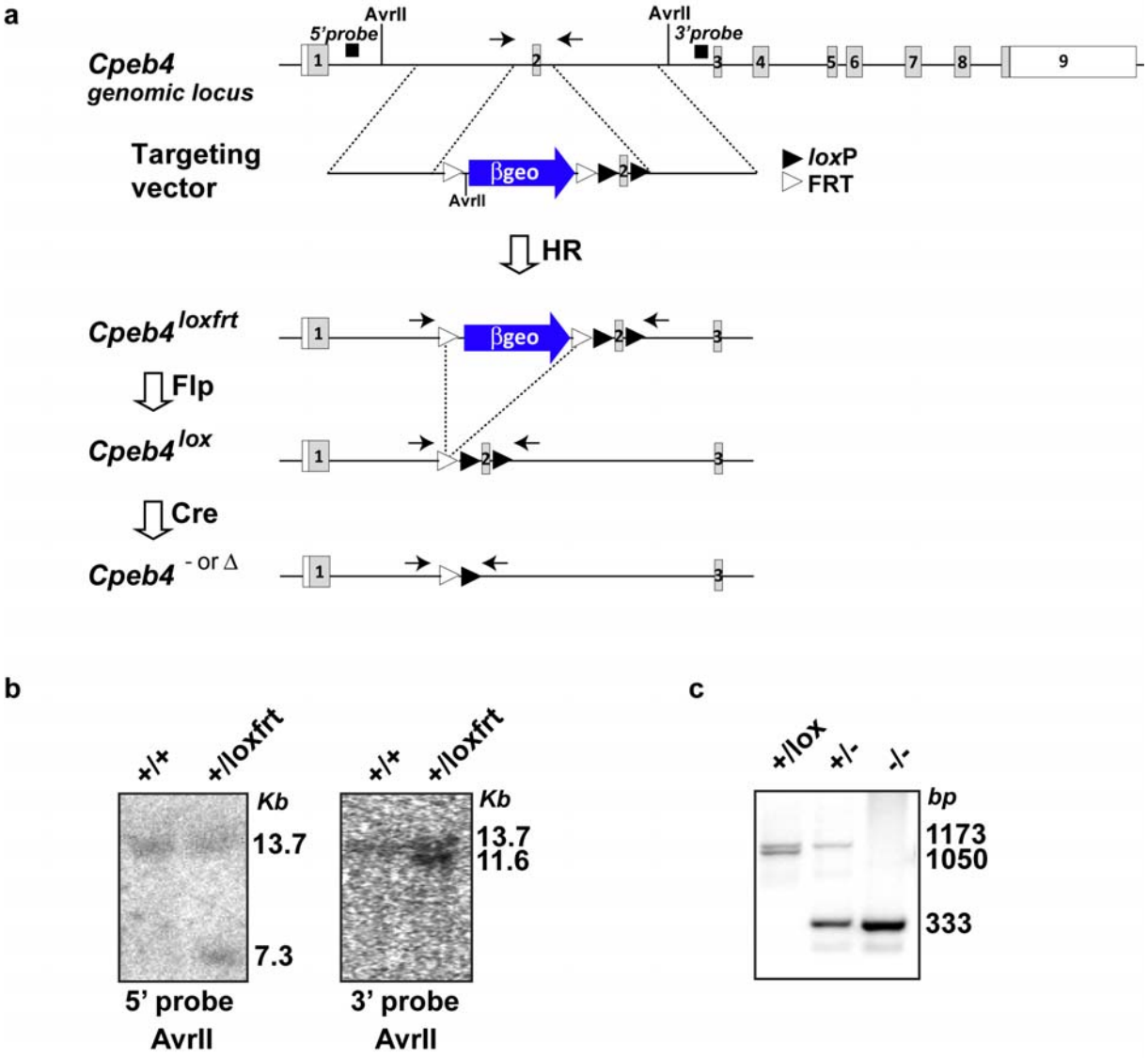

Supplementary figure 5. Generation of CPEB4-deficient mice. **a.** Schematic representation of the Cpeb4 alleles used in this study. The mouse Cpeb4 locus encoding CPEB4 contains 9 exons (boxes) including non-coding (open boxes) or protein-coding (grey boxes) sequences. *lox*P (black triangles) and FRT (white triangles) sites were used to flank exon2 or the bgeo cassette (blue), which encodes for β-galactosidase and the neo-resistance gene. The bgeo cassette contains poly-A sequences for termination of transcription and is preceded by a spliced acceptor so that, expression of β-galactosidase and the neo-resistance gene is driven by the CPEB4 regulatory elements. The βgeo cassette was subsequently deleted by mating Cpeb4$^{+/loxfrt}$ with Flp mice [139]. Further excision of exon2 was achieved by Cre mediated DNA recombination leading to a frame-shift and loss of function Cpeb4- allele. Inducible activation of Cre by tamoxifen turns the conditional Cpeb4^{lox} allele into the deleted Cpeb4Δ allele. HR, homologous recombination. **b.** Southern blot analysis from genomic DNA of Cpeb4 $^{+/loxfrt}$ mice. DNA was digested with AvrII and hybridized with the 5' and 3' probes. The position of both probes is shown in panel a. **c.** PCR amplification of wild-type (+), conditional (lox) and null (-) Cpeb4 alleles using the oligonucleotides represented by arrows in panel a. **In collaboration with Gonzalo Fernandez-Miranda.**

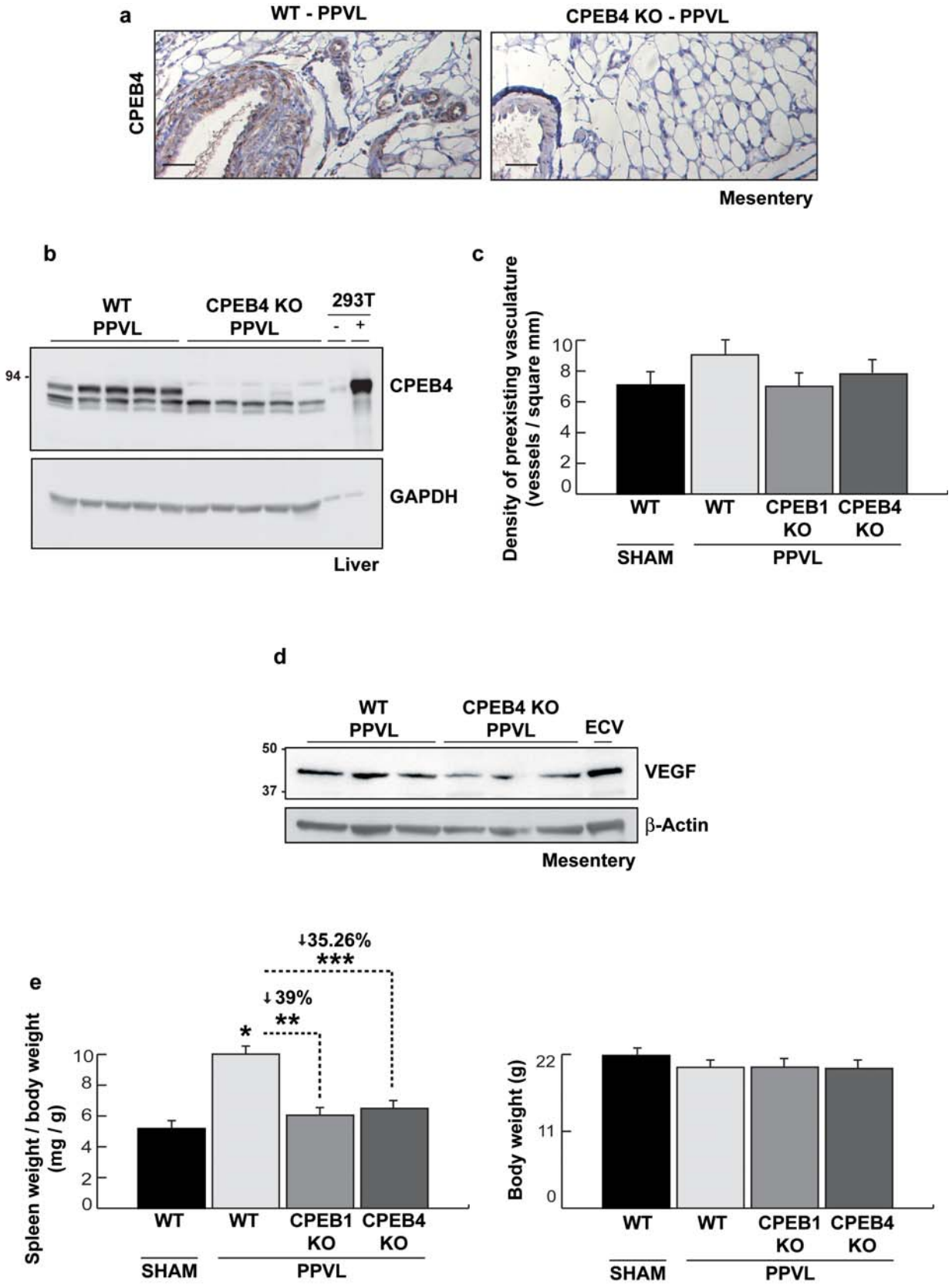

Supplementary figure 6. Studies in CPEB1 and CPEB4 inducible knockout mice a. Representative photomicrograghs of CPEB4 immunostained mesentery sections from wild

type (WT) mice and CPEB4 knockout (KO) mice, 8 days after inducing portal hypertension by partial portal vein ligation (PPVL). Scale bar: 50 μ
m. **b.** Western blotting of CPEB4 protein in the liver of WT mice and CPEB4 KO mice, 8 days after PPVL. Results demonstrate effective depletion of CPEB4 in the liver of CPEB4 KO mice. **c.** Quantification of the vascular density of preexisting vessels (vessels per square millimeter) in the mesentery of wild type mice and the CPEB1 and CPEB4 knockout mice after PPVL. Results from wild type mice subjected to a control sham operation (SHAM) are also shown. Data are as mean±S.E.M. **d.** Western blotting of VEGF protein in the mesentery of WT mice and CPEB4 KO mice, 8 days after PPVL. Results demonstrate reduction of VEGF protein in response to CPEB4 depletion in the mesentery of portal hypertensive mice. **e.** Measurement of spleen weight per body weight *(left)* and body weight *(right)* in WT mice and CPEB1 and CPEB4 knockout mice, 8 days after inducing portal hypertension by PPVL, and also in WT mice subjected to a sham operation. WT mice presented splenomegaly after PPVL, compared with WT mice subjected to a sham operation (SHAM). The increased spleen weight of PPVL mice was significantly prevented by CPEB1 or CPEB4 depletion. Data are as mean±S.E.M. **P*=0.005, ***P*=0.01, *** *P*=0.008. **In collaboration with Mercedes Fernandez's group, Gonzalo Fernandez-Miranda and Carlos Maillo.**

REFERENCES

1. Wacker, A. & Gerhardt, H. Endothelial development taking shape. *Current opinion in cell biology* **23**, 676-685 (2011).
2. Gerhardt, H. VEGF and endothelial guidance in angiogenic sprouting. *Organogenesis* **4**, 241-246 (2008).
3. Adams, R.H. & Alitalo, K. Molecular regulation of angiogenesis and lymphangiogenesis. *Nature reviews. Molecular cell biology* **8**, 464-478 (2007).
4. Phng, L.K. & Gerhardt, H. Angiogenesis: a team effort coordinated by notch. *Developmental cell* **16**, 196-208 (2009).
5. Nagy, J.A., Dvorak, A.M. & Dvorak, H.F. VEGF-A and the induction of pathological angiogenesis. *Annual review of pathology* **2**, 251-275 (2007).
6. Karamysheva, A.F. Mechanisms of angiogenesis. *Biochemistry. Biokhimiia* **73**, 751-762 (2008).
7. Ferrara, N. & Davis-Smyth, T. The biology of vascular endothelial growth factor. *Endocrine reviews* **18**, 4-25 (1997).
8. Ferrara, N. Role of vascular endothelial growth factor in regulation of physiological angiogenesis. *American journal of physiology. Cell physiology* **280**, C1358-1366 (2001).
9. Chung, A.S. & Ferrara, N. Developmental and pathological angiogenesis. *Annual review of cell and developmental biology* **27**, 563-584 (2011).
10. Dvorak, H.F. Vascular permeability factor/vascular endothelial growth factor: a critical cytokine in tumor angiogenesis and a potential target for diagnosis and therapy. *Journal of clinical oncology : official journal of the American Society of Clinical Oncology* **20**, 4368-4380 (2002).
11. Adamis, A.P.*, et al.* Increased vascular endothelial growth factor levels in the vitreous of eyes with proliferative diabetic retinopathy. *American journal of ophthalmology* **118**, 445-450 (1994).
12. Aiello, L.P.*, et al.* Suppression of retinal neovascularization in vivo by inhibition of vascular endothelial growth factor (VEGF) using soluble VEGF-receptor chimeric proteins. *Proceedings of the National Academy of Sciences of the United States of America* **92**, 10457-10461 (1995).
13. Fernandez, M.*, et al.* Angiogenesis in liver disease. *Journal of hepatology* **50**, 604-620 (2009).

14. Sanz-Cameno, P., Trapero-Marugan, M., Chaparro, M., Jones, E.A. & Moreno-Otero, R. Angiogenesis: from chronic liver inflammation to hepatocellular carcinoma. *Journal of oncology* **2010**, 272170 (2010).
15. Bosch, J., Pizcueta, P., Feu, F., Fernandez, M. & Garcia-Pagan, J.C. Pathophysiology of portal hypertension. *Gastroenterology clinics of North America* **21**, 1-14 (1992).
16. Abraldes, J.G., Angermayr, B. & Bosch, J. The management of portal hypertension. *Clinics in liver disease* **9**, 685-713, vii (2005).
17. Lee, S.S., Girod, C., Braillon, A., Hadengue, A. & Lebrec, D. Hemodynamic characterization of chronic bile duct-ligated rats: effect of pentobarbital sodium. *The American journal of physiology* **251**, G176-180 (1986).
18. Abraldes, J.G., Pasarin, M. & Garcia-Pagan, J.C. Animal models of portal hypertension. *World journal of gastroenterology : WJG* **12**, 6577-6584 (2006).
19. Vorobioff, J., Bredfeldt, J.E. & Groszmann, R.J. Hyperdynamic circulation in portal-hypertensive rat model: a primary factor for maintenance of chronic portal hypertension. *The American journal of physiology* **244**, G52-57 (1983).
20. Aller, M.A., Arias, J.L., Cruz, A. & Arias, J. Inflammation: a way to understanding the evolution of portal hypertension. *Theoretical biology & medical modelling* **4**, 44 (2007).
21. Core, L.J. & Lis, J.T. Transcription regulation through promoter-proximal pausing of RNA polymerase II. *Science* **319**, 1791-1792 (2008).
22. Kapranov, P*., et al.* RNA maps reveal new RNA classes and a possible function for pervasive transcription. *Science* **316**, 1484-1488 (2007).
23. Shatkin, A.J. & Manley, J.L. The ends of the affair: capping and polyadenylation. *Nature structural biology* **7**, 838-842 (2000).
24. Shuman, S. Structure, mechanism, and evolution of the mRNA capping apparatus. *Progress in nucleic acid research and molecular biology* **66**, 1-40 (2001).
25. Furuichi, Y., LaFiandra, A. & Shatkin, A.J. 5'-Terminal structure and mRNA stability. *Nature* **266**, 235-239 (1977).
26. Sonenberg, N. Cap-binding proteins of eukaryotic messenger RNA: functions in initiation and control of translation. *Progress in nucleic acid research and molecular biology* **35**, 173-207 (1988).
27. Patel, A.A. & Steitz, J.A. Splicing double: insights from the second spliceosome. *Nature reviews. Molecular cell biology* **4**, 960-970 (2003).

28. Smith, C.W. & Valcarcel, J. Alternative pre-mRNA splicing: the logic of combinatorial control. *Trends in biochemical sciences* **25**, 381-388 (2000).
29. Wang, Z. & Burge, C.B. Splicing regulation: from a parts list of regulatory elements to an integrated splicing code. *RNA* **14**, 802-813 (2008).
30. Matlin, A.J., Clark, F. & Smith, C.W. Understanding alternative splicing: towards a cellular code. *Nature reviews. Molecular cell biology* **6**, 386-398 (2005).
31. Wahle, E. & Kuhn, U. The mechanism of 3' cleavage and polyadenylation of eukaryotic pre-mRNA. *Progress in nucleic acid research and molecular biology* **57**, 41-71 (1997).
32. Zhao, J., Hyman, L. & Moore, C. Formation of mRNA 3' ends in eukaryotes: mechanism, regulation, and interrelationships with other steps in mRNA synthesis. *Microbiology and molecular biology reviews : MMBR* **63**, 405-445 (1999).
33. Gil, A. & Proudfoot, N.J. Position-dependent sequence elements downstream of AAUAAA are required for efficient rabbit beta-globin mRNA 3' end formation. *Cell* **49**, 399-406 (1987).
34. Gil, A. & Proudfoot, N.J. A sequence downstream of AAUAAA is required for rabbit beta-globin mRNA 3'-end formation. *Nature* **312**, 473-474 (1984).
35. Takagaki, Y., Ryner, L.C. & Manley, J.L. Four factors are required for 3'-end cleavage of pre-mRNAs. *Genes & development* **3**, 1711-1724 (1989).
36. MacDonald, C.C., Wilusz, J. & Shenk, T. The 64-kilodalton subunit of the CstF polyadenylation factor binds to pre-mRNAs downstream of the cleavage site and influences cleavage site location. *Molecular and cellular biology* **14**, 6647-6654 (1994).
37. Murthy, K.G. & Manley, J.L. The 160-kD subunit of human cleavage-polyadenylation specificity factor coordinates pre-mRNA 3'-end formation. *Genes & development* **9**, 2672-2683 (1995).
38. Meyer, S., Urbanke, C. & Wahle, E. Equilibrium studies on the association of the nuclear poly(A) binding protein with poly(A) of different lengths. *Biochemistry* **41**, 6082-6089 (2002).
39. Keller, R.W.*, et al.* The nuclear poly(A) binding protein, PABP2, forms an oligomeric particle covering the length of the poly(A) tail. *Journal of molecular biology* **297**, 569-583 (2000).

40. Mangus, D.A., Evans, M.C. & Jacobson, A. Poly(A)-binding proteins: multifunctional scaffolds for the post-transcriptional control of gene expression. *Genome biology* **4**, 223 (2003).
41. Tian, B., Hu, J., Zhang, H. & Lutz, C.S. A large-scale analysis of mRNA polyadenylation of human and mouse genes. *Nucleic acids research* **33**, 201-212 (2005).
42. Hook, A.G. & Kellems, R.E. Localization and sequence analysis of poly(A) sites generating multiple dihydrofolate reductase mRNAs. *The Journal of biological chemistry* **263**, 2337-2343 (1988).
43. Setzer, D.R., McGrogan, M., Nunberg, J.H. & Schimke, R.T. Size heterogeneity in the 3' end of dihydrofolate reductase messenger RNAs in mouse cells. *Cell* **22**, 361-370 (1980).
44. Wahle, E. & Ruegsegger, U. 3'-End processing of pre-mRNA in eukaryotes. *FEMS microbiology reviews* **23**, 277-295 (1999).
45. Jenal, M.*, et al.* The poly(A)-binding protein nuclear 1 suppresses alternative cleavage and polyadenylation sites. *Cell* **149**, 538-553 (2012).
46. Bava, F.A.*, et al.* CPEB1 coordinates alternative 3'-UTR formation with translational regulation. *Nature* (2013).
47. Zhang, H., Lee, J.Y. & Tian, B. Biased alternative polyadenylation in human tissues. *Genome biology* **6**, R100 (2005).
48. Mayr, C. & Bartel, D.P. Widespread shortening of 3'UTRs by alternative cleavage and polyadenylation activates oncogenes in cancer cells. *Cell* **138**, 673-684 (2009).
49. Licatalosi, D.D.*, et al.* HITS-CLIP yields genome-wide insights into brain alternative RNA processing. *Nature* **456**, 464-469 (2008).
50. Flavell, S.W.*, et al.* Genome-wide analysis of MEF2 transcriptional program reveals synaptic target genes and neuronal activity-dependent polyadenylation site selection. *Neuron* **60**, 1022-1038 (2008).
51. Ji, Z., Lee, J.Y., Pan, Z., Jiang, B. & Tian, B. Progressive lengthening of 3' untranslated regions of mRNAs by alternative polyadenylation during mouse embryonic development. *Proceedings of the National Academy of Sciences of the United States of America* **106**, 7028-7033 (2009).

52. Nagalakshmi, U.*, et al.* The transcriptional landscape of the yeast genome defined by RNA sequencing. *Science* **320**, 1344-1349 (2008).

53. Cole, C.N. & Scarcelli, J.J. Transport of messenger RNA from the nucleus to the cytoplasm. *Current opinion in cell biology* **18**, 299-306 (2006).

54. Stewart, M. Ratcheting mRNA out of the nucleus. *Molecular cell* **25**, 327-330 (2007).

55. Strasser, K.*, et al.* TREX is a conserved complex coupling transcription with messenger RNA export. *Nature* **417**, 304-308 (2002).

56. Aguilera, A. Cotranscriptional mRNP assembly: from the DNA to the nuclear pore. *Current opinion in cell biology* **17**, 242-250 (2005).

57. Moore, M.J. From birth to death: the complex lives of eukaryotic mRNAs. *Science* **309**, 1514-1518 (2005).

58. Preiss, T. & M, W.H. Starting the protein synthesis machine: eukaryotic translation initiation. *BioEssays : news and reviews in molecular, cellular and developmental biology* **25**, 1201-1211 (2003).

59. Gebauer, F. & Hentze, M.W. Molecular mechanisms of translational control. *Nature reviews. Molecular cell biology* **5**, 827-835 (2004).

60. Wells, S.E., Hillner, P.E., Vale, R.D. & Sachs, A.B. Circularization of mRNA by eukaryotic translation initiation factors. *Molecular cell* **2**, 135-140 (1998).

61. Pestova, T.V.*, et al.* Molecular mechanisms of translation initiation in eukaryotes. *Proceedings of the National Academy of Sciences of the United States of America* **98**, 7029-7036 (2001).

62. Lorsch, J.R. & Herschlag, D. Kinetic dissection of fundamental processes of eukaryotic translation initiation in vitro. *The EMBO journal* **18**, 6705-6717 (1999).

63. Pestova, T.V.*, et al.* The joining of ribosomal subunits in eukaryotes requires eIF5B. *Nature* **403**, 332-335 (2000).

64. Shin, B.S.*, et al.* Uncoupling of initiation factor eIF5B/IF2 GTPase and translational activities by mutations that lower ribosome affinity. *Cell* **111**, 1015-1025 (2002).

65. Jackson, R.J., Hellen, C.U. & Pestova, T.V. The mechanism of eukaryotic translation initiation and principles of its regulation. *Nature reviews. Molecular cell biology* **11**, 113-127 (2010).

66. Spahn, C.M. & Nierhaus, K.H. Models of the elongation cycle: an evaluation. *Biological chemistry* **379**, 753-772 (1998).

67. Ramakrishnan, V. Ribosome structure and the mechanism of translation. *Cell* **108**, 557-572 (2002).

68. Kapp, L.D. & Lorsch, J.R. The molecular mechanics of eukaryotic translation. *Annual review of biochemistry* **73**, 657-704 (2004).

69. Kisselev, L.L. & Buckingham, R.H. Translational termination comes of age. *Trends in biochemical sciences* **25**, 561-566 (2000).

70. Hellen, C.U. & Sarnow, P. Internal ribosome entry sites in eukaryotic mRNA molecules. *Genes & development* **15**, 1593-1612 (2001).

71. Balvay, L., Soto Rifo, R., Ricci, E.P., Decimo, D. & Ohlmann, T. Structural and functional diversity of viral IRESes. *Biochimica et biophysica acta* **1789**, 542-557 (2009).

72. Hellen, C.U. IRES-induced conformational changes in the ribosome and the mechanism of translation initiation by internal ribosomal entry. *Biochimica et biophysica acta* **1789**, 558-570 (2009).

73. Kieft, J.S. Viral IRES RNA structures and ribosome interactions. *Trends in biochemical sciences* **33**, 274-283 (2008).

74. Komar, A.A. & Hatzoglou, M. Cellular IRES-mediated translation: the war of ITAFs in pathophysiological states. *Cell Cycle* **10**, 229-240 (2011).

75. Spriggs, K.A., Stoneley, M., Bushell, M. & Willis, A.E. Re-programming of translation following cell stress allows IRES-mediated translation to predominate. *Biology of the cell / under the auspices of the European Cell Biology Organization* **100**, 27-38 (2008).

76. Lewis, S.M. & Holcik, M. For IRES trans-acting factors, it is all about location. *Oncogene* **27**, 1033-1035 (2008).

77. Bastide, A.*, et al.* An upstream open reading frame within an IRES controls expression of a specific VEGF-A isoform. *Nucleic acids research* **36**, 2434-2445 (2008).

78. Ray, P.S.*, et al.* A stress-responsive RNA switch regulates VEGFA expression. *Nature* **457**, 915-919 (2009).

79. Kurosu, T.*, et al.* HuR keeps an angiogenic switch on by stabilising mRNA of VEGF and COX-2 in tumour endothelium. *British journal of cancer* **104**, 819-829 (2011).

80. Tang, K., Breen, E.C. & Wagner, P.D. Hu protein R-mediated posttranscriptional regulation of VEGF expression in rat gastrocnemius muscle. *American journal of physiology. Heart and circulatory physiology* **283**, H1497-1504 (2002).

81. Onesto, C., Berra, E., Grepin, R. & Pages, G. Poly(A)-binding protein-interacting protein 2, a strong regulator of vascular endothelial growth factor mRNA. *The Journal of biological chemistry* **279**, 34217-34226 (2004).

82. Du, M.*, et al.* VEGF gene expression is regulated post-transcriptionally in macrophages. *The FEBS journal* **273**, 732-745 (2006).

83. Ray, P.S. & Fox, P.L. A post-transcriptional pathway represses monocyte VEGF-A expression and angiogenic activity. *The EMBO journal* **26**, 3360-3372 (2007).

84. Villalba, A., Coll, O. & Gebauer, F. Cytoplasmic polyadenylation and translational control. *Current opinion in genetics & development* **21**, 452-457 (2011).

85. Mendez, R. & Richter, J.D. Translational control by CPEB: a means to the end. *Nature reviews. Molecular cell biology* **2**, 521-529 (2001).

86. Richter, J.D. CPEB: a life in translation. *Trends in biochemical sciences* **32**, 279-285 (2007).

87. Radford, H.E., Meijer, H.A. & de Moor, C.H. Translational control by cytoplasmic polyadenylation in Xenopus oocytes. *Biochimica et biophysica acta* **1779**, 217-229 (2008).

88. Pique, M., Lopez, J.M., Foissac, S., Guigo, R. & Mendez, R. A combinatorial code for CPE-mediated translational control. *Cell* **132**, 434-448 (2008).

89. Belloc, E. & Mendez, R. A deadenylation negative feedback mechanism governs meiotic metaphase arrest. *Nature* **452**, 1017-1021 (2008).

90. Barnard, D.C., Ryan, K., Manley, J.L. & Richter, J.D. Symplekin and xGLD-2 are required for CPEB-mediated cytoplasmic polyadenylation. *Cell* **119**, 641-651 (2004).

91. Wang, X.P. & Cooper, N.G. Comparative in silico analyses of cpeb1-4 with functional predictions. *Bioinformatics and biology insights* **4**, 61-83 (2010).

92. Keleman, K., Kruttner, S., Alenius, M. & Dickson, B.J. Function of the Drosophila CPEB protein Orb2 in long-term courtship memory. *Nature neuroscience* **10**, 1587-1593 (2007).

93. Hasegawa, E., Karashima, T., Sumiyoshi, E. & Yamamoto, M. C. elegans CPB-3 interacts with DAZ-1 and functions in multiple steps of germline development. *Developmental biology* **295**, 689-699 (2006).

94. Si, K.*, et al.* A neuronal isoform of CPEB regulates local protein synthesis and stabilizes synapse-specific long-term facilitation in aplysia. *Cell* **115**, 893-904 (2003).

95. Hake, L.E. & Richter, J.D. CPEB is a specificity factor that mediates cytoplasmic polyadenylation during Xenopus oocyte maturation. *Cell* **79**, 617-627 (1994).

96. Fernandez-Miranda, G. & Mendez, R. The CPEB-family of proteins, translational control in senescence and cancer. *Ageing research reviews* **11**, 460-472 (2012).

97. Balatsos, N.A., Nilsson, P., Mazza, C., Cusack, S. & Virtanen, A. Inhibition of mRNA deadenylation by the nuclear cap binding complex (CBC). *The Journal of biological chemistry* **281**, 4517-4522 (2006).

98. Copeland, P.R. & Wormington, M. The mechanism and regulation of deadenylation: identification and characterization of Xenopus PARN. *RNA* **7**, 875-886 (2001).

99. Gao, M., Fritz, D.T., Ford, L.P. & Wilusz, J. Interaction between a poly(A)-specific ribonuclease and the 5' cap influences mRNA deadenylation rates in vitro. *Molecular cell* **5**, 479-488 (2000).

100. Kim, J.H. & Richter, J.D. Opposing polymerase-deadenylase activities regulate cytoplasmic polyadenylation. *Molecular cell* **24**, 173-183 (2006).

101. Cao, Q. & Richter, J.D. Dissolution of the maskin-eIF4E complex by cytoplasmic polyadenylation and poly(A)-binding protein controls cyclin B1 mRNA translation and oocyte maturation. *The EMBO journal* **21**, 3852-3862 (2002).

102. Cao, Q., Kim, J.H. & Richter, J.D. CDK1 and calcineurin regulate Maskin association with eIF4E and translational control of cell cycle progression. *Nature structural & molecular biology* **13**, 1128-1134 (2006).

103. Minshall, N., Reiter, M.H., Weil, D. & Standart, N. CPEB interacts with an ovary-specific eIF4E and 4E-T in early Xenopus oocytes. *The Journal of biological chemistry* **282**, 37389-37401 (2007).

104. Sarkissian, M., Mendez, R. & Richter, J.D. Progesterone and insulin stimulation of CPEB-dependent polyadenylation is regulated by Aurora A and glycogen synthase kinase-3. *Genes & development* **18**, 48-61 (2004).

105. Mendez, R.*, et al.* Phosphorylation of CPE binding factor by Eg2 regulates translation of c-mos mRNA. *Nature* **404**, 302-307 (2000).

106. Pascreau, G., Delcros, J.G., Cremet, J.Y., Prigent, C. & Arlot-Bonnemains, Y. Phosphorylation of maskin by Aurora-A participates in the control of sequential protein synthesis during Xenopus laevis oocyte maturation. *The Journal of biological chemistry* **280**, 13415-13423 (2005).

107. Kim, J.H. & Richter, J.D. RINGO/cdk1 and CPEB mediate poly(A) tail stabilization and translational regulation by ePAB. *Genes & development* **21**, 2571-2579 (2007).

108. Wakiyama, M., Imataka, H. & Sonenberg, N. Interaction of eIF4G with poly(A)-binding protein stimulates translation and is critical for Xenopus oocyte maturation. *Current biology : CB* **10**, 1147-1150 (2000).

109. Gebauer, F. & Richter, J.D. Mouse cytoplasmic polyadenylylation element binding protein: an evolutionarily conserved protein that interacts with the cytoplasmic polyadenylylation elements of c-mos mRNA. *Proceedings of the National Academy of Sciences of the United States of America* **93**, 14602-14607 (1996).

110. Tay, J., Hodgman, R. & Richter, J.D. The control of cyclin B1 mRNA translation during mouse oocyte maturation. *Developmental biology* **221**, 1-9 (2000).

111. Novoa, I., Gallego, J., Ferreira, P.G. & Mendez, R. Mitotic cell-cycle progression is regulated by CPEB1 and CPEB4-dependent translational control. *Nature cell biology* **12**, 447-456 (2010).

112. Eliscovich, C., Peset, I., Vernos, I. & Mendez, R. Spindle-localized CPE-mediated translation controls meiotic chromosome segregation. *Nature cell biology* **10**, 858-865 (2008).

113. Kurihara, Y.*, et al.* CPEB2, a novel putative translational regulator in mouse haploid germ cells. *Biology of reproduction* **69**, 261-268 (2003).

114. Theis, M., Si, K. & Kandel, E.R. Two previously undescribed members of the mouse CPEB family of genes and their inducible expression in the principal cell layers of the hippocampus. *Proceedings of the National Academy of Sciences of the United States of America* **100**, 9602-9607 (2003).

115. Chen, P.J. & Huang, Y.S. CPEB2-eEF2 interaction impedes HIF-1alpha RNA translation. *The EMBO journal* **31**, 959-971 (2012).

116. Vogler, C.*, et al.* CPEB3 is associated with human episodic memory. *Frontiers in behavioral neuroscience* **3**, 4 (2009).

117. Ortiz-Zapater, E.*, et al.* Key contribution of CPEB4-mediated translational control to cancer progression. *Nature medicine* **18**, 83-90 (2012).

118. Ernoult-Lange, M.*, et al.* Nucleocytoplasmic traffic of CPEB1 and accumulation in Crm1 nucleolar bodies. *Molecular biology of the cell* **20**, 176-187 (2009).

119. Lin, C.L., Evans, V., Shen, S., Xing, Y. & Richter, J.D. The nuclear experience of CPEB: implications for RNA processing and translational control. *RNA* **16**, 338-348 (2010).

120. Peng, S.C., Lai, Y.T., Huang, H.Y., Huang, H.D. & Huang, Y.S. A novel role of CPEB3 in regulating EGFR gene transcription via association with Stat5b in neurons. *Nucleic acids research* **38**, 7446-7457 (2010).

121. Kan, M.C.*, et al.* CPEB4 is a cell survival protein retained in the nucleus upon ischemia or endoplasmic reticulum calcium depletion. *Molecular and cellular biology* **30**, 5658-5671 (2010).

122. Caldeira, J.*, et al.* CPEB1, a novel gene silenced in gastric cancer: a Drosophila approach. *Gut* **61**, 1115-1123 (2012).

123. Groisman, I.*, et al.* Control of cellular senescence by CPEB. *Genes & development* **20**, 2701-2712 (2006).

124. Burns, D.M. & Richter, J.D. CPEB regulation of human cellular senescence, energy metabolism, and p53 mRNA translation. *Genes & development* **22**, 3449-3460 (2008).

125. Dong, Q.G.*, et al.* A general strategy for isolation of endothelial cells from murine tissues. Characterization of two endothelial cell lines from the murine lung and subcutaneous sponge implants. *Arteriosclerosis, thrombosis, and vascular biology* **17**, 1599-1604 (1997).

126. Ben-Shoshan, J.*, et al.* Hypoxia-inducible factor-1alpha and -2alpha additively promote endothelial vasculogenic properties. *Journal of vascular research* **46**, 299-310 (2009).

127. Morgan, M., Iaconcig, A. & Muro, A.F. CPEB2, CPEB3 and CPEB4 are coordinately regulated by miRNAs recognizing conserved binding sites in paralog positions of their 3'-UTRs. *Nucleic acids research* **38**, 7698-7710 (2010).

128. Mejias, M.*, et al.* Beneficial effects of sorafenib on splanchnic, intrahepatic, and portocollateral circulations in portal hypertensive and cirrhotic rats. *Hepatology* **49**, 1245-1256 (2009).

129. Mejias, M.*, et al.* Relevance of the mTOR signaling pathway in the pathophysiology of splenomegaly in rats with chronic portal hypertension. *Journal of hepatology* **52**, 529-539 (2010).
130. Huang, S.P.*, et al.* Interleukin-6 increases vascular endothelial growth factor and angiogenesis in gastric carcinoma. *Journal of biomedical science* **11**, 517-527 (2004).
131. Wei, L.H.*, et al.* Interleukin-6 promotes cervical tumor growth by VEGF-dependent angiogenesis via a STAT3 pathway. *Oncogene* **22**, 1517-1527 (2003).
132. Groppo, R. & Richter, J.D. CPEB control of NF-kappaB nuclear localization and interleukin-6 production mediates cellular senescence. *Molecular and cellular biology* **31**, 2707-2714 (2011).
133. Hagele, S., Kuhn, U., Boning, M. & Katschinski, D.M. Cytoplasmic polyadenylation-element-binding protein (CPEB)1 and 2 bind to the HIF-1alpha mRNA 3'-UTR and modulate HIF-1alpha protein expression. *The Biochemical journal* **417**, 235-246 (2009).
134. Alexandrov, I.M.*, et al.* Cytoplasmic polyadenylation element binding protein deficiency stimulates PTEN and Stat3 mRNA translation and induces hepatic insulin resistance. *PLoS genetics* **8**, e1002457 (2012).
135. Garcia-Tsao, G. & Bosch, J. Management of varices and variceal hemorrhage in cirrhosis. *The New England journal of medicine* **362**, 823-832 (2010).
136. Llovet, J.M.*, et al.* Sorafenib in advanced hepatocellular carcinoma. *The New England journal of medicine* **359**, 378-390 (2008).
137. Bava, F.A.*, et al.* CPEB1 coordinates alternative 3'-UTR formation with translational regulation. *Nature* **495**, 121-125 (2013).
138. Raymond, C.S. & Soriano, P. High-efficiency FLP and PhiC31 site-specific recombination in mammalian cells. *PloS one* **2**, e162 (2007).
139. Rodriguez, C.I.*, et al.* High-efficiency deleter mice show that FLPe is an alternative to Cre-loxP. *Nature genetics* **25**, 139-140 (2000).
140. Ruzankina, Y.*, et al.* Deletion of the developmentally essential gene ATR in adult mice leads to age-related phenotypes and stem cell loss. *Cell stem cell* **1**, 113-126 (2007).

141. Belloc, E., Pique, M. & Mendez, R. Sequential waves of polyadenylation and deadenylation define a translation circuit that drives meiotic progression. *Biochemical Society transactions* **36**, 665-670 (2008).

142. Niranjanakumari, S., Lasda, E., Brazas, R. & Garcia-Blanco, M.A. Reversible cross-linking combined with immunoprecipitation to study RNA-protein interactions in vivo. *Methods* **26**, 182-190 (2002).

143. Bahlmann, F.H.*, et al.* Erythropoietin regulates endothelial progenitor cells. *Blood* **103**, 921-926 (2004).